Universitat
de les Illes Balears

Title: Gravitational lensing effects on detection of gravitational waves from black hole binary systems.

AUTHOR: Héctor Estellés Estrella

Master's Thesis

Master's degree in Physics
(With a speciality/Itinerary Astrophysics & Relativity)

at the

UNIVERSITAT DE LES ILLES BALEARS

Academic year 2016/2017

Date 30/06/2017

UIB Master's Thesis Supervisor Sascha Husa

Abstract

Gravitational wave astronomy has become a reality after the first gravitational wave detections done by advanced LIGO detectors. The availability of accurate waveform templates is crucial for the optimal detection of signals, and for the reliable identification of the source, in order to filter the astrophysical signals from the noise of the detector. In this work we treat a phenomenon that can significantly affect the gravitational wave signal: gravitational lensing. The presence of matter inhomogeneities in the propagating path of gravitational waves from the source to the detector can modify the signals, both in amplitude and phase. If these effects are not included in the search templates, there can be a loss of detected signals. However, as in the well-known case of gravitational lensing of light, lensing magnification can increase the number of detectable events if lensing effects are included in the search templates. For gravitational lensing of light, the geometrical optics framework is sufficient for analyzing almost all astrophysical situations of interest, but in the last decade the work of Takahashi, Nakamura and others showed that for lensing of gravitational waves the correct framework is wave optics.

In this work we discuss the fundamental theory for understanding lensing effects on gravitational wave signals in the wave optics formalism, and we study two interesting situations of lensing of coalescing black hole binary signals, currently the only detected systems by gravitational wave detectors. First, we study how the signal-to-noise ratio of a lensed signal can decrease by the employ of unlensed templates for the search, and how the estimated binary parameters can be biased with respect the right ones due to the incomplete templates. Second, we study the increase in the number of detectable events per year for advanced LIGO due to lensing magnification if lensing effects are included in the templates.

Contents

1 Introduction

A new era in astronomy has begun with the direct detection of gravitational waves by the LIGO Scientific Collaboration. The two gravitational wave signals detected in 2015, GW150914 and GW151226, opened a new branch in observational astronomy: gravitational wave astronomy, robusted by the recent third detection GW170104.

Being theoretically predicted by Albert Einstein only one year after his theory of General Relativity was published in 1915, it took almost a century to directly confirm the existence of gravitational waves (although an indirect observation in 1973 of gravitational waves through the lost of energy of a binary pulsar deserved a Nobel prize for Taylor and Hulse in 1993). Einstein itself was skeptic about the possibility of detect gravitational waves, because they are so tiny that an incredible amount of technology has been needed to finally detect them. At the present time, three advanced gravitational wave detectors are operating in Observational Runs registering a huge amount of data on which new gravitational wave signals will be found during the following years. They are both LIGO detectors, in Hanford and Livingston (USA), and VIRGO detector in Cascina, Italy. They have enough sensitivity in the frequency range from 20 Hertz to a few thousand of Hertz to detect the last inspiral orbits, merger and ringdown of coalescing binary system, the most promising source of gravitational waves for these detectors due to the available theoretical models for searching the signals. Other kinds of signal could be detected in the following years by these detectors, such as gravitational waves from spinning neutron stars, supernova explosions, cosmic strings cusps, and maybe new unexpected sources.

Besides the relevance of the discovery of gravitational waves themselves (along with the first evidence of the existence of black hole binary systems), gravitational waves provide a new powerful way to study astrophysical and cosmological phenomena, complementary but essentially different to the study of the electromagnetic spectrum initiated almost half a millennium ago by Galileo's telescope. The strong regime of gravity can be observed for the first time in Science's history. Information about black hole's nature can help theoretical physics in resolving some of the most intriguing problems in current physics as the black hole information puzzle (the study of quasinormal modes in gravitational waves signals from black hole binaries could prove the validity of the no-hair theorem and other elements involved in this paradox). The study of gravitational wave emission from binary neutron systems and supernova explosions could enlighten unclear aspects about their inner structure, equations of state, formation and evolution of these systems. Also, gravitational waves from supermassive black hole binaries could provide a new method to measure cosmological distances, and therefore provide information about cosmological parameters and dark energy. Maybe in a not-so-far future, sensitive enough detectors could bring us information about inflation and the Plank epoch of the Universe. Summarizing, a new and exciting way of looking the Universe has walked its first steps.

As a recent branch of Science, the study of gravitational waves has an ongoing theoretical and experimental development with a increasing interest from the science community. In this work we will treat a not so much studied phenomena of gravitational waves: gravitational lensing of gravitational waves due to matter inhomogeneities in the

propagation path from the source emitting them to Earth's detectors. Gravitational lensing of light is a well-known phenomena, with a rich contribution to astronomy and astrophysics. One should expect that gravitational waves interact also with the matter they find in their propagation. Besides the potential information that this lensing could bring about the lenses, for gravitational wave detection is interesting to see what are the possible effects that this phenomenon provokes on detections. As in the light case, one could expect a magnification of the signals, leading to an increase of the number of detections. However, as we will see in this work, due to the different nature in the emission of gravitational waves and light, for gravitational waves one has to deal with interference phenomena, that could lead to a potential loss of signals if lensing effects are not included in the search.

1.1 Work structure

This work is structured as follows:

- In Section 2 we give a brief introduction to General Relativity, the current theoretical framework for gravitational phenomena, being both gravitational waves and gravitational lensing predictions of this theory, without an analog in the previous theory of gravitation. We introduce the basic ideas of the theory, and develop some of the tools that we will need in the rest of the work.

- In Section 3 we introduce gravitational lensing in its geometrical optics approximation. This approximation is valid for light, but for gravitational waves we will see that even in the valid geometrical optic limit one needs to include interference effects. This section provides some definitions of interesting quantities in lensing that we will employ in the wave optics treatment, and besides it gives an idea of why lensing has to occur according to General Relativity.

- In Section 4, we emphasize the need of a wave optics treatment of lensing of gravitational waves and develop the needed structure to study lensing in this regime. We focus on the amplification factor, the key quantity in wave optics lensing, and we discuss the general behavior of this quantity. Propagation of gravitational waves through empty space is also discussed.

- In Section 5 we present the emission of gravitational waves by black hole binary systems, since we will focus on lensing of these signals. For the moment, they constitute the only detected system by gravitational wave detectors, so it is justified to focus on them. We comment the general aspects of emission theory, from Post-Newtonian approximations to the phenomenological model that we will employ in this work. We also include the emission from spinning neutron stars, although a planned analysis of lensing for these signals does not appear here finally.

- In Section 6 we sketch the basic features of detection of gravitational waves, and some data analysis tools that we will employ to extract conclusions from lensed signals.

- In Section 7, we present the results of this work. Essentially we treat how lensing affects the detectability of gravitational waves. In the first situation we study how

potentially detectable signals can be lost if one does not include lensing effects on the search template. The second situation study the inverse scenario, how the number of detectable events could increase because lensing magnification if one employs a lensed template bank to search the signals.

- In Section 8 we comment some conclusions of this work.

1.2 Notation and units

We will follow the standard notation conventions in General Relativity. For tensorial indices, we denote spacetime indices with Greek letters running from 0 to 3, with the time component corresponding to 0. We denote spacelike indices with latin letters running from 1 to 3. We employ the Einstein summation convention, in which repeated indices up and down in a expression mean summation over all the possible values. For example:

$$x^{\mu}y_{\mu} \equiv \sum_{\mu=0}^{3} x^{\mu}y_{\mu} \ .$$

We use geometrized units in which the Newton's constant G and the speed of light are settled to one:

$$G = c = 1 \ .$$

In these units, mass, length and time has the same dimensions. The two more employed units in this work are the solar mass M$\odot$ and megaparsecs Mpc, both in dimensions of time. In geometrized units, the conversion of these units into seconds is:

$$M_{\odot} = 4.925 \times 10^{14} s \ ,$$
$$Mpc = 1.029 \times 10^{-6} s \ .$$

2 A brief introduction to General Relativity

Both gravitational phenomena related to this work, gravitational lensing and gravitational waves, are consequence of our current theory of gravitation, General Relativity developed by Albert Einstein and published in 1915. Thus, the most natural first step is to give an introduction to the concepts that we will employ during the rest of the work. A complete and mathematically rigorous presentation of General Relativity is out of the scope of this work. Instead, we will present the needed concepts for the work in a handy way.

2.1 The Equivalence Principle: gravitation as inertia

The key idea of General Relativity is to interpret gravitation as an inertial phenomenon. Instead of considering gravity as an usual interaction between bodies, like electromagnetism, or as in the previous theory of gravitation due to Isaac Newton, General Relativity states that gravitation is a consequence of the geometry of spacetime. Spacetime gets curved by the presence of energy and matter on it, and energy and matter travel along spacetime according to its curved geometry.

Einstein was motivated to discover the real nature of gravity by the Equivalence Principle, which oldest form was realized by Galileo and stated by Isaac Newton. Consider the second Newton's law:

$$\mathbf{F} = m_i \mathbf{a} \ , \tag{1}$$

where $\mathbf{F}$ is the sum of forces experimented by a particle, $\mathbf{a}$ is the acceleration of that particle, and m_i is the inertial mass of the particle, a quantity that in some sense measures the amount of inertia (how much force is needed to give some acceleration). And now consider Newton's gravitational force:

$$\mathbf{F}_g(\mathbf{x}) = -m_g U(\mathbf{x}) \hat{\mathbf{r}} \ , \tag{2}$$

where $U(\mathbf{x})$ is the gravitational potential in the position $\mathbf{x}$, and m_g is the gravitational charge of the particle, i.e, a quantity that measures how strong the particle feels the gravitational interaction (think for example in the electric charge q in Coulomb's law, it has the same role). Using both equations, the acceleration of a particle due to a gravitational field is:

$$\mathbf{a} = -\frac{m_g}{m_i} U(\mathbf{x}) \hat{\mathbf{r}} \ . \tag{3}$$

Again, to see the similarity, think about the acceleration of a charged particle in an electric potential $\phi(\mathbf{x})$: $\mathbf{a} = \pm(q/m_i)\phi(\mathbf{x})\hat{\mathbf{r}}$.

Galileo experimentally realized (the famous, and perhaps apocryphal, experiment of the Tower of Pisa) that all bodies fall with the same acceleration on the Earth's gravitational potential, regardless of their mass. Thus, Newton stated the principle of equivalence between the gravitational charge (that has dimensions of mass) and the inertial mass:

$$m_g = m_i \ . \tag{4}$$

This is a non trivial statement. Regardless being quantities with the same dimensions, the role of m_g and m_i is entirely different. This equality (proved to a high degree of accuracy by later experiments) led Einstein to think in the relation between inertia an gravitation. After some though experiments, Einstein stated a more general version of the Equivalence Principle:

> The outcome of any local experiment in a freely falling laboratory is independent of the velocity of the laboratory and its location in spacetime.

What this sentence means is that in some type of reference systems (freely falling ones) one cannot feel the existence of a gravitational field locally (i.e, for regions of the spacetime small enough to consider the gravitational field homogeneous). This naturally leave to the assumption that gravitation is an inertial effect. If you consider the freely falling systems as the true inertial systems, then in them you do not experience any gravitational force because that force does not exist. You realize locally the presence of gravitation (for example, when you drop an object in Earth's surface from some height) when you are not in an inertial frame. In the Earth's surface we are accelerated by the electromagnetic force between our feet and the ground. The gravitational force we see on falling object in Earth's surface is not a true force. Is a fictitious inertial force, as in the Coriolis effect, where we see a non-existing force due to be in a non-inertial coordinate system.

The keyword is *locally*. If you observe the movement of bodies far away from you, then you realize again some kind of force acing on them. But this is because you are not in *their* inertial frames. Inertial frames exist locally. This conclusion led Einstein to assume that spacetime is not flat (in a flat spacetime, like in Minkowski spacetime of special relativity, one can define global reference systems). Spacetime has a curved geometry, and the objects inhabiting spacetime travel according to this geometry.

2.2 The geometry of spacetime

So far we were talking about spacetime without explain what we meant. Spacetime is a concept born with the new physical paradigm that Einstein installed in 1905 with his theory of Special Relativity. Thus, it is interesting to see what is spacetime and what is its mathematical structure in the special relativistic case, and after that generalize. Besides, during the rest of the work we will refer often to the spacetime of Special Relativity: Minkowski spacetime (due to its mathematical formalization by Hermann Minkowski in 1907). After that, we will generalize the basic ideas to the more general mathematical structure of Riemann geometry.

2.2.1 Flat spacetime: Minkowski

In the revolutionary picture of Special Relativity, time and space become relative to the observers. Consider a physical event as something that happens at some time and somewhere. An observer with an associated reference frame can characterize events by four numbers, according to his reference frame: one number measuring the time when the event happened according to the reference clock of the observer, and three numbers measuring the position where the event happened according to the observer's spatial reference system (consider for example three rigid rods with length rules attached to

the observer). For two different events, the observer can measure the time interval Δt and the space interval $\Delta \mathbf{x}$ between them. So far all these things hold in Galilean physics.

The new thing introduced by Special Relativity is that observers moving with a relative velocity measure distinct time intervals Δt and spatial intervals $\Delta \mathbf{x}$ between two events. The only invariant (i.e, observer independent) interval is the spacetime interval: $(\Delta s)^2 = (\Delta \mathbf{x})^2 - (\Delta t)^2$ due to the universality of the speed of light $c = 1$ (in natural units) established by Einstein's principle of relativity.

The continuum set of all events is what we call spacetime. So in the lowest level spacetime is a set of points (the events), but Special Relativity charges more structure into it. If we define a coordinate system on the spacetime, i.e, we assign to each event four numbers in a one-to-one correspondence $\{x^\mu(p)\} = \{x^0(p), x^1(p), x^2(p), x^3(p)\}$, then we see that Minskowski spacetime is (topologically) equivalent to $\mathbb{R}^4$. Of course, $\mathbb{R}^4$ is a vector space, so Minskowski spacetime is itself a vector space. But Special Relativity gives another extra structure: the spacetime interval is a norm in this vector space, it is the norm of the 4-vector joining the two events. A norm defined on a vector space gives you a metric space.

Consider we have a position vector s with components (x^0, x^1, x^2, x^3). The length of this vector is the spacetime interval between the origin and the position s, and the length of a vector is given by its norm. The square norm is then:

$$length(s)^2 = s^2 = ||s||^2 = s \cdot s = -(x^0)^2 + (x^1)^2 + (x^2)^2 + (x^3)^2 \ . \tag{5}$$

The inner product defining that norm is:

$$s \cdot s = \eta_{\mu\nu} x^\mu x^\nu = (x^0, x^1, x^2, x^3) \begin{pmatrix} -1 & 0 & 0 & 0 \\ 0 & 1 & 0 & 0 \\ 0 & 0 & 1 & 0 \\ 0 & 0 & 0 & 1 \end{pmatrix} \begin{pmatrix} x^0 \\ x^1 \\ x^2 \\ x^3 \end{pmatrix} \ . \tag{6}$$

The matrix $\eta_{\mu\nu} = diag(-1, 1, 1, 1)$ is called the Minkowski (or flat) metric. Actually, the matrix are the components of the metric in a reference system. The metric itself is 2-covariant tensor, i.e, a map from pairs of vectors to real numbers, but we will talk better about this in the general scenario. In Minkowski, the metric $\eta_{\mu\nu}$ has the same components in all inertial coordinate systems (for accelerated reference systems the components will change).

We can easily see that the norm defined by Minkowski metric is indefinite, i.e, the norms can be positive, negative, and zero even if the vector is not the zero vector. A metric which gives indefinite norms and has only one minus sign in its diagonal form is called Lorentzian metric. Consider for example the vector $(1, 1, 0, 0)$. It is obviously not the zero vector but its norm is zero. Negative norm vectors are called timelike vectors, positive norm vector are called spacelike vectors, and zero norm vector are called lightlike or null vectors. Consider again the spacetime interval in its infinitesimal form:

$$ds^2 = \eta_{\mu\nu} dx^\mu dx^\nu = -(dx^0)^2 + (d\mathbf{x})^2 \tag{7}$$

The component x^0 is the time component (in our convention) so we rename $x^0 = t$ (remember, in units $c = 1$). If we have a null interval between two infinitesimally close events, then we have $d\mathbf{x} = \pm dt$ or what is the same, the particle moving between these two events has a speed $v = |d\mathbf{x}/dt| = 1 = c$ so it moves at the speed of light. For preserving causality, information (which is carried by energy or matter) cannot propagate speeder than light, so the speed of all physical objects moving in the spacetime have to fulfill $|d\mathbf{x}/dt| \leq 1$.

Now let us consider the inertial paths of objects (particles, bodies or fields) in Minkowski spacetime, which we call geodesics for now on. If they are not subject to external forces, they will move with constant velocity, thus describing straight paths in spacetime. A straight path is defined by its tangent vector, and according to what we said before physical objects can only move in paths with timelike or null tangent vectors. These paths are called timelike and null geodesics. In particular, massive particles and fields move along timelike geodesics, and massless particles and fields (as light or gravitational waves) move along null geodesics.

2.2.2 Manifolds and tensors

Now we turn back our attention to the general situation. Minkowski spacetime is no longer valid for representing the general spacetime of General Relativity. The required generalization has to take into account the Equivalence Principle, which we can reformulate as spacetime has to look locally like Minkowski spacetime, but it can have another global topology. So we need a mathematical structure that looks like $\mathbb{R}^4$ in small enough regions and that has a Lorentzian metric structure which reduces to Minkowski metric in those regions. This is achieved by a Lorentzian manifold (of four dimensions). First, let us see what is a manifold.

Consider a set of points p called M which satisfies the following conditions:

- There are open subsets of points in which exists a one-to-one map from points of M to points of a region of $\mathbb{R}^4$, i.e, we can assign a system of coordinates to a region of the set (generally one cannot assign a global coordinate system to the entire set). Each open subset with this one-to-one map defined on it is called a chart.

- In a region shared by two or more charts, one can change from one coordinate system to another by a set of invertible differentiable functions. These coordinate transformations are called diffeomorphisms.

- The union of all charts is called an atlas. If the atlas is maximal, i.e, it is formed by all possible charts that can be defined on the set, then the set is a (differentiable) manifold.

We want to express the laws of Physics in a coordinate independent way, because coordinate systems are an artifact introduced by observers in order to use the mathematical tools of $\mathbb{R}^4$. A physical observable (a quantity that can be measured) has to be independent on the choice of a particular coordinate system by a particular observer. So we need to introduce in the manifold coordinate independent objects. This objects are called tensors. Let's start with the simplest class of tensors: vectors (besides scalars

quantities, that are trivial tensors).

It can be shown that at each point of the manifold we can construct a 4-dimensional vector space [Wald, sec. 2.2] called Tangent Vector Space T_pM. One useful basis for the vector space is the set of directional derivatives along the coordinates directions x^μ, evaluated at the point p. This is called the coordinate basis:

$$\{\frac{\partial}{\partial x^\mu}\} \equiv \{\partial_{x^\mu}\} = \{\partial_{x^0}, \partial_{x^1}, \partial_{x^2}, \partial_{x^3}\} \ , \tag{8}$$

(we do not explicitly write the dependence on the point p in order to not complicate excessively the notation, but all quantities are evaluated in p because the vector space is defined only in p).

The basis allows us to write all the vectors v of T_pM as linear combinations of the basis vectors:

$$v = v^\mu \partial_\mu \ . \tag{9}$$

where the numbers $v^\mu(x(p))$ are the components of the vector in that coordinate system and depend on the coordinates of the point p. If we make a coordinate transformation $x^\mu \rightarrow y^\mu(x)$ from the system x^μ to the system y^μ, using the chain rule the basis transforms as:

$$\partial_{y^\mu} = \frac{\partial}{\partial y^\mu(x)} = \left(\frac{\partial x^\nu}{\partial y^\mu}\right) \frac{\partial}{\partial x^\nu} = J^\nu{}_\mu \partial_{x^\nu} \ , \tag{10}$$

where $J^\nu{}_\mu$ is the inverse Jacobian of the coordinate transformation. It can be shown [Wald, page 17] that the vector components transform as:

$$v'^\mu = \left(\frac{\partial y^\mu}{\partial x^\nu}\right) v^\nu = J_\nu{}^\mu v^\nu \ , \tag{11}$$

where $J_\nu{}^\mu$ is the Jacobian of the transformation. So the entire vector transform as:

$$v' = v'^\mu \partial_{y^\mu} = J_\alpha{}^\gamma J^\beta{}_\gamma v^\alpha \partial_{x^\beta} = \delta^\beta_\alpha v^\alpha \partial_{x^\beta} = v^\alpha \partial_{x^\alpha} = v \ , \tag{12}$$

it is invariant under coordinate transformations, as we wanted.

The next class of tensor we can construct from vectors are the covectors. It can be shown [Wald, page 19] that there is a one-to-one map from each vector on T_pM to the real numbers. These maps are called covectors, and form a vector space called the Cotangent Space or the Dual Space T^*_pM defined on the same point as T_pM. The coordinate dual basis for these covectors are the coordinate differentials dx^μ, and in this basis we can write all covectors ω in T^*_pM as linear combinations of the dual basis:

$$\omega = \omega_\mu dx^\mu \ . \tag{13}$$

Now the transformations under a change of coordinates are the inverse of the vector case: the covector components transforms with the inverse Jacobian of the coordinate transformation and the dual basis covectors transform with the Jacobian.

Finally, we can define more general tensors using the tensor product to form a basis of the class of tensors we want. For example, we can form a vector space $\mathbb{T}^0_2$ of rank-2 covariant tensors using the basis $\{dx^\mu \otimes dx^\nu\}$:

$$T = T_{\mu\nu} dx^\mu \otimes dx^\nu \ . \tag{14}$$

This is a multi-linear map from elements of the Cartesian space $T_pM \times T_pM$ (pairs of vectors) to real numbers. In general, the components of a tensor of arbitrary rank will transform with a Jacobian for each upstairs index and an inverse Jacobian for each downstairs index.

So far, we have define tensors on a point. There is no global vector space associated with the manifold. However we can define tensor fields. A tensor field of some rank is a map that assign to each point in a region of the manifold a tensor of that rank. For example, a vector field $v(x)$ assigns a vector to each point of the region where is defined. Now the components of tensor fields are functions of the coordinates: $T^{\mu\nu} = T^{\mu\nu}(x)$. We usually talk about tensors fields without writing explicitly the word *field*.

2.2.3 Metric tensor and Curvature

Once we have a manifold and the invariant objects living in it, tensors, we turn into the question of how describing the geometry of spacetime. For talking about geometry we need to talk about distances and angles. This is achieved, as in the case of Minkowski spacetime, defining an inner product in the vector space of each point: defining a metric field in the manifold.

As we have seen when we talked about tensors, a 2-rank covariant tensor is a map from pairs of vectors to the real numbers. So for defining a metric we need that class of tensor. The metric has to be symmetric and has to have Lorentzian signature, because we want the inner product to be the same as in Minkowski in regions small enough of the manifold (because of the Equivalence Principle). And finally, we want an invertible metric because we want to define a inner product in the cotangent space as well. So the spacetime metric has to be a non-degenerate symmetric 2-rank covariant tensor:

$$g = g_{\mu\nu}(x) dx^\mu \otimes dx^\nu \ . \tag{15}$$

Being non-degenerate means that the components matrix $g_{\mu\nu}(x)$ has non-zero determinant at each point, so we can invert it to obtain an inverse metric:

$$g^{-1} = g^{\mu\nu}(x) \partial_{x^\mu} \otimes \partial_{x^\nu} \ , \tag{16}$$

which satisfies $g^{\mu\nu} g_{\nu\rho} = \delta^\mu_\rho$. Closely related to the metric is the line element. If we compute the inner product (with the metric) of an infinitesimal displacement vector δx^μ, we obtain:

$$g(\delta x, \delta x) = g_{\mu\nu} \delta x^\mu \delta x^\nu \equiv ds^2 \ , \tag{17}$$

where the line element ds^2 is the infinitesimal generalization of the spacetime interval in Minkowski. Given the line element we have the metric components, so it is usual to specify a metric giving its associated line element.

Besides defining an inner product in the tangent space (and an inner product in the cotangent space with the inverse metric), the metric allow us to map from tensors of one class to tensors of another class. For example, the metric allow us to identify each vector in the tangent space of a point with one and only one covector of the cotangent space of that point:

$$v_\mu = g_{\mu\nu} v^\nu \ . \tag{18}$$

In general, we can "up and down" indices of tensor (rigorously, map tensors of different ranks) contracting indices with the metric.

For talking about the geometry of spacetime we need to take into account the behavior of a region of points, but so far our physical quantities (described by tensors) are defined in one point. We need to see how tensors change when they are displaced to adjacent points: we need to derivate. But the usual partial derivative operators ∂_μ, when acting on a tensor, do not return a tensor, i.e, they return a coordinate dependent quantity [Wald, sec. 3.1]. We need to generalize the derivative operators in order to return tensors when they act on tensors. This is achieved introducing a connection on the manifold: $\Gamma^\mu_{\nu\rho}$, which components do not transform as tensors. So we demand that the terms arising from the transformation of $\Gamma^\mu_{\nu\rho}$ (acting on a tensor) exactly cancel the terms arising in the transformation of ∂_μ (acting on that tensor). With that, we can define the covariant derivatives of vectors and covectors as:

$$\nabla_\nu v^\mu(x) \equiv \frac{\partial v^\mu(x)}{\partial x^\nu} + \Gamma^\mu_{\nu\rho}(x) v^\rho(x) \ , \tag{19}$$

$$\nabla_\nu \omega_\mu(x) \equiv \frac{\partial \omega_\mu(x)}{\partial x^\nu} - \Gamma^\rho_{\mu\nu}(x) \omega_\rho(x) \ . \tag{20}$$

It is straightforward to generalize for any tensor class: simply add a term as in (19) for each upstairs index an a term as in (20) for each downstairs index. For example, the covariant derivative of the metric is:

$$\nabla_\alpha g_{\mu\nu} = \partial_\alpha g_{\mu\nu} - \Gamma^\rho_{\alpha\nu} g_{\mu\rho} - \Gamma^\rho_{\alpha\mu} g_{\rho\nu} \ . \tag{21}$$

There is a hole class of connections compatible with out requirement of defining a covariant derivative, but in General Relativity we choose just one, that has the additional property of making zero the covariant derivative of the metric $\nabla_\alpha g_{\mu\nu} = 0$. Then we talk about a metric compatible connection, and solving the last equation equal to zero one finds the symbols of that connection [Wald, page 36], which are called the Christoffel symbols:

$$\Gamma^\rho_{\mu\nu} = \frac{1}{2} g^{\rho\lambda} (\partial_\mu g_{\lambda\nu} + \partial_\nu g_{\mu\lambda} - \partial_\lambda g_{\mu\nu}) \ . \tag{22}$$

As we said repeatedly, the Equivalence Principle tells us that any spacetime has to look like Minkowski spacetime locally. It can be shown [Carot, sec. 1.3] that we can always set a coordinate system in which the metric diagonalizes to $g_{\mu\nu} = diag(-1, 1, 1, 1)$, at least in one point. These coordinates are called normal coordinates, and are valid in some small enough region. In this coordinate system, the first derivatives of the metric, and therefore the Christoffel symbols, are zero. We can do a Taylor expansion of the metric in this region around the point ($x = 0$) in which is flat:

$$g_{\mu\nu}(x) = g_{\mu\nu}(0) + \frac{1}{2} \frac{\partial^2 g_{\mu\nu}(x)}{\partial x^\alpha \partial x^\beta} x^\alpha x^\beta + O(x^3) \ . \tag{23}$$

Thus, the metric is approximately flat in a region such that the second term is $\ll 1$. So we see that the second derivatives of the metric in some sense capture the essence of spacetime not being flat in larger regions. We can define a curvature tensor field in terms of the second derivatives of the metric, or equivalently in terms of derivatives of the Christoffel symbols, since these contain first derivatives of the metric. This is the Riemann curvature tensor [Wald, sec. 3.2], whose components are:

$$R^\alpha{}_{\mu\beta\nu} = \partial_\beta \Gamma^\alpha_{\mu\nu} - \partial_\nu \Gamma^\alpha_{\mu\beta} + \Gamma^\alpha_{\beta\lambda} \Gamma^\lambda_{\mu\nu} - \Gamma^\alpha_{\nu\lambda} \Gamma^\lambda_{\mu\beta} \ . \tag{24}$$

2.2.4 The motion of inertial particles: Geodesics

The Riemann curvature tensor field describes the curvature at each point of the manifold, so knowing the Riemann at all points is equal to know the geometry of spacetime. Now we can ask how matter and energy moves along spacetime. First of all, we can describe a path or a curve in spacetime using some parametrization of the coordinate system: $x^\mu(\lambda)$. The parameter λ is a real valued function that for each point in the curve assigns one value. This is how trajectories are usually defined in Physics. Consider for example a mechanical problem for one particle. After solving the equations of motion, what one generally obtains is a time parametrized solution of the position: $\mathbf{x}(t)$. In our case the parameter is arbitrary, but for the motion of massive particles, which are described by timelike paths, the proper time is a natural parameter.

We are interested here in the paths of inertial objects, those who are not affected by any external force (remember that we are no longer considering gravity as a force). There are several ways of deriving the equation of these paths, which are called geodesics. Since we will mention at some point in this work the concept of parallel transport, let us introduce the parallel transport and derive the geodesic equation from it.

Consider we want to know how the value of a tensor change as we transport it along some curve in spacetime (this is a little sloppy, since as we remarked before tensors spaces are defined in each point, and for different points we have different tensor spaces; but consider that transport is a map between the geometry of one point and the geometry of another, and then under this map we can assign tensors from one point to tensors from other point). This is simply the derivative of the tensor along the curve, i.e, the covariant derivative in the direction of the tangent vector to the curve. For example, for vectors we have:

$$\frac{Dv^\mu}{d\lambda} = t^\nu \nabla_\nu v^\mu \ , \tag{25}$$

where $t^\mu = dx^\mu/d\lambda$ is the tangent vector to the curve. Geodesics in some sense are a generalization of straight lines in flat spacetime, since the motion of force-free particles in flat spacetime is described by straight lines. A straight line in flat geometry can be though as a path whose tangent vector remains parallel to itself in all points of the path, i.e, that after transporting it along the path, the vector is self-parallel, so its derivative along the path is proportional to itself. Then we say that the tangent vector is parallely transported along the curve. So we can use the same criteria: a geodesic (a inertial path in spacetime) is a path whose tangent vector is parallely transported along it,

$$t^\nu \nabla_\nu t^\mu = c t^\mu \ . \tag{26}$$

This is for an arbitrary parameter. However, it can be shown that there is a family of parameters for which the derivative of the tangent vector is zero (the vector remains the same vector). These are called affine parameters. With the definition of the covariant derivative (19) and the tangent vector, we can rewrite the last equation (in affine parameterization) as:

$$\frac{dx^\nu}{d\lambda}\left[\frac{\partial}{\partial x^\nu}\left(\frac{dx^\mu}{d\lambda}\right)\right] + \Gamma^\mu_{\nu\lambda}\frac{dx^\nu}{d\lambda}\frac{dx^\lambda}{d\lambda} = 0 \ . \tag{27}$$

Using the chain rule backwards for the first term:

$$\frac{d^2x^\mu}{d\lambda^2} + \Gamma^\mu_{\nu\lambda}\frac{dx^\nu}{d\lambda}\frac{dx^\lambda}{d\lambda} = 0 \ . \tag{28}$$

This is the geodesic equation in affine parameterization. It is a second order ordinary differential equation in λ, so given two initial conditions $x^\mu(\lambda = 0)$ and $t^\mu(\lambda = 0)$ it has always a unique solution. Geodesics can be timelike, spacelike or null, according to the norm of their tangent vectors. In this work we will interested in null geodesics, the paths followed by light and gravitational waves since they are massless fields.

2.3 Einstein equations

Now that we know how to characterize the curvature (i.e, the non-flatness) of spacetime and how physical entities move across it, it is time to see what generates the curvature. We mentioned the Equivalence Principle as the way Einstein got into the structure of spacetime. Another, more philosophical conjecture gave him the idea of how spacetime gets curved. It is the Mach conjecture, from the physicist and philosopher Ernst Mach. There are many formulations of the conjecture, but in some sense it says that the presence of matter in one region of spacetime should affect which reference frames are inertial in another. The conclusion is that Einstein stated that the energy and matter content of spacetime determines its curvature. And that is the idea behind the Einstein field equations of General Relativity. We need to see them, because in this work we will derive the wave equation of gravitational waves linearizing them. But before we need to talk about energy and matter.

2.3.1 Energy-momentum tensor

We introduced tensors as a way to express physical quantities in a coordinate independent way. We can compress the measurable quantities of some matter and energy configuration into a tensorial expression: the energy-momentum tensor. It is a generalization of the stress tensor employed in continuum media dynamics:

$$T^{\mu\nu}(x) = \begin{pmatrix} \epsilon & \pi^1 & \pi^2 & \pi^3 \\ \pi^1 & p^1 & \sigma^{12} & \sigma^{13} \\ \pi^2 & \sigma^{12} & p^2 & \sigma^{23} \\ \pi^3 & \sigma^{13} & \sigma^{23} & p^3 \end{pmatrix} \ , \tag{29}$$

where:

- $T^{00} = \epsilon$ is the energy density. It takes into account the rest mass density and other forms of energy. For example, for a perfect fluid is simply $\epsilon = \rho_0(1 + u)$ where ρ_0 is the mass density of the fluid and u its internal energy.
- $T^{0i} = \pi^i$ is the linear momentum density in the ith direction, or equivalently the flux of energy density in that direction.
- $T^{ii} = p^i$ is the flux of the ith component of linear momentum in the direction ith, i.e, the normal stress in that direction. In the case of a medium with isotropic stresses, it is just the pressure.

- $T^{ij} = \sigma^{ij}$ is the flux of the ith component of linear momentum in the direction jth. It is the shear stress.

The energy-momentum tensor is a symmetric tensor. We can see it because of the equalities we mentioned above. For example, the $0i$ component is the flux of energy density in the ith direction, but this is completely equivalent to the density of linear momentum in the ith direction, the component $i0$. Finally, if we want to preserve local conservation of the physical quantities, we have to demand that the energy-momentum tensor has zero divergence:

$$\nabla_\nu T^{\mu\nu} = 0 \ . \tag{30}$$

2.3.2 Einstein tensor

Once we have some energy and matter configuration defined by the energy-momentum tensor, we can look for the equation relating the curvature produced by this configuration. We have established that the curvature is measured by the Riemann tensor $R^\alpha{}_{\mu\beta\nu}$. It is a 4-rank tensor, so in order to find a equation relating the information of the curvature to the energy-momentum tensor (which is 2-ranked) we need to decompose it. Without entering into the details, from the Riemann tensor we can obtain a traceless part, the Weyl tensor, and a trace part, which is the Ricci tensor (being a trace, we have to contract two indices of the Riemann tensor, so the Ricci tensor is a 2-ranked tensor). The Ricci tensor is defined as:

$$R_{\mu\nu} = R^\alpha{}_{\mu\alpha\nu} = g^{\alpha\beta} R_{\alpha\mu\beta\nu} \ . \tag{31}$$

Besides, the Ricci tensor is symmetric as the energy-momentum tensor, due to the symmetric properties of the Riemann tensor. So one can try the following equation:

$$R_{\mu\nu} = \kappa T_{\mu\nu} \ , \tag{32}$$

where κ is some proportionality constant and $T_{\mu\nu} = g_{\mu\alpha} g_{\nu\beta} T^{\alpha\beta}$. But one can show that $\nabla^\nu R_{\mu\nu} \neq 0$ in general, and by the local conservation law of $T^{\mu\nu}$, we need in the left hand side a tensor with vanishing divergence. Using the Bianchi identities, one can construct a unique tensor from the Riemann that fulfill that condition [Wald, page 40], and it was found by Einstein, the Einstein tensor:

$$G_{\mu\nu} = R_{\mu\nu} - \frac{1}{2} g_{\mu\nu} R \ , \tag{33}$$

where $R = R^\mu{}_\mu = g^{\mu\nu} R_{\mu\nu}$ is the scalar curvature, the trace of the Ricci tensor.

2.3.3 Einstein equations

We finally have the equations relating the curvature of spacetime with the energy-matter content on it, the Einstein field equations:

$$G_{\mu\nu} = 8\pi T_{\mu\nu} \ , \tag{34}$$

where the proportionality constant was fixed for matching the Poisson equation for the gravitational potential in the Newtonian limit (in geometrized units $G = c = 1$). In section 4.2 we will see that linearizing the Einstein equations in the vacuum we find a wave equation governing the propagation of gravitational waves, and in section 5.1 we will use the wave equation with an energy-momentum tensor source to derive a approximated formula of production of gravitational waves by accelerated sources.

3 Lensing in the geometrical optics limit

Gravitational lensing of light was one of the first consequences predicted by Albert Einstein of his theory of General Relativity (GR) published in 1915. Likewise, it was one of the first experimental proofs GR was successful to pass: the observation by Eddington and his team of star positions during the solar eclipse of May 29, 1919.

In this section, we analyze the behavior of light rays propagating in a non-flat background spacetime, and see how their trajectories (null geodesics of the spacetime) deviate respect to the trajectories in a flat spacetime. The analysis is taken without taking into account the wave behavior of light, in the so called geometrical optics approximation. Gravitational waves, as we will see, propagate along null geodesics too, so in a first approximation geometrical lensing should be a valid description for gravitational waves. For light this is a valid approximation in almost all astrophysical situations of interest, although for gravitational waves we will discuss later in this work that the approximation breaks down in astrophysically relevant regimes. Besides, due to the different nature of emission of light and gravitational waves by astrophysical sources, the geometrical limit includes extra terms for gravitational waves.

3.1 Perturbed Minkowski metric

We start choosing a suitable spacetime metric for which we will study the behavior of null geodesics. Our Universe is almost spatially flat, i.e, at a concrete value of the cosmological time, the spatial 3-surfaces have a flat geometry. Our Universe is also suffering a cosmological expansion, so we cannot associate it with Minkowski spacetime. Actually, our Universe is well described by a Friedmann-Robertson-Walker metric, of the form:

$$ds^2 = -dt^2 + a(t)^2 d\Sigma^2 \ , \tag{35}$$

where the spatial metric is:

$$d\Sigma^2 = \frac{1}{1-k^2r^2}dr^2 + r^2(d\theta^2 + \sin^2\theta d\phi^2) \ , \tag{36}$$

where $k = \{1, 0, -1\}$ determines the topology of the spatial sections. The current observational situation suggests that $k = 0$, and we see that for this value the spatial metric is the flat metric in spherical coordinates. Thus, the difference between the spatially flat FRW metric and Minkowski is the scale factor $a(t)$ which encodes the cosmological expansion. However, for small regions of propagation (small times compared with the typical scale of expansion) we can deal with Minkowski metric as a starting point. In fact, we will see that for the scales involved in lensing, we will need to include cosmological effects, but we can correct later the needed quantities. So we start with the Minkowski metric:

$$ds^2 = -dt^2 + \delta_{ij}dx^i dx^j \ , \tag{37}$$

where δ_{ij} is the Kronecker delta.

Lensing is produced by the presence of matter inhomogeneities in the propagation path of light rays (or gravitational waves). In this work we will treat as lenses compact

objects, like black holes or massive stars. We can treat the curvature they produce in the weak field limit: essentially we assume that the lenses are slow-moving (their intrinsic velocities are slow compared with the speed of light $v \ll 1$) and that the curvature they produce has a characteristic radius much longer than the size of these objects. These conditions are fulfilled by the typical lenses we consider in this work. Thus, we can consider that the lens energy-momentum tensor is dominated by the energy density component:

$$T^{00}(x) = \rho(x), \quad T^{i0} = T^{ij} \approx 0 \ . \tag{38}$$

Because we expect a small curvature produced by these systems, we can consider that the metric they produce is Minskowki plus a perturbation:

$$g_{\mu\nu} = \eta_{\mu\nu} + \gamma_{\mu\nu} \ , \tag{39}$$

whit $|\gamma_{\mu\nu}| \ll |\eta_{\mu\nu}|$. We will not develop here how the Einstein equations simplify in this scenario (the procedure is analogous to the derivation of the wave equation that we will treat later in this work, essentially one linearizes the Einstein equations to first order in the perturbation), but essentially we can neglect the time derivatives of $\gamma_{\mu\nu}$ since as the lenses are slow-moving, the geometry will change slow as well. For the spatial derivatives we have the following equations:

$$\Delta\bar{\gamma}_{00} = -16\pi\rho \ , \tag{40a}$$
$$\Delta\bar{\gamma}_{ij} = 0 \ , \tag{40b}$$

where $\bar{\gamma}_{\mu\nu}$ is the traceless part of the perturbation, and Δ is the flat Laplacian operator. One can solve these equations to obtain:

$$\gamma_{\mu\nu}(x) = U(x) \ , \tag{41}$$

with $U(x)$ being a function satisfying the Poisson equation:

$$\Delta U = 4\pi\rho \ . \tag{42}$$

This is of course the equation of the Newtonian gravitational potential generated by the lens mass density ρ. Thus, the metric we will use to derive lensing phenomena is the perturbed Minkowski metric:

$$ds^2 = -(1+2U)dt^2 + (1-2U)\delta_{ij}dx^i dx^j \ . \tag{43}$$

The complete procedure to derive this metric can be seen in [Wald, sec. 4.4].

3.2 Deviation angle

Now that we have a spacetime on where fields propagate, we can study the details of the propagation. We will closely follow the explanation given in [Carroll, sec. 7.3]. Let us consider null geodesics $x^\mu(\lambda)$ in this spacetime, which satisfy the geodesic equation in the affine parametrization:

$$\frac{d^2x^\mu}{d\lambda^2} + \Gamma^\mu_{\rho\sigma}\frac{dx^\rho}{d\lambda}\frac{dx^\sigma}{d\lambda} = 0 \ . \tag{44}$$

It is natural to split the geodesics into two pieces: a path that corresponds to the null geodesic in the background (i.e, the actual geodesic when $U = 0$), and a deviation path, that we can regard as a perturbation to the background geodesic:

$$x^\mu(\lambda) = x^\mu(\lambda)^{(0)} + x^\mu(\lambda)^{(1)} \ . \tag{45}$$

In order to treat $x^\mu(\lambda)^{(1)}$ as a perturbation (i.e, evaluate quantities along $x^\mu(\lambda)^{(0)}$ and solve for $x^\mu(\lambda)^{(1)}$) one has to assume that the Newtonian potential U varies negligibly between the background and true geodesics, i.e, that $x^{i(1)}\partial_i U \ll U$. However, as discussed in [Carroll, page 288], one can circumvent this restriction considering short paths and then add them up to assemble a larger path.

We can define the tangent vectors of the splitted paths:

$$k^\mu \equiv \frac{dx^{\mu(0)}}{d\lambda} \ , \tag{46}$$

$$l^\mu \equiv \frac{dx^{\mu(1)}}{d\lambda} \ . \tag{47}$$

Essentially, k^μ is the wave vector of the light ray, and l^μ is a deviation vector. Since $x^\mu(\lambda)$ is a null geodesic, it satisfies:

$$g_{\mu\nu}\frac{dx^\mu}{d\lambda}\frac{dx^\nu}{d\lambda} = 0 \ . \tag{48}$$

Putting (46) and (47) into (48), we see that to zeroth order we have $(k^0)^2 = (\vec{\mathbf{k}})^2 \equiv k^2$, and we will use it as the definition of the quantity k. To first order in U, we have:

$$\begin{aligned} 2\eta_{\mu\nu}k^\mu l^\nu + \gamma_{\mu\nu}k^\mu k^\nu = 0 \ , \\ -kl^0 + \mathbf{l}\cdot\mathbf{k} = 2k^2U \ . \end{aligned} \tag{49}$$

since terms involving $\gamma_{\mu\nu}l^\nu$ or $l^\mu l^\nu$ are second order in U. Shortly, we will use the last relation to prove that $\mathbf{l}$ and $\mathbf{k}$ are orthogonal to first order. But first, let us apply the geodesic equation. From our metric (43), we can compute the Christoffel symbols: $\Gamma^0_{0i} = \Gamma^i_{00} = \partial_i U$ and $\Gamma^i_{jk} = \delta_{jk}\partial^i U - \delta^i_k\partial_j U - \delta^i_j\partial_k U$, and the others are zero. We see that all the Christoffel symbols are of first order, so the zeroth order term of the equation is just the equation of a straight line:

$$\frac{d^2x^{\mu(0)}}{d\lambda^2} = 0 \ , \tag{50}$$

as one should expect since Minkowski geodesics are straight lines (in inertial coordinates, at least). To first order (neglecting terms like Γl since they are second order in U) we see:

$$\frac{dl^\mu}{d\lambda} = -\Gamma^\mu_{\rho\sigma}k^\rho k^\sigma \ . \tag{51}$$

Separating time and spatial components:

$$\frac{dl^0}{d\lambda} = -2k(\mathbf{k}\cdot\vec{\nabla}U) \ , \tag{52}$$

$$\frac{d\mathbf{l}}{d\lambda} = -2k^2\vec{\nabla}U + 2(\mathbf{k}\cdot\vec{\nabla}U)\mathbf{k} \equiv -2k^2\vec{\nabla}_\perp U \ , \tag{53}$$

where $\vec{\nabla}_\perp U = \vec{\nabla} U - \vec{\nabla}_\parallel U = \vec{\nabla} U - k^{-2}(\mathbf{k}\cdot\vec{\nabla}U)\mathbf{k}$ is the transverse gradient to the background path. We can integrate the time part, to obtain:

$$\begin{aligned} l^0 &= \int \frac{dl^0}{d\lambda} d\lambda = -2k \int (\mathbf{k}\cdot\vec{\nabla}U) d\lambda = -2k \int (\frac{d\mathbf{x}}{d\lambda}\cdot\vec{\nabla}U) d\lambda \\ &= -2k \int \vec{\nabla}U \cdot d\mathbf{x} = -2kU \end{aligned} \tag{54}$$

and if we replace this result in equation (49), we see that in effect $\mathbf{l}$ and $\mathbf{k}$ are orthogonal to first order in U:

$$\mathbf{l}\cdot\mathbf{k} = kl^0 + 2k^2U = -2k^2U + 2k^2U = 0 \ . \tag{55}$$

This result allows us to interpret the change of $\vec{\mathbf{l}}$ along the background geodesic as the angle $\hat{\alpha}$ by which $\vec{\mathbf{k}}$ is deviated. This angle is called the deviation angle (sometimes deflection angle), and is the basic quantity in geometrical lensing. From the spatial part of the first order term of the geodesic equation (53), we can compute this angle:

$$\hat{\alpha} \equiv -\frac{\Delta\mathbf{l}}{k} = -\frac{1}{k}\int \frac{d\mathbf{l}}{d\lambda} d\lambda = 2k \int \vec{\nabla}_\perp U d\lambda = 2\int \vec{\nabla}_\perp U ds \ , \tag{56}$$

where $s = k\lambda$ is the physical spatial distance traversed. The minus sign in the definition of $\hat{\alpha}$ comes from the fact that we define the angle as measured by an observer looking backward along the geodesic.

3.3 Thin lens approximation: The lens equation

The next step is to consider another simplification of the problem, in order to get analytic expressions for the deviation angle. We assume the so called thin lens approximation: all the deflection takes place at a single distance, in the lens plane. This assumption is valid if the following conditions are satisfied:

- The intrinsic velocities of the source, the lens and the observer are non-relativistic, i.e, small compared to c.
- The gravitational potential of the lens is non-relativistic, i.e, is small compared to c^2.

As discussed in [Wambsganss], for light these assumptions are justified in all astrophysical situations of interest. For gravitational waves, the assumptions are still fulfilled and we will employ the thin lens approximation too, but in the context of wave optics instead of geometrical optics.

In Figure 1 we display the basic configuration of a lensing situation in the thin lens approximation. We have a lens plane, defined as the plane orthogonal to the line-of-sight of the center-of-mass of the lens (L), and we have a source plane, parallel to the lens plane, containing the source (S). ξ is the position in the lens plane where the deflection takes place. η is the source position in the source plane.

Let us analyze the optical setup of Figure 3.3: $\hat{\alpha}$ (in the figure called $\tilde{\alpha}$) is the deviation angle we computed before, the angle by which the light ray coming from the

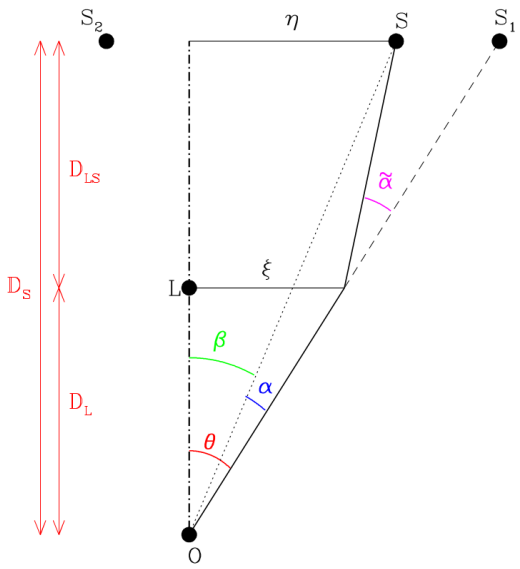

Figure 1: Optical setup of a lensing scenario (Reprinted from [Wambsganss, page 12])

source S deviates when it reaches the lens plane. From the observer's viewpoint, this translates in the observation of an image (S1), which is related to the observed source by an angle α, called reduced deviation angle. We can also define the angle between the source and the lens, β, and between the image and the lens, θ.

Let's derive the relation between the angles and distances involved in Figure 1. As we will see later, lensing effects are more important as η is smaller, so we can consider that ξ and η are much smaller than the distances to the source and the lens, and because of that the angles involved will be tiny ($\ll 1$) so we can apply the small angle approximation. From the figure, we see that:

$$\sin\theta \simeq \sin\beta + \sin\alpha \ , \tag{57}$$

and in the small angle approximation this translates to:

$$\theta = \beta + \alpha \ . \tag{58}$$

Now we realize that $D_S \sin\alpha \simeq D_{LS} \sin\hat{\alpha}$, so in the small angle approximation: $\alpha = \dfrac{D_{LS}}{D_S}\hat{\alpha}$. Now we can write the lens equation:

$$\theta = \beta + \frac{D_{LS}}{D_S}\hat{\alpha} \ . \tag{59}$$

It is the key equation in geometrical lensing, since it relates the angle of the observed images (θ) (we will talk about the images soon) with the position of the source respect to the lens (characterized by the angle β) and the deviation angle $\hat{\alpha}$, that contains the physics of the lensing. The next step is compute this angle for a lens model and analyze the lens equation.

3.4 Cosmological distances and redshift

Concerning the distances reflected in Figure 3.3, we remember that at the beginning of this section we commented the need of a cosmological metric, since in general the

distances involved are cosmological (with non-zero redshift). For simplicity, we omitted the cosmological nature of the spacetime and considered a simpler Minkowskian perturbed one. So now we need to take this into account in order to define the distances. There are various ways of defining meaningful distances in cosmology: the proper motion distance, the luminosity distance, and the angular diameter distance are three of the most common choices (see [Carroll, sec. 8.5] or [Schneider, Ehlers & Falco, sec. 4.5.2] for a more detailed discussion). Here we are going to employ the angular diameter distance, since this is the standard one in lensing.

The angular diameter distance is defined as the ratio between the physical size of the object (R) and the angular size it forms in the sky for an observer (δ):

$$d_A = \frac{R}{\delta} \ . \tag{60}$$

This definition is practical for observational purposes, since the angular size is what we measure with the telescope, and the proper size can be inferred from other observed quantities, like the brightness and so on. However, to see the dependence of the definition on the choice of a cosmological model, let's relate the angular diameter distance with the luminosity distance, which has a more direct cosmological interpretation. The luminosity distance is defined as:

$$d_L^2 = \frac{L}{4\pi F} \ , \tag{61}$$

where L is the absolute luminosity of the source and F is the flux measured by the observer (energy per unit time per unit area). The definition comes from the fact that in flat space the flux at a distance r from the source (assuming spherical wave fronts) is precisely $F = \dfrac{L}{A(r)} = \dfrac{L}{4\pi r^2}$, where $A(r)$ is the area of the wavefront at a distance r.

However, in a cosmological expanding universe, the flux will be diluted due to cosmological redshift. The basic idea is the following. Consider the flat FRW metric (35), we said that the difference between Minkowski metric and this metric is the scale factor $a(t)$, which is a monotonic increasing function of the cosmological time t. Due to this factor, the spatial metric is different at different values of the cosmological time. So if a photon is emitted at some time t_1 with wavelength λ_1, at some posterior time t_2 it will have a different wavelength λ_2, since the spatial metric has changed (and then distances are measured different). One can prove that the quotient between the different wavelengths is equal to the quotient between the scale factors at those times:

$$\frac{a(t_2)}{a(t_1)} = \frac{\lambda_2}{\lambda_1} \equiv (1+z) \ , \tag{62}$$

where z is the redshift.

There are two ways in which the flux is redshifted: first, the wavelength of the photons, and then their energy $\hbar\omega$, will be redshifted: $\lambda_z = (1+z)\lambda$, $E_z = E/(1+z)$, and second, the wave fronts will be time delayed, since two photons emitted with a difference in time of δt will reach the same sphere with a time difference of $(1+z)\delta t$. Thus for the flux we obtain $F = \dfrac{L}{(1+z)^2 A}$, where now A is the area of a comoving

sphere at distance d_L. Using the flat FRW metric as a good approximation to our Universe, one can compute the luminosity distance as a function of the cosmological parameters of the model:

$$d_L = (1+z)\frac{1}{H_0}\int \frac{dz'}{\Omega_m(1+z')^3 + \Omega_k(1+z')^2 + \Omega_\Lambda} \ , \tag{63}$$

where H_0 is the Hubble parameter at the present time and Ω_i are the cosmological densities of matter, spatial curvature, and vacuum energy. The Hubble constant can be measured with observations, but the densities are derived quantities that depend on the cosmological model employed.

Now we can relate the luminosity distance with the angular diameter distance. In 1933, [Etherington] proved the reciprocity theorem, which essentially states that many geometrical properties are invariant when one transposes the roles of source and observer in astronomical observations. With this theorem one can prove that:

$$d_L = (1+z)^2 d_A \ . \tag{64}$$

3.5 Circular-symmetric models: effective potential

A useful assumption in order to model a lens is to consider that the mass density distribution of the lens is, at least, axially symmetric respect to the plane's normal at the origin. Since in the thin lens approximation we assume that all the lensing effect takes place at the lens plane, we can define a 2-dimensional effective potential in the plane, which will be circular-symmetric. First, we derive the deviation angle for the simplest model of a lens, the so-called point mass lens, and then generalize to more general models. Nevertheless, in this work we will employ exclusively the point mass lens model, because despite of its simplicity, is a good approximation when lensing is produced by a compact object, like a star, a black hole, and so on. As we will see later, this kind of lenses are important in the wave optics regime of gravitational waves lensing. However, for considering galactic or halos lensing other models are more accurate.

Let us start with the Newtonian potential generated by a particle of mass M:

$$U = -\frac{GM}{r^2} = -\frac{GM}{\sqrt{\xi^2+n^2}} \ , \tag{65}$$

where $\boldsymbol{\xi}$ is the position in the lens plane where the ray hits it (the mass is at the origin of the lens plane coordinates), and $\mathbf{n}$ is a normal direction to the plane. For computing the deviation angle (56) we need to take the transverse gradient of the potential (in this case a directional derivative in $\boldsymbol{\xi}$) and integrate for all the physical distance traveled by the ray:

$$\vec{\nabla}_\perp U = \hat{\boldsymbol{\xi}}\frac{\partial}{\partial \xi}U = \frac{GM}{(\xi^2+n^2)^{3/2}}\boldsymbol{\xi} \ , \tag{66}$$

$$\hat{\alpha} = 2GM\xi\int_{-\infty}^{+\infty}\frac{dn}{(\xi^2+n^2)^{3/2}} = \frac{4GM}{\xi} \ . \tag{67}$$

Now let us consider a more general model, in which we have a 3-dimensional mass density configuration, but axially symmetric with respect to the normal to the lens

plane at the origin. Since in the thin lens approximation we assume that all the deviation effect takes place at the lens plane, we can define an effective surface mass density projecting the mass density distribution into the plane:

$$\Sigma(\xi) = \int_0^{D_S} \rho(\vec{r})dn = \int_0^{D_S} \rho(\xi, n)dn \ , \tag{68}$$

and we can define an effective 2-D potential, the deflecting potential, projecting the original potential:

$$\psi(\xi) = \int_0^{D_S} U(\vec{r})dn = \int_0^{D_S} U(\xi, n)dn \ . \tag{69}$$

We can express the deviation angle in terms of this potential simply as:

$$\hat{\alpha} = \vec{\nabla}_\perp \psi = \frac{\partial}{\partial \xi}\psi(\xi) \ . \tag{70}$$

Because the axial symmetry of the density distribution $\rho(\vec{r})$, the surface distribution $\Sigma(\xi)$ and the deflecting potential are circular-symmetric in the lens plane. Using the Gauss theorem, is easy to see that for a fixed radial distance in the lens plane ξ, only the (effective) mass inside a circle of this radius can contribute to the potential, and this potential is precisely the same as in the point mass case, but with a mass function of ξ:

$$\hat{\alpha} = \frac{4GM(\xi)}{\xi} = \frac{4G}{\xi}\int_0^{\xi} \Sigma(\xi')d\xi' \ . \tag{71}$$

Of course, for a point mass lens, the surface density is simply $\Sigma(\xi) = M\delta(\xi)$ where $\delta(\xi)$ is the Dirac delta distribution function. The deflecting potential for a point mass lens has a logarithmic behavior.

3.6 Einstein radius, images, magnification and time delay

Now we focus on the point mass lens model and see how the lens equation looks within it:

$$\theta = \beta + \frac{D_{LS}}{D_S}\frac{4GM}{\xi} \ . \tag{72}$$

We can relate ξ with the angle θ: $D_L \sin\theta \simeq \xi$ and with the small angle approximation $\xi = D_L\theta$, so the lens equation becomes an equation relating the angular position of the image θ with the angular position of the source β:

$$\theta = \beta + \frac{D_{LS}}{D_L D_S}\frac{4GM}{\theta} \ . \tag{73}$$

Consider the special case in which source, lens and observer are collinear. In this case, $\beta = 0$, and we have a quadratic equation for θ:

$$\theta^2 = 4GM\frac{D_{LS}}{D_L D_S} \ , \tag{74}$$

and the solution is called the Einstein (angular) radius:

$$\theta_E = \sqrt{\frac{4GMD_{LS}}{D_L D_S}} \ . \tag{75}$$

By the circular symmetry, the images form a ring around the lens, at an angular separation of θ_E. In general, for $\beta \neq 0$, we can express the lens equation in terms of the Einstein radius:

$$\theta^2 - \beta\theta - \theta_E^2 = 0 \ , \tag{76}$$

which has the solutions:

$$\theta_{1,2} = \frac{1}{2}\left(\beta \pm \sqrt{\beta^2 + 4\theta_E^2}\right) \ . \tag{77}$$

For the point mass lens model, there are always two images, which positions are given by $\theta_{1,2}$. The negative solution is always inside the Einstein radius, and the positive is always outside.

We can talk now about the magnification of these images. The magnification is defined as the ratio between the solid angles of the image and the source, and, since surface brightness is conserved by lensing, it is also the ratio between the luminosity of the image and the source:

$$\mu = \frac{\theta d\theta}{\beta d\beta} \ . \tag{78}$$

For the point mass lens model, using the lens equation we can express the magnification as:

$$\mu_{1,2} = \left(1 - \left[\frac{\theta_E}{\theta_{1,2}}\right]^4\right)^{-1} = \frac{y^2+2}{2y\sqrt{y^2+4}} \pm \frac{1}{2} \ , \tag{79}$$

where $y = \beta/\theta_E$ is the normalized impact parameter: the (angular) separation between the source and the lens in terms of the Einstein radius. It's easy to see that since the minus solution to the lens equation is always inside the Einstein ring ($\theta_2 < \theta_E$), its magnification is negative, i.e, the image is mirror inverted. The plus solution has always a positive magnification. An easy calculation shows that the difference between the two magnification is always one (in this model):

$$\mu_1 + \mu_2 = 1 \ . \tag{80}$$

The total magnification, defined as the sum of the absolute value of the two magnifications, is always larger than one, and in fact is infinite for $y = 0$, which is a consequence of the geometrical approximation:

$$\mu_T = |\mu_1| + |\mu_2| = \frac{y^2+2}{2y\sqrt{y^2+4}} \ . \tag{81}$$

Finally, we turn to the time delay of the images, i.e, the time interval for the observer between the arrival of the signal from the source and the arrival of the image signal. There are two delaying factors: the first is a geometrical one, that is, the different path lengths traversed by the image, and the second is a gravitational delay produced by the potential at the lens plane. Here we just put the expression resulting from the calculation. The calculation itself is done in [Schneider, Ehlers & Falco, sec. 5.3]:

$$\tau(\theta,\beta) = (1+z_L)\frac{D_L D_S}{D_{LS}}\left(\frac{1}{2}(\theta-\beta)^2 - \frac{D_{LS}}{D_S}\psi(\theta)\right) \ . \tag{82}$$

The values of θ that extremize the time delay are the positions of the images, i.e, the solutions to the lens equation. To see this, consider the derivative of the time delay with respect to β:

$$\begin{aligned} \frac{\partial \tau(\theta,\beta)}{\partial \theta} &= (1+z_L)\frac{D_L D_S}{D_{LS}}(\theta - \beta - \frac{D_{LS}}{D_S}\frac{\partial \psi(\theta)}{\partial \theta}) \\ &= (1+z_L)\frac{D_L D_S}{D_{LS}}(\theta - \beta - \alpha) \ , \end{aligned} \tag{83}$$

so if we equal this derivative to zero, we recover the lens equation:

$$\theta - \beta - \alpha = 0 \ . \tag{84}$$

This is just the Fermat principle of optics, that states that lensed images always extremize the light travel time.

4 Lensing of gravitational waves: Wave optics

Both light and gravitational waves have wave nature. In both cases, the propagation of the field (the electromagnetic field in the light case, and the dynamical degrees of freedom of the spacetime metric in the second case) obeys a wave equation (we will soon derive the wave equation for gravitational waves), so the field can suffer wave effects such as diffraction and interference. When these effects become relevant, the geometrical picture becomes incomplete. In this section we will introduce the framework of wave optics lensing of gravitational waves. We will also review the basic features of propagation of gravitational waves in a flat background.

4.1 The inaccuracy of geometrical optics: diffraction effect

For giving an order of magnitude estimation on what frequency regime the geometrical optics approximation breaks down, let's consider a circular ring of rays part of the same wave front inciding on a point mass lens, in a circumference of radius ξ with the lens in its center. From the results of the previous sections, the deviation angle is:

$$\hat{\alpha} = \frac{4GM}{\xi} = \frac{2R_S}{\xi} \ , \tag{85}$$

where $R_S = 2GM$ is the Schwarzschild radius of the lens. The rays are focused into a single point, at a focal distance d_F which obeys the optical relation:

$$\frac{\xi}{d_F} = \tan\hat{\alpha} \simeq \hat{\alpha} \ , \tag{86}$$

so

$$d_F \simeq \frac{\xi^2}{2R_S} \ . \tag{87}$$

The focus of all the surface of rays into a single point is the responsible of the infinite magnification result of geometrical optics.

In the geometrical picture, we are implicitly assuming that the photons or the gravitons that form the field, are particles which incide with complete accuracy at a distance ξ from the lens, or at least that the uncertainty in the transverse position, $\Delta\xi$, is much smaller than ξ. But they are quanta of the field, and they have to obey the Heisenberg principle which states that $\Delta k_\perp \Delta\xi \geq \hbar$ where $\Delta k_\perp$ is the uncertainty in the transverse momentum of the particle. So $\Delta k_\perp \geq \dfrac{\hbar}{\Delta\xi} \geq \dfrac{\hbar}{\xi}$. The angular spreading of the particle can be defined as the quotient between the transverse momentum uncertainty and the momentum in the propagation direction:

$$\Delta\hat{\alpha}_s \equiv \frac{\Delta k_\perp}{k_\parallel} \geq \frac{1}{\xi}\frac{\hbar}{k_\parallel} = \frac{\lambda\!\!\!^{-}}{\xi} \ , \tag{88}$$

where $\lambda\!\!\!^{-}$ is the reduced wavelength of the particle. Propagating to a distance d_F, this defines a transverse spread:

$$\Delta y_s = d_F \Delta\hat{\alpha}_s = \frac{\lambda\!\!\!^{-}\xi}{2R_S} \ . \tag{89}$$

In order to obtain a great focusing, the spreading has to be much smaller than the impact parameter, $\Delta y_s \ll \xi$, so $\lambda\!\!\!^{-} \ll 2R_S$. In that regime, the geometrical approximation is valid since very little energy is spread by the lens. However, when $\lambda\!\!\!^{-} \sim R_S$, one cannot achieve big magnifications because the wave is spread out, i.e, is diffracted by the lens. So in this regime the geometrical picture is incomplete and we need to analyze the more general situation of wave optics.

4.2 The wave equation

In order to derive the equation governing the propagation of gravitational waves, we start with the background metric (43):

$$ds^2 = \bar{g}_{\mu\nu}dx^\mu dx^\nu = -(1+2U)dt^2 + (1-2U)\delta_{ij}dx^i dx^j \ . \tag{90}$$

We will denote all the quantities evaluated with this background metric with a bar above them.

Consider now a perturbation of this background, which defines a new metric:

$$g_{\mu\nu} = \bar{g}_{\mu\nu} + h_{\mu\nu} \ , \tag{91}$$

where $h_{\mu\nu}$ is a perturbation in the sense that in our coordinate system, its components are much smaller than the background components:

$$|h_{\mu\nu}| \ll |\bar{g}_{\mu\nu}| \ . \tag{92}$$

This condition is coordinate-dependent, so we require that exists a coordinate system on which this condition holds, valid on a sufficiently large region of spacetime.

Choosing a coordinate system (or more precisely a class of them) breaks the diffeomorphism invariance, but the perturbation still has a residual gauge symmetry. Under a transformation of coordinates of the form:

$$x^\mu \to x'^\mu = x^\mu + \xi^\mu(x) \tag{93}$$

the perturbation transforms as:

$$h_{\mu\nu}(x) \to h'_{\mu\nu}(x') = h_{\mu\nu}(x) - (\bar{\nabla}_\mu \xi_\nu + \bar{\nabla}_\nu \xi_\mu) \ , \tag{94}$$

where $h^{\mu\nu}(x)$ and $h'^{\mu\nu}(x')$ represent the same physical perturbation. Actually, this is only true if the functions ξ^μ contain only high frequency modes (that is, that the scale in which ξ^μ varies is of the same order than the scale on which h varies). We also require that $|\bar{\nabla}_\nu \xi_\mu| \leq |h_{\mu\nu}|$. For a generic function, the transformation may make that the separation between the background and the perturbation disappears [Maggiore, sec. 1.6].

Our goal is to obtain a wave equation governing the evolution of the perturbation, which is what we will call a gravitational wave. The procedure is to linearize the Einstein equations (express them to first order in $h^{\mu\nu}$). So the first step is to compute the linearized Christoffel symbols of this metric. The inverse metric to first order in

h is $g^{\mu\nu} = \bar{g}^{\mu\nu} - h^{\mu\nu}$, so it is straightforward to show that the linearized Christoffel symbols are:

$$\begin{aligned}\Gamma^{\mu}_{\nu\rho} &= \frac{1}{2}g^{\mu\sigma}(\partial_\nu g_{\rho\sigma} + \partial_\rho g_{\nu\sigma} - \partial_\sigma g_{\nu\rho}) \\ &= \bar{\Gamma}^{\mu}_{\nu\rho} + \frac{1}{2}\tilde{g}^{\mu\sigma}(\partial_\nu h_{\rho\sigma} + \partial_\rho h_{\nu\sigma} - \partial_\sigma h_{\nu\rho}) + O(h^2) \ ,\end{aligned} \tag{95}$$

where $\bar{\Gamma}^{\mu}_{\nu\rho}$ are the Christoffel symbols of the background metric, that we have already computed.

In order to linearize the Riemann tensor, we simplify the task choosing a (local) inertial coordinate system in the background in which $\bar{\Gamma}^{\mu}_{\nu\rho} = 0$ (but, of course, not their derivatives). Thus, the complete Christoffel symbols are of order $\Gamma^{\mu}_{\nu\rho} = O(h)$ and the terms $\Gamma\Gamma$ are of order $\sim O(h^2)$. So in this coordinate system, the Riemann tensor (24) reads as:

$$R^{\mu}{}_{\nu\rho\sigma} = \partial_\rho \Gamma^{\mu}_{\nu\sigma} - \partial_\sigma \Gamma^{\mu}_{\nu\rho} + O(h^2) \ . \tag{96}$$

Performing the calculation and then replacing the partial derivatives of $h_{\mu\nu}$ by background covariant derivatives (we can do it since $\partial_\mu = \bar{\nabla}_\mu$ because $\bar{\Gamma}^{\mu}_{\nu\rho} = 0$ in the system where we compute the Riemann tensor) we arrive at:

$$\begin{aligned}R_{\mu\nu\rho\sigma} = \bar{R}_{\mu\nu\rho\sigma} + \frac{1}{2}(&\bar{\nabla}_\rho\bar{\nabla}_\nu h_{\mu\sigma} + \bar{\nabla}_\sigma\bar{\nabla}_\mu h_{\nu\rho} - \bar{\nabla}_\rho\bar{\nabla}_\mu h_{\nu\sigma} - \bar{\nabla}_\sigma\bar{\nabla}_\nu h_{\mu\rho} \\ &+ h_\mu{}^\tau \bar{R}_{\tau\nu\rho\sigma} - h_\nu{}^\tau \bar{R}_{\tau\mu\rho\sigma}) \ .\end{aligned} \tag{97}$$

Since this expression is written in terms of tensorial (i.e, coordinate independent) quantities, the result is valid in all coordinates systems (that preserve the conditions mentioned above).

Thus, we have a background term and a linear one: $R_{\mu\nu\rho\sigma} = \bar{R}_{\mu\nu\rho\sigma} + {}^{(1)}R_{\mu\nu\rho\sigma}$. For getting the Ricci tensor, we have to contract with the full metric: $R_{\mu\nu} = g^{\alpha\beta}R_{\alpha\mu\beta\nu} = (\bar{g}^{\alpha\beta} - h^{\alpha\beta})(\bar{R}_{\alpha\mu\beta\nu} + {}^{(1)}R_{\alpha\mu\beta\nu})$. The linear term in h is therefore: ${}^{(1)}R_{\mu\nu} = \bar{g}^{\alpha\beta}\,{}^{(1)}R_{\alpha\mu\beta\nu} - h^{\alpha\beta}\bar{R}_{\alpha\mu\beta\nu}$ and doing the calculation:

$${}^{(1)}R_{\mu\nu} = \frac{1}{2}(\bar{\nabla}^\alpha\bar{\nabla}_\mu h_{\nu\alpha} + \bar{\nabla}^\alpha\bar{\nabla}_\nu h_{\mu\alpha} - \bar{\nabla}^\alpha\bar{\nabla}_\alpha h_{\mu\nu} - \bar{\nabla}_\mu\bar{\nabla}_\nu h) + h^{\alpha\beta}\bar{R}_{\alpha\mu\beta\nu} \ , \tag{98}$$

where h is the trace of $h_{\mu\nu}$. We can simplify this expression using the residual gauge symmetry (94) to choose a gauge condition, the transverse-traceless Lorentz gauge $\bar{\nabla}^\alpha h_{\mu\alpha} = 0$ and $h = 0$. We will prove in the following section that in a flat background the residual gauge symmetry allows us to choose this gauge condition. The derivation is analogous in curved background, but some subtleties arise by the more restrictive nature of the gauge freedom (94). Nevertheless, it can be proven that for the physical scenarios we are interested in, the extra restrictions do not suppose a problem [Maggiore, sec. 1.6]. In order to apply this gauge to the last expression, we need to permute the order of the covariant derivatives. In flat background it is not a problem since ordinary derivatives commute. However, in our case the commutation produces extra terms, but we can neglect them since all involve the background Christoffel symbols, which are of order $\Gamma \sim \partial_\mu U$ with the perturbation or derivatives of it, so all terms are at least second order.

The resulting expression for the complete Ricci tensor (to first order) is:

$$R_{\mu\nu} = \bar{R}_{\mu\nu} + \frac{1}{2}\bar{\Box}h_{\mu\nu} + h^{\alpha\beta}\bar{R}_{\alpha\mu\beta\nu} \ , \tag{99}$$

where $\bar{\Box} = \bar{\nabla}^{\alpha}\bar{\nabla}_{\alpha}$ is the d'Alembertian operator of the background. Since the background metric is itself a solution of the Einstein vacuum equations, $\bar{R}_{\mu\nu} = 0$, and the linearized Einstein equations are:

$$\bar{\Box}h_{\mu\nu} + 2h^{\alpha\beta}\bar{R}_{\alpha\mu\beta\nu} = 0 \ . \tag{100}$$

The second term can be neglected. To see this, let's look at the orders of magnitude involved. The Riemann tensor of the background contains second order derivatives of the background metric, which varies significantly in a characteristic scale L_B. So the second term is of order $h^{\alpha\beta}\bar{R}_{\alpha\mu\beta\nu} \sim O(h/L_B^2)$. The d'Alembertian term contains second derivatives of the perturbation $h_{\mu\nu}$, which varies in a typical scale $\lambda\!\!\!^{-}$ (the reduced wavelength), so the term is of order $\bar{\Box}h_{\mu\nu} \sim O(h/\lambda\!\!\!^{-2})$. Now, for the class of sources we will consider in this work, the minimum frequency of the detectable GWs is of order 10 Hz, so the largest wavelengths are of order 30 Mm, much shorter than the typical curvature radius of a weakly curved spacetime. So $h/L_B^2 \ll h/\lambda\!\!\!^{-2}$ and we can neglect the background Riemann term:

$$\bar{\Box}h_{\mu\nu} = 0 \ . \tag{101}$$

This is the wave equation of the perturbation, which we can call now a gravitational wave in its own right.

4.3 Gravitational waves propagating in flat spacetime

Before looking for the solutions to the wave equation we have derived above, it is useful to study the solutions in flat spacetime, i.e, when $U = 0$. In this case, the d'Alembertian operator is the flat d'Alembertian:

$$\Box h_{\mu\nu} = (-\partial_t^2 + \Delta)h_{\mu\nu} = 0 \ , \tag{102}$$

where Δ is the flat space Laplace operator:

$$\Delta = \partial_x^2 + \partial_y^2 + \partial_z^2 \ , \tag{103}$$

but it is convenient to clarify some aspects of the gauge conditions used in the derivation of the wave equation before discussing the solutions.

4.3.1 The Lorentz Transverse-Traceless gauge

In order to derive the wave equation in the last section, we mentioned the use of the Lorentz transverse-traceless gauge. In flat spacetime it is more easy to see how apply this gauge condition, and after that we can analyze the properties of the solution in this gauge.

First of all let us mention a notation subtlety. In the wave equation (102) the tensor $h_{\mu\nu}$ is traceless because we applied that condition in the derivation of the equation.

But in general, without the choice of a gauge condition, the perturbation $h_{\mu\nu}$ has non-vanishing trace. Let us denote the traceless part of this tensor as:

$$\bar{h}_{\mu\nu} = h_{\mu\nu} - \frac{1}{2}\eta_{\mu\nu}h \ , \tag{104}$$

where $h = h^{\mu}_{\ \mu}$. We will see that after applying the full gauge condition, $\bar{h}_{\mu\nu} = h_{\mu\nu}$, but for the moment the two tensors are different. The Lorentz gauge condition (often called De Donder gauge condition, or harmonic gauge condition) is applied to the traceless part:

$$\partial^{\nu}\bar{h}_{\mu\nu} = \partial^{\nu}h_{\mu\nu} - \frac{1}{2}\eta_{\mu\nu}\partial^{\nu}h = 0 \ . \tag{105}$$

Is this condition allowed by the residual gauge freedom of the linearized theory? Remember the residual gauge symmetry we have (now in flat spacetime):

$$h'_{\mu\nu}(x') = h_{\mu\nu}(x) - (\partial_{\mu}\xi_{\nu} + \partial_{\nu}\xi_{\mu}) \ . \tag{106}$$

We can see how the trace transforms contracting indices:

$$h'(x') = h(x) - 2\partial^{\mu}\xi_{\mu} \ . \tag{107}$$

So the divergence of $\bar{h}_{\mu\nu}$ will transform as:

$$\begin{aligned}
\partial^{\nu}\bar{h}'_{\mu\nu} &= \partial^{\nu}h'_{\mu\nu} - \frac{1}{2}\eta_{\mu\nu}\partial^{\nu}h' \\
&= \partial^{\nu}h_{\mu\nu} - \frac{1}{2}\eta_{\mu\nu}\partial^{\nu}h - (\partial^{\nu}\partial_{\mu}\xi_{\nu} + \partial^{\nu}\partial_{\nu}\xi_{\mu} - \eta_{\mu\nu}\partial^{\nu}\partial^{\alpha}\xi_{\alpha}) \\
&= \partial^{\nu}\bar{h}_{\mu\nu} - \partial^{\nu}\partial_{\mu}\xi_{\nu} + \partial^{\alpha}\partial_{\mu}\xi_{\alpha} - \Box\xi_{\mu} \\
&= \partial^{\nu}\bar{h}_{\mu\nu} - \Box\xi_{\mu} \ .
\end{aligned} \tag{108}$$

Thus, if initially the divergence is equal to some function $\partial^{\nu}\bar{h}'_{\mu\nu} = f_{\mu}(x)$, then we can make a gauge transformation setting the divergence to zero choosing a coordinate transformation ξ_{μ} satisfying:

$$\Box\xi_{\mu} = f_{\mu}(x) \ . \tag{109}$$

This equation always has solutions in terms of the Green's functions of the d'Alembertian operator:

$$\xi_{\mu}(x) = \int d^4y G(x-y) f_{\mu}(y) \ , \tag{110}$$

so we can always choose the Lorentz gauge condition for the traceless tensor $\bar{h}_{\mu\nu}$. But from the derivation above, one can see that the Lorentz condition does not exhaust the gauge freedom of the linearized theory. Once we have set that condition, we can always apply another coordinate transformation that will leave the condition untouched if it satisfies $\Box\xi_{\mu} = 0$. So we have the freedom for specify four functions ξ_{μ} in order to fix completely the gauge. This is completely equivalent to choose a particular coordinate system. Therefore, we have four extra conditions besides the four conditions imposed by the Lorentz gauge. One particular choose of these conditions that is very appropriate for studying the propagation outside the source is the so-called transverse-traceless (TT) condition, mentioned during the derivation of the wave equation in the previous section.

We choose ξ_0 in order to make the trace of $h_{\mu\nu}$ equal to zero (so as we said before with this condition $\bar{h}_{\mu\nu} = h_{\mu\nu}$), and we choose the three ξ_i in order to make $h_{0i} = 0$. With the last conditions, the Lorentz condition for the time index $\partial^0 h_{00} + \partial^i h_{0i} = 0$ reads as $\partial^0 h_{00} = 0$, so the time-time component of the perturbation metric is constant in time. This correspond to a static perturbation to the static part of the gravitational field, and does not propagate because is static. So for the gravitational wave propagation, this condition is equivalent to $h_{00} = 0$. Summarizing, the TT gauge conditions are:

$$h_{0\mu} = 0 \ , \tag{111a}$$

$$h = 0 \ , \tag{111b}$$

$$\partial^j h_{ij} = 0 \ . \tag{111c}$$

So the gravitational wave (in this gauge) is a pure spatial traceless tensor field. We have reduced the originally ten independent component of $h_{\mu\nu}$ to six with the Lorentz condition, and finally to only two independent components with the transverse-traceless conditions.

Let us emphasize the counting of degrees of freedom. We have arrived to two independent components of $h_{\mu\nu}$, i.e, two degrees of freedom for the gravitational wave. One can think that this only applies to linearized theory but in fact is true for General Relativity and the complete metric tensor $g_{\mu\nu}$. Initially one has 10 independent components of $g_{\mu\nu}$ because is a 2-rank symmetric tensor in a 4-dimensional manifold (so its components form a 4×4 symmetric matrix). But in order to get the Einstein field equations describing the evolution of $g_{\mu\nu}$, we apply the Bianchi identities $\nabla^\nu G_{\mu\nu} = 0$. This imposes four conditions on the Einstein tensor, so we have only six independent components of the Einstein tensor and therefore only six independent evolution field equations. The remaining four equations are constrains, the so-called Hamiltonian and Momentum constraints. These constraints only contain one time derivative of the corresponding metric component, so four of the metric components are just initial conditions that the metric must satisfy. This reduces the degrees of freedom from ten to six. But the Bianchi identities are tensorial, i.e, independent of coordinates, so we have still the diffeomorphism freedom to specify the coordinate system, so four extra conditions can be applied to the metric, giving only two authentic physical degrees of freedom.

Regarding the name of the gauge condition, the traceless part in clear, but analyzing the solutions to the wave equation in the following section will be clear why is called transverse too.

4.3.2 Plane wave solutions to the wave equation in a flat background

The solutions to the flat sourceless wave equation (102) are plane wave solutions:

$$h_{\mu\nu}(x) = A_{\mu\nu} \exp(i k_\alpha x^\alpha) \ , \tag{112}$$

where $A_{\mu\nu}$ is a tensor with constant components and k_μ is a 1-form with constant components too. Applying the d'Alembertian to this solution should give us back the wave equation:

$$\Box h_{\mu\nu} = \eta^{\alpha\beta} \partial_\alpha \partial_\beta h_{\mu\nu} = \eta^{\alpha\beta} k_\alpha k_\beta h_{\mu\nu} = 0 \ . \tag{113}$$

For being generically true, k_μ must be a null covector:

$$\eta^{\mu\nu}k_\mu k_\nu = k_\mu k^\mu = 0 \ . \tag{114}$$

The vector k^μ is called the wave vector, with components $k^\mu = (\omega, \mathbf{k})$, where ω is the frequency of the wave and $\mathbf{k}$ characterizes the direction of propagation of the wave. The null normalization condition gives us the dispersion relation $\omega^2 = |\mathbf{k}|^2$, so the group velocity (and also the phase velocity) of the wave is $v = \partial\omega/\partial|\mathbf{k}| = 1$, the speed of light in our geometrized units. So gravitational waves propagates at the speed of light, on null geodesics, and are therefore a massless tensor field.

As we have seen before, in the TT gauge we only have spatial components of the gravitational wave, so $A_{\mu\nu} = A_{ij}$ is a pure spatial tensor. Applying the Lorentz condition (reduced to a spatial divergence due to the TT conditions) $\partial^i h_{ij} = 0$:

$$k^i A_{ij} = 0 \ , \tag{115}$$

that is, the projection of A_{ij} onto the direction of propagation is zero, i.e, the wave is transverse to the propagation direction, for that the name of the gauge condition. Without lost of generality, consider a Cartesian system $\{x, y, z\}$ with the wave propagating in the direction z. Then, the transverse condition reads as:

$$\hat{\mathbf{z}} \cdot A = (0,0,1) \cdot \begin{pmatrix} A_{xx} & A_{xy} & A_{xz} \\ A_{xy} & A_{yy} & A_{yz} \\ A_{xz} & A_{yz} & A_{zz} \end{pmatrix} = (A_{xz}, A_{yz}, A_{zz}) = \vec{0} \ . \tag{116}$$

We also have the traceless condition:

$$Tr(A) = A_{xx} + A_{yy} = 0 \quad \Rightarrow \quad A_{yy} = -A_{xx} \ . \tag{117}$$

It is common to rename the components A_{xx} and A_{xy} as h_+ and $h_\times$ because of the effect that each polarization has on the proper distances parallel to the wave as the wave passes through space. So finally the wave tensor in this coordinate system reads as:

$$h_{ij}(t,z) = \begin{pmatrix} h_+ & h_\times & 0 \\ h_\times & -h_+ & 0 \\ 0 & 0 & 0 \end{pmatrix} \cos[\omega(t-z)] \ , \tag{118}$$

since we are interested only in the real part, and since $k = \omega$ due to the dispersion relation.

4.4 The Eikonal approximation

Returning to the wave equation in our perturbed Minkowskian background, it no longer admits plane wave solutions since the background d'Alembertian contains extra terms involving the potential U appearing in the Christoffel symbols of the covariant derivatives.

But we can simplify the equation before looking for the solutions, treating only the propagation of a scalar wave, due to the Eikonal approximation, which we are now going to explain (for a more detailed explanation, see for example [Maggiore, sec. 1.5]

or [Baraldo, Hosoya & Nakamura, Appendix A]).

Consider that L_C is the typical scale in which the amplitude or the wavelength or the polarization tensor vary (the smaller of these quantities). We can consider solutions to the wave equation which a part that varies rapidly in a scale λ, i.e, the phase, and an amplitude part which varies slowly in the scale L_C. So an ansatz to the wave equation could be of the form:

$$h_{\mu\nu}(x) = \{A_{\mu\nu}(x) + \epsilon B_{\mu\nu}(x) + \epsilon^2 C_{\mu\nu}(x) + \ldots\} e^{iS(x)/\epsilon} \ , \tag{119}$$

where ϵ is a fictitious parameter (set to one at the end) to take into account the order of the terms in the quantity λ/L_C. Substituting this ansatz into the wave equation, to the leading and next-to-leading order we obtain:

$$0 = -\frac{1}{\epsilon^2} A_{\mu\nu} \bar{\nabla}_\alpha S \bar{\nabla}^\alpha S + \frac{i}{\epsilon} (2\bar{\nabla}_\alpha A_{\mu\nu} \bar{\nabla}^\alpha S + A_{\mu\nu} \bar{\nabla}^\alpha \bar{\nabla}_\alpha S + i B_{\mu\nu} \bar{\nabla}_\alpha S \bar{\nabla}^\alpha S) \ . \tag{120}$$

From the leading order term, and assuming that $A_{\mu\nu}$ is non-vanishing, we see that:

$$\bar{\nabla}_\alpha S \bar{\nabla}^\alpha S = g^{\mu\nu} \partial_\mu S \partial_\nu S = 0 \tag{121}$$

since S is a scalar. This is the (generalization of the) Eikonal equation of classical optics, and it defines the characteristic wave fronts. If we define the wave vector as $k_\mu = \partial_\mu S$, as in the case of plane wave solutions, we see that $k^\mu k_\mu = 0$, so it is a null vector. Furthermore, since k_μ is a gradient, $\bar{\nabla}_\mu k_\nu = \bar{\nabla}_\nu k_\mu$, it is easy to show that:

$$k^\mu \bar{\nabla}_\mu k_\nu = 0, \tag{122}$$

which is the geodesic equation (44). So gravitons propagate along null geodesics of the background metric (43).

The next-to-leading order term reads as:

$$2\bar{\nabla}_\alpha A_{\mu\nu} \bar{\nabla}^\alpha S + A_{\mu\nu} \bar{\nabla}^\alpha \bar{\nabla}_\alpha S = 0 \ , \tag{123}$$

since the third term is vanishing due to the Eikonal equation. Now we can split the amplitude tensor $A_{\mu\nu}$ into a scalar amplitude $A = \sqrt{\frac{1}{2} A^*_{\mu\nu} A^{\mu\nu}}$ and a normalized polarization tensor $e_{\mu\nu} = \dfrac{1}{A} A_{\mu\nu}$, so $A_{\mu\nu} = A e_{\mu\nu}$. Applying the gauge condition $\bar{\nabla}^\alpha h_{\mu\alpha} = 0$, we see that the lowest order yields $e_{\mu\nu} k^\nu = 0$, so the polarization tensor is transverse to the null geodesics (as in the flat case). In terms of the amplitude, we can write eq. (123) as:

$$\bar{\nabla}_\alpha (A^2 k^\alpha) = 0 \ , \tag{124}$$

which give us the conservation law of the number of gravitons, i.e, the amplitude decreases as the rays diverge from each other.

Finally, for the polarization tensor, eq. (123) implies that:

$$k^\alpha \bar{\nabla}_\alpha e_{\mu\nu} = 0 \ , \tag{125}$$

thus the polarization tensor is parallely transported along the geodesics, so its change is low frequency (i.e, is of the order of U) and hence we can treat it as constant in our

observational situation and focus on the propagation of the scalar amplitude (including the phase), which we rename as $\phi(x)$. The scalar wave equation becomes:

$$\bar{\Box}\phi(x) = 0 \ . \tag{126}$$

Finally, we can always express the d'Alembertian of a scalar function as:

$$\partial_\mu(\sqrt{-\det \bar{g}}\bar{g}^{\mu\nu}\partial_\nu\phi) = 0 \ . \tag{127}$$

4.5 The Amplification Factor

Now we are going to derive the most important quantity in wave optical lensing: the amplification factor. Our discussion follows closely that of [Takahashi & Nakamura]. In diffraction theory it is common to express the last equation (127) in the frequency domain, in order to obtain a (inhomogeneous) Helmholtz equation. We can decompose the scalar wave into its Fourier modes:

$$\phi(t, \vec{\mathbf{r}}) = \int_{-\infty}^{\infty} df \tilde{\phi}(\omega, \vec{\mathbf{r}}) e^{-i2\pi ft} \ . \tag{128}$$

From the metric (43), we can compute $\sqrt{-\det \bar{g}} = (1-2U)^2$ and the inverse metric $\bar{g}^{\mu\nu} = diag(\frac{-1}{1-2U}, \frac{1}{1-2U}, \frac{1}{1-2U}, \frac{1}{1-2U})$, and putting the Fourier transform into equation (127), we obtain an equation for each mode with frequency f:

$$(\Delta + \omega^2)\tilde{\phi}(f, \vec{\mathbf{r}}) = 4\omega^2 U \tilde{\phi}(f, \vec{\mathbf{r}}) \ , \tag{129}$$

where Δ is the flat space Laplacian operator and $\omega = 2\pi f$, where f is the frequency of that mode of the gravitational wave.

The last equation is an inhomogeneous Helmholtz equation, and it can be solved using Kirchhoff's integral theorem (see, for example, [Born & Wolf, sec. 8.3.1]). It is useful to introduce the amplification factor, defined as the quotient between the lensed waves (solutions to equation (127)) and the unlensed waves (solutions to the equation with $U = 0$) for a given value of $\vec{\mathbf{r}}$:

$$F(f) \equiv \frac{\tilde{\phi}^L(f)}{\tilde{\phi}(f)} \ . \tag{130}$$

Using the thin lens approximation of section [3.3], and the fact that the frequency is redshifted by a quantity $1 + z_L$, the amplification factor can be computed as:

$$F(f) = \frac{D_S \xi_0^2 (1+z_L)}{D_L D_{LS}} \frac{f}{i} \int d^2\mathbf{x} \ \exp[2\pi i f t_d(\mathbf{x}, \mathbf{y})] \ , \tag{131}$$

[Schneider, Ehlers & Falco, sec. 4.7], where $\mathbf{x} \equiv \boldsymbol{\xi}/\xi_0$ is a normalized position in the lens plane (ξ_0 is the normalization constant of the length, which we will set as the Einstein radius), $\mathbf{y} \equiv \boldsymbol{\eta} D_L/\xi_0 D_S$ is the source position, and $t_d(\mathbf{x}, \mathbf{y})$ is the arrival time of the wave from $\mathbf{y}$ through $\mathbf{x}$ to the observer, and it can be computed as:

$$t_d(\mathbf{x}, \mathbf{y}) = \frac{D_S \xi_0^2 (1+z_L)}{D_L D_{LS}} \left[\frac{1}{2}|\mathbf{x} - \mathbf{y}|^2 - \psi(\mathbf{x}) + \phi_m(\mathbf{y})\right] \ , \tag{132}$$

where $\psi(\mathbf{x})$ is the effective bidimensional deflecting potential defined in (69) but defined dimensionless, so it obeys the 2D Poisson equation:

$$\Delta_x \psi(\mathbf{x}) = 2\frac{\Sigma}{\Sigma_c} \ , \tag{133}$$

(remember that Σ is the surface mass density of the lens, defined in (68), and Σ_c is its critical value) and $\phi_m(\mathbf{y})$ is a function for making the minimum value of the arrival time equal to zero.

4.5.1 Point mass lens model amplification factor

For the point mass lens model, we choose the normalization constant ξ_0 equal to the Einstein radius (75), and the critical density Σ_c as the value of the lens mass M_L spread uniformly over the area of the Einstein ring, so $\Sigma_c = D_S/(4\pi D_L D_{LS})$. The surface density of a point mass lens is simply $\Sigma = M_L \delta^2(\boldsymbol{\xi})$, so we can solve for the deflecting potential obtaining $\psi(\mathbf{x}) = \ln x$. With these results, we can integrate equation (131) to obtain:

$$F(f) = \exp\left[\frac{\pi\omega}{4} + i\frac{\omega}{2}\left(\ln\left(\frac{\omega}{2}\right) - 2\phi_m(y)\right)\right]\Gamma\left(1 - \frac{i}{2}\omega\right)\ {}_1F_1\left(\frac{i}{2}\omega, 1; \frac{i}{2}\omega y^2\right) \ , \tag{134}$$

where $\omega = 8\pi M_{Lz} f$ is a dimensionless frequency, $M_{Lz} = (1 + z_L)M_L$ is the redshifted lens mass, Γ is the Gamma function, ${}_1F_1$ is the confluent hypergeometric function, and the offset of the arrival time is $\phi_m(y) = (x_m - y)^2/2 - \ln x_m$, where $x_m = (y + \sqrt{y^2+4})/2$ are the normalized positions of the images in the lens plane.

The amplification factor depends on the lens mass and the relative position between the source and the lens with respect to the observer by the two following quantities:

- The dimensionless mass-weighted frequency:

$$\omega = 8\pi M_{Lz} f \ . \tag{135}$$

  As we can see, this parameter measures the relation between the wavelength and the Schwarzschild radius of the lens:

$$8\pi M_{Lz} f = 4\pi R_S f = 2\frac{R_S}{\lambda} \ , \tag{136}$$

  so when $\omega \gg 1$, then $\lambda \ll R_S$ and we are in the regime where geometrical optics should be expected to be a good approximation (in the next subsection we will discuss that this is not completely true). When $\omega \lesssim 1$, then we are in the region where diffraction is important and the magnification is small.

- The impact parameter:

$$y = \eta\sqrt{\frac{D_S}{4M_L D_L D_{DL}}} \ . \tag{137}$$

  It depends on the optical setup of distances. For a given value of η (the dimensionful position of the source in the source plane with its origin in the point where the line-of-sight observer-lens crosses it), the impact parameter increases

as the source is further away. It decreases when the lens mass is larger, since a more massive lens produces stronger potentials. It decreases also with the distant from the observer to the lens, and with the distance from the lens to the source. So this mutual relation between the different distances in one single parameter complicates the analysis of the situation, because there is a degeneracy in the distances: different configurations will appear with the same value of y, and y is the quantity that will appear in the measured gravitational wave.

4.5.2 Amplitude and phase modulation

As a complex function, the amplification factor has modulus $|F(f)|$ and argument $\theta_F(f)$. The modulus will affect the amplitude of the scalar gravitational wave, and the argument will affect its phase.

We can treat $F = F(\omega, y)$ as a function of the two explicit parameters that appear in the expression, ω and y. Let us plot the function for a range of ω and different values of the impact parameter y. When we study in section 7 lensing effects over coalescing binary signals, we will have the situation of a varying ω, since the signal varies its frequency with time, but a fixed impact parameter, since the observational time for these signals for ground-based detectors as LIGO is small (seconds as most) compared with the times in which the impact parameter varies due to the relative movement between the lens and the source. However, for the case of continuous signals from isolated neutron stars, we are in a situation where the signal is almost monochromatic, so ω is expected to have an unique value (or a very narrow range of values), but the impact parameter y is expected to change over the whole observational time, which can be months or even years.

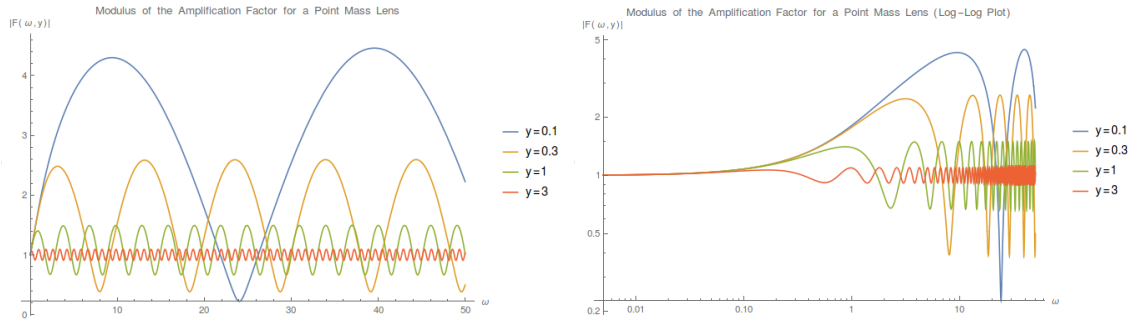

(a) Linear plot

(b) Double logarithmic plot

Figure 2: Modulus of the Amplification factor as a function of ω for different values of y

In Figure 2 we can see the oscillatory behavior of the modulus $|F|$. For small values of the impact parameter y (so small angles between the lens and the source with respect to the observer), one can get considerable amplification of the signals. We can think in the modulus of F as a magnification, defined as in the case of geometrical optics (remember section 3). It seems that the oscillatory behavior depends only on the impact parameter (however the impact parameter depends on the lens mass). For greater values of y, one observes shorter periods of oscillation.

In the logarithmic plot 2(b), wee see that for $\omega \lesssim 1$ the amplification amplitude is of order 1, because in this regime is expected diffraction to be great, so the signal cannot focus, as discussed in section 4.1. However, it is not clear that one reach the geometrical optics limit when ω increases. The magnifications begin to be important as ω increases, but we have the oscillatory behavior so even in regions with a large ω, we can have no magnification or even have the signal weakened! (in some intervals the magnification is less than one, so the lensed signal is weaker than the original signal).

If we plot for even larger ω, we approach the geometrical optics limit. There are some time-cost problems associated with the computation of the amplification factor F at large values of $y^2\omega$, due to the bad behavior of the Confluent Hypergeometric function ${}_1F_1(a, b; z)$ in the region of large imaginary z, so in the next plot we only show F for a tiny value of y, in order to achieve larger values of ω:

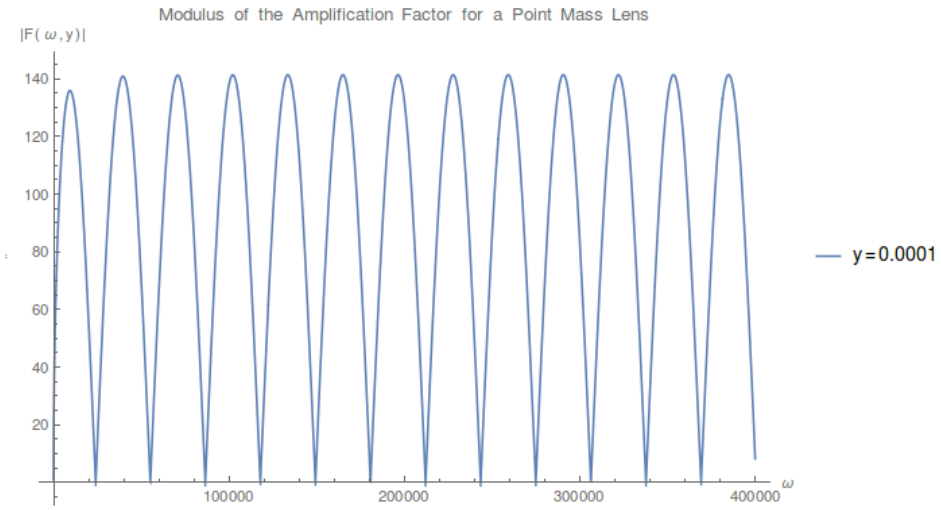

Figure 3: Behavior of —F— for large values of ω

However, as we see in the above plot, there is no suggestion that the oscillations cease to exist at some value of ω. It seems that the oscillations depends completely on the value of y. So a priori it is not true that we recover the geometrical optics limit of section 3 increasing the mass of the lens. It is true that since y depends on $1/\sqrt{M_L}$, a larger mass will imply a smaller y, and then a longer oscillation period, so for some frequency ranges, one can have an approximately geometrical limit behavior (in the sense of section 3), but that would be a coincidence independent of the relation between M_L and λ.

In fact, we will see in the next subsection that taking the limit $\omega \to \infty$, which by the discussion of section 4.1 is taking the geometrical optics limit, returns the expression of magnification of section 3 but with an interference sinusoidal term. But first we are going to see what is the behavior of the argument of F, which will affect the phase of the gravitational wave signal.

In Figure 4, we see a similar behavior as for the modulus. When $\omega \lesssim 1$, the argument is close to zero and the signal will not have a large modulation in its phase. As ω gets larger, we see an oscillatory variation of the argument. For smaller y, the

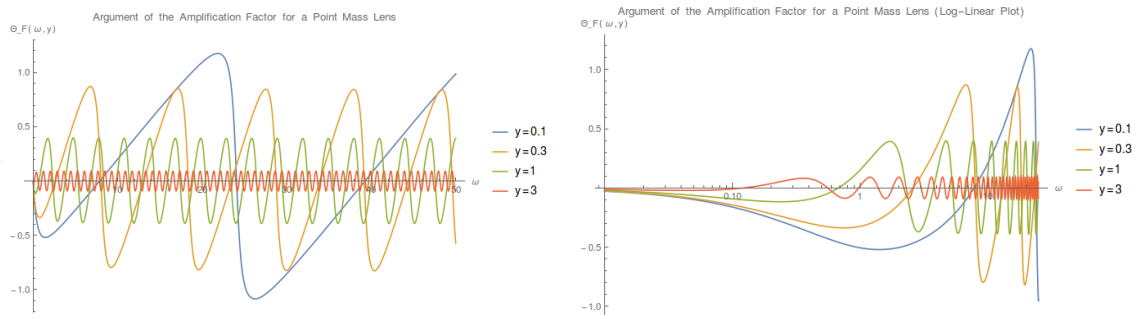

(a) Linear plot

(b) Logarithmic linear plot

Figure 4: Argument of the Amplification factor as a function of ω for different values of y

period of this oscillations is longer and the reached values are larger. As y gets larger, the range of values that take the argument is shorter, so we does not expect a great phase modulation.

4.5.3 Taking the geometrical optics limit on F

For taking the geometrical optics limit of the amplification factor $F(f)$ it is useful to employ the general expression (131), that we remember here:

$$F(f) = \frac{D_S \xi_0^2 (1+z_L)}{D_L D_{LS}} \frac{f}{i} \int d^2\mathbf{x} \ \exp[2\pi i f t_d(\mathbf{x},\mathbf{y})] \ . \tag{138}$$

The limit $\omega \to \infty$ discussed above is equivalent to take the limit $f \gg t_d^{-1}$, where t_d is the time delay between images. This is because in the geometrical limit, one can consider that the two images are resolvable with enough accuracy due to the lack of diffraction, so in order to achieve that it is needed that the time delay between them are great enough. Taking that limit on the general expression of the amplification factor, the imaginary exponential oscillates very quickly, so one can consider that only the stationary points of $t_d(\mathbf{x},\mathbf{y})$ contribute to the integral because the rest of contributions cancel each other. The stationary points $\mathbf{x}_j$ of the time delay are given by:

$$\frac{\partial t_d(\mathbf{x},\mathbf{y})}{\partial \mathbf{x}} = 0 \ , \tag{139}$$

which in fact are the image positions in the lens plane, as we discussed in section 3.6. Then, in the geometrical optics limit the integral over $\mathbf{x}$ reduces to a sum for the image positions $\mathbf{x}_j$:

$$F(f) = \sum_j |\mu_j|^{1/2} \exp[2\pi i f t_{d,j} - i\pi n_j] \ , \tag{140}$$

where μ_j is the magnification of each image as defined in (78), $t_{d,j}$ is the time delay of each image, and $n_j = \{0, 1, 1/2\}$ depending on $\mathbf{x}_j$ being a minimum, maximum or a saddle point of $t_d(\mathbf{x},\mathbf{y})$.

For a point mass lens model, we have always two images, one is a minimum of the arrival time ($n_+ = 0$) and the other is a maximum ($n_- = 1$). Joining the phases for the two time delays into a relative time delay between the two images $\Delta t_d = t_{d,-} - t_{d,+}$,

one obtains the following expression for the geometrical optics limit of the point mass lens amplification factor:

$$F(f) = |\mu_+|^{1/2} - i|\mu_-|^{1/2} e^{2\pi i f \Delta t_d} \ , \tag{141}$$

where each magnification is given by the expression of section 3.6:

$$\mu_\pm = \frac{1}{2} \pm \frac{y^2+2}{2y\sqrt{y^2+4}} \ , \tag{142}$$

and the relative time delay between the double images is:

$$\Delta t_d = 4M_{Lz}\left(\frac{1}{2}y\sqrt{y^2+4} + \ln\left(\frac{\sqrt{y^2+4}+y}{\sqrt{y^2+4}-y}\right)\right) \ . \tag{143}$$

Taking the modulus of the amplification factor $F(f)$ in this limit, we obtain the total magnification of the signal:

$$|F(f)| = |\mu_+| + |\mu_-| + 2|\mu_+\mu_-|^{1/2}\sin(2\pi f \Delta t_d) \ . \tag{144}$$

The first two terms are just the total magnification defined in section 3.6 in the geometrical optics formalism, but we got an extra term that takes into account interference effects. As we can see, if we combine the factor $4M_{Lz}$ with the factor $2\pi f$ of the sinus, we get ω, so the oscillation is given by $\sin(\omega f(y))$ where $f(y)$ is a function of y only. That proves our claim that the period of the oscillations in the plots above seemed to depend only on the value of y (of course, if we vary the amplification factor in the physical frequency range, the period of the oscillation will depend on M_{Lz}).

The argument of the amplification factor $F(f)$ in this limit is:

$$\arctan\left(\frac{-|\mu_-|^{1/2}\cos(2\pi f \Delta t_d)}{|\mu_+|^{1/2} + |\mu_-|^{1/2}\sin(2\pi f \Delta t_d)}\right) \ . \tag{145}$$

The two expressions (144) and (145) reflect well what we observed in the plots of the amplification factor, for $\omega \gg 1$:

- The modulus and the argument of F oscillates with a period dependent of the value of y (again, if we plot versus the physical frequency, the redshifted lens mass M_{Lz} will affect this period too).
- The amplitude of this oscillation (the difference between maximum and minimum values of the modulus and the argument in each case) increases as y decrease, because each magnification decreases (in absolute value) as the impact parameter increases.

We have seen that taking the geometrical optics limit, we recover the expression of the total magnification of section 3.6 with an added interference effect. However, the amplification factor obtained for a point mass lens is independent of the case we are treating: light or gravitational waves, because in the derivation we are using a scalar wave function, which is insensitive to the different tensorial nature of the two fields. One should wonder why this interference nature is not seen in gravitational lensing of

light. The explanation of why this interference is not seen in lensed light waves is done in [Schneider, Ehlers & Falco, page 219]. Basically, the argument of the sinus in the interference term is $\sim f\Delta t_d$, which for the high frequencies of light is a very sensitive frequency-dependent quantity. Light emission by astrophysical sources is usually incoherent, or with a very short coherence time (there are exceptions as some radio sources and line emission spectra provided by atomic decays). One generally needs to average the light reception in a frequency bandwidth inversely proportional to the coherence time. So if the coherence time is much smaller than the time delay Δt_d, the sinus is averaged over a lot of periods and of course the average gives zero, so the interference term disappears.

But the situation with gravitational waves from astrophysical sources as binaries is different. The production of gravitational waves is a coherent process. The frequency may be time dependent but at each moment the source is producing a wave with a specific frequency and a specific phase, as we will see in section 5. In light emission, the incoherence comes from the fact that a lot of atoms and particles are generating photons with different thermal frequencies, so you don not have a wave with a defined phase, but a lot of waves with different frequencies and phases summed up, so you cannot measure the phase when you observe that wave and you average over frequencies. For a stochastic background of gravitational waves, the situation will be similar to light, but we do not consider this kind of detection in this work.

Thus, for astrophysical gravitational wave lensing you cannot ignore the interference term that appears in the geometrical optics limit from wave optics. For large ω you could use the limit expressions (144) and (145) of this section, but you cannot use the expressions of section 3.6.

4.6 Lensing probability

Let us conclude this section by commenting about how to compute the probability of a signal being lensed due to a point mass lens. We will use it later in this work to estimate how the number of detectable events could increase for aLIGO due to lensing.

We will use the formula of [Takahashi & Nakamura], that is borrowed from the formula derived in [Schneider, Ehlers & Falco, sec. 12.2.1] for light (remember that as we are working with a scalar wave function, the results of wave optics are valid for both light and gravitational waves regardless their different tensorial nature, as long as the Eikonal approximation applies):

$$P(z_s) = \frac{3}{2}\Omega_{co} y^2 \int_0^{z_s} dz_L \frac{(1+z_L)^2}{H(z_L)/H_0} \frac{H_0 D_{LS}(z_L, z_s) H_0 D_L(z_L)}{H_0 D_S(z_s)} \ , \tag{146}$$

where z_s is the redshift of the source, z_L is the redshift of the lens, H_0 is the Hubble constant at the present time (zero redshift), $H(z_L)$ is the Hubble constant at the lens redshift, and Ω_{co} is the cosmological density of compact objects.

As we see, the lensing probability depends on y^2, since πy^2 is the (dimensionless) area of the lens for which the impact parameter is between 0 and y. The dependence

on the distances D_L, D_S and D_{LS} takes into account the solid angle in the source plane for which the source is lensed in a solid angle in the lens plane. The cosmological factors appear due to the cosmological nature of the distances, and finally the integral in the lens redshift is for summing all the possible lenses between the source and the observer.

5 Sources of Gravitational Waves and Waveforms

Now that we have developed the basic theory of propagation and lensing of gravitational waves, we need to obtain expressions for astrophysical gravitational wave signals in order to study lensing effects on them. We expect that there are several astrophysical phenomena that create strong enough GW signals to be detected by ground-based gravitational wave detectors. At this time, the LIGO observatories in Hanford and Livingston are the most sensitive gravitational wave detectors we have. In this section, we will present the main astrophysical sources detectable by LIGO and the form of the GW signals they produce. We will focus on two cases: isolated neutron stars, which produce almost monochromatic signals, and the coalescence of compact binaries, which are already observed by aLIGO.

5.1 Mass quadrupole formula

In order to get a feeling about how gravitational waves are produced by typical sources, we first derive the quadrupole formula, which is the lowest order term in a multipole expansion over flat spacetime. This is, we neglect the gravitational effect of the source in the near field regime where gravitational waves are produced (weak field sources), and expand in low velocities. These assumptions break down in the case of compact binaries coalescence, where in the last orbits before the merger the binaries can reach relativistic velocities, and the region of production of GWs is small enough to take into account the curvature produced by the system. Therefore, for getting more accurate analytic expressions it is necessary to use the Post-Newtonian expansion, which we will treat later in this section.

In this section we will follow very closely the explanation given in [Maggiore, sec. 3.1-3.3]. We will explicitly write c and G in order to analyze the several expansions that will appear.

5.1.1 Weak field approximation

If the radius of curvature generated by the source is much greater than the typical size of the region of production of GWs, then we can consider the linearized Einstein equation in a flat background, but this time including the energy-momentum tensor of the source:

$$\Box \bar{h}_{\mu\nu} = -\frac{16\pi G}{c^4} T_{\mu\nu} \ , \tag{147}$$

(the bar appearing over h is because in the presence of matter, the traceless-transverse gauge cannot be employed, so now in general the perturbation h has trace, but the wave equation applies to the traceless part (104)). As a linear differential equation, the solution will involve the Green's functions of the d'Alembertian operator, satisfying:

$$\Box G(x - x') = \delta^4(x - x') \ , \tag{148}$$

so the solutions are:

$$\bar{h}_{\mu\nu}(x) = -\frac{16\pi G}{c^4} \int d^4x' G(x - x') T_{\mu\nu}(x') \ . \tag{149}$$

A specific solution to the Green's function equation will depend on the boundary conditions imposed. As we are dealing with a radiation problem, the appropriate boundary conditions are the Kirchhoff-Sommerfeld "no-incoming radiation" boundary conditions. Basically, we are imposing that at past null infinity there is no incoming radiation. Or in other words, we are only looking for ongoing modes of the wave equation. The correct Green's function in this situation is the retarded Green's function:

$$G(x-x') = -\frac{1}{4\pi|\mathbf{x}-\mathbf{x'}|}\delta(ct_{ret}-ct') \ , \tag{150}$$

where the retarded time is:

$$t_{ret} = t - \frac{|\mathbf{x}-\mathbf{x'}|}{c} \ , \tag{151}$$

that is, if the wave is radiated at a position $\mathbf{x'}$ within the source, and reaches a point $\mathbf{x}$ at a time t, then subtracting the time $|\mathbf{x}-\mathbf{x'}|/c$ the wave spent propagating from $\mathbf{x'}$ to $\mathbf{x}$ (remember it travels at light speed c) we obtain the time at which the wave started to be radiated, t_{ret}. So the solution to the inhomogeneous wave equation (147) is:

$$\bar{h}_{\mu\nu}(x) = \frac{4G}{c^4}\int d^3x' \frac{1}{|\mathbf{x}-\mathbf{x'}|} T_{\mu\nu}\left(t - \frac{|\mathbf{x}-\mathbf{x'}|}{c}, \mathbf{x'}\right) \ . \tag{152}$$

Outside of the source, we can project this solution to the TT-gauge:

$$h^{TT}_{ij}(t,\mathbf{x}) = \frac{4G}{c^4}\Lambda_{ij,kl}(\hat{\mathbf{x}})\int d^3x' \frac{1}{|\mathbf{x}-\mathbf{x'}|} T_{kl}\left(t - \frac{|\mathbf{x}-\mathbf{x'}|}{c}, \mathbf{x'}\right) \ , \tag{153}$$

where $\Lambda_{ij,kl}(\mathbf{n})$ is the projection tensor that depends on the orientation $\mathbf{n} = \mathbf{x}/r$ of the point $\mathbf{x}$ at which we evaluate the wave. The last expression only depends on the integral of the spatial components of the energy momentum tensor. But since we have imposed the Lorentz gauge to the solutions, $\partial^\nu \bar{h}_{\mu\nu}(x) = 0$, it follows from the sourced wave equation (147) that $\partial^\nu T_{\mu\nu}(x) = 0$, i.e, the energy-momentum tensor is a conserved quantity, and we can relate the time and the time-space components to the spatial components.

Since we are interest in the values of the wave at the lens distance or the detector distance from the source, and since these distances $|\mathbf{x}| \equiv r$ are much greater than the typical size d of the source, we can expand:

$$|\mathbf{x}-\mathbf{x'}| = r - \mathbf{x'}\cdot\mathbf{n} + O(d^2/r) \ , \tag{154}$$

(since the integration poins $\mathbf{x'}$ are always inside the source, so $|\mathbf{x'}| \ll |\mathbf{x}| = r$). We retain only to lowest order in the denominator, and to first order in $\mathbf{x'}$ in the energy-momentum tensor, giving:

$$h^{TT}_{ij}(t,\mathbf{x}) = \frac{1}{r}\frac{4G}{c^4}\Lambda_{ij,kl}(\mathbf{n})\int d^3x' \ T_{kl}\left(t - \frac{r}{c} + \frac{\mathbf{x'}\cdot\mathbf{n}}{c}, \mathbf{x'}\right) \ . \tag{155}$$

5.1.2 Slow-moving approximation

Now we are going to apply another approximation, that the sources are slow-moving, i.e, that their characteristic velocities v are much slower than the speed of light c. Let us start noticing that if the source has a characteristic motion frequency ω_s, or a

range of frequencies with maximum frequency ω_s, and a characteristic size d, then the velocities inside the source are of order $v \sim \omega_s d$. Now if we consider that the source is slow-moving, $v \ll c$, then $\omega_s d \ll c$. If we Fourier transform the energy-momentum tensor:

$$T_{kl}\left(t - \frac{r}{c} + \frac{\mathbf{x'}\cdot\mathbf{n}}{c}, \mathbf{x'}\right) = \int \frac{d^4k}{(2\pi)^4}\tilde{T}_{kl}(\omega,\mathbf{k})\exp[-i\omega(t-r/c+\mathbf{x'}\cdot\mathbf{n}/c)+i\mathbf{k}\cdot\mathbf{x'}]\ , \quad (156)$$

then, since the integral is over the source points $\mathbf{x'}$, the term $\omega\mathbf{x'}\cdot\mathbf{n}/c$ is bounded to be less or equal than $\omega_s d/c$, and by the non-relativistic velocities discussed above:

$$\frac{\omega\mathbf{x'}\cdot\mathbf{n}}{c} \lesssim \frac{\omega_s d}{c} \ll 1 \quad (157)$$

so we can expand the exponential:

$$\exp[-i\omega(t-r/c+\mathbf{x'}\cdot\mathbf{n}/c)+i\mathbf{k}\cdot\mathbf{x'}] = e^{-i\omega(t-r/c)}\left(1 - i\frac{\omega}{c}x'^i n^i + \frac{1}{2}\left(-i\frac{\omega}{c}\right)^2 x'^i x'^j n^i n^j + \dots\right)\ , \quad (158)$$

which is equivalent to make a Taylor expansion of T_{kl} in the parameter $\mathbf{x'}\cdot\mathbf{n}/c$:

$$T_{kl}\left(t - \frac{r}{c} + \frac{\mathbf{x'}\cdot\mathbf{n}}{c}, \mathbf{x'}\right) \simeq T_{kl}(t-r/c,\mathbf{x'}) + \frac{x'^i n^i}{c}\partial_0 T_{kl} + \frac{1}{2c^2}x'^i x'^j n^i n^j \partial_0^2 T_{kl} + \dots \quad (159)$$

where the derivatives are computed at the retarded time points $(t - r/c, \mathbf{x'})$.

5.1.3 Momenta of the energy-momentum tensor

If we plug the last expansion of the energy-momentum tensor into the far-from-the-source TT-gauge solution (155), we can identify the integral terms as the (time derivatives of the) momenta of the stress tensor (the spatial part of the energy-momentum tensor), with these momenta defined as:

$$S_{ij}(t) = \int d^3x\ T_{ij}(t,\mathbf{x})\ , \quad (160a)$$

$$S_{ij}{}^k(t) = \int d^3x\ T_{ij}(t,\mathbf{x})x^k\ , \quad (160b)$$

$$S_{ij}{}^{kl}(t) = \int d^3x\ T_{ij}(t,\mathbf{x})x^k x^l\ , \quad (160c)$$

and so on. In terms of these momenta, and knowing that $\partial_0 = c\partial_t$, equation (155) becomes:

$$h_{ij}^{TT}(t,\mathbf{x}) = \frac{1}{r}\frac{4G}{c^4}\Lambda_{ij,kl}(\mathbf{n})\left[S_{kl}(t_{ret}) + \frac{1}{c}\dot{S}_{kl}{}^i(t_{ret})n_i + \frac{1}{2c^2}\ddot{S}_{kl}{}^{ij}(t_{ret})n_i n_j + \dots\right]\ . \quad (161)$$

Physically, it is more useful to express the stress momenta in terms of the energy density (T^{00}/c^2) momenta and linear momentum density (T^{0i}/c) momenta (do not confuse the mathematical term moment of a continuous function with the physical term momentum as in the energy-momentum tensor). This is because the stress tensor momenta depend on the distribution of stresses inside the source, which is difficult to

determine, while the energy density momenta and the linear momentum momenta are easier to obtain. The energy density momenta are:

$$M(t) = \frac{1}{c^2}\int d^3x\ T^{00}(t,\mathbf{x})\ , \tag{162a}$$

$$M^i(t) = \frac{1}{c^2}\int d^3x\ T^{00}(t,\mathbf{x})x^i\ , \tag{162b}$$

$$M^{ij}(t) = \frac{1}{c^2}\int d^3x\ T^{00}(t,\mathbf{x})x^ix^j\ , \tag{162c}$$

and so on. And the momentum density momenta are:

$$P^i(t) = \frac{1}{c}\int d^3x\ T^{0i}(t,\mathbf{x})\ , \tag{163a}$$

$$P^{i,j}(t) = \frac{1}{c}\int d^3x\ T^{0i}(t,\mathbf{x})x^j\ , \tag{163b}$$

$$P^{i,jk}(t) = \frac{1}{c}\int d^3x\ T^{0i}(t,\mathbf{x})x^jx^k\ , \tag{163c}$$

and so on.

As we discussed before, the energy-momentun tensor is conserved, and we can use this to relate the momenta of the stress tensor to the energy density and momentum density momenta. Using that $\partial_0 T^{00} = -\partial_i T^{0i}$, we can identify the energy momenta with the momentum momenta, and we can use $\partial_0 T^{i0} = -\partial_j T^{ij}$ to relate the momentum momenta with the stress momenta, and integrating over a volume V larger than the source volume (the energy-momentum tensor will vanish on the boundary of this volume), one can found the following relations:

$$\dot{M} = 0\ , \tag{164a}$$

$$\dot{M}^i = P^i\ , \tag{164b}$$

$$\dot{M}^{ij} = P^{i,j} + P^{j,i}\ , \tag{164c}$$

and

$$\dot{P}^i = 0\ , \tag{165a}$$

$$\dot{P}^{i,j} = S^{ij}\ , \tag{165b}$$

$$\dot{P}^{i,jk} = S^{ij,k} + S^{ik,j}\ . \tag{165c}$$

Using (164c) with (165b), we can express:

$$\ddot{M}^{ij} = S^{ij}\ . \tag{166}$$

Thus we are relating the zeroth moment of the stress tensor to the second time derivative of the quadrupole moment of the energy density.

5.1.4 Quadrupole radiation

If we stay at the lowest order in the slow-velocity expansion, we arrive at the quadrupole formula:

$$h_{ij}^{TT}(t,\mathbf{x})_{quad} = \frac{1}{r}\frac{2G}{c^4}\Lambda_{ij,kl}(\mathbf{n})\ddot{M}^{kl}(t-r/c)\ . \tag{167}$$

Let us take a look at the physical meaning of the formula:

- The values of the gravitational wave components decrease with $1/r$. Mathematically, this is a consequence of the nature of the d'Alembertian operator, which retarded Green's function introduces this dependence on the distance. This is important for distinguish the dynamical contribution of the quadrupole moment from the static contribution, which falls as $1/r^3$. So far from the source, the dynamical part (the gravitational wave) dominate over the static potential part.

- It depends on the quadrupole moment of the energy density. This is a difference from electromagnetism, where one can get radiation from a dipole moment. In both cases, monopole radiation is forbidden by the charge conservation an mass (energy) conservation. For dipole moment radiation, you need a changing dipole moment, i.e, an oscillating center of charge. In the case of electromagnetism, nothing stops a center of electric charge to be oscillating, but in the case of gravitation a oscillating center of density in an isolated system will violate momentum conservation. In fact, we can see this in our derivation of the quadrupole formula. Equation (165a) is the expression of the momentum conservation, and it is the reason that we cannot have a dipole contribution from (164b).

- The weak coupling of gravitation with matter, incarnated in the factor G/c^4, as well as in general the quadrupole moment, which in some sense measure the shape of the system, is smaller than the dipole moment, make gravitational radiation extremely weaker than electromagnetic radiation. In order to have a signal strong enough to be detected at the Earth, it is needed great massive sources with great accelerations.

Now we can split (167) into its polarizations, plus and cross, and see the dependence of each on the components of the (second time derivative) quadrupole moment. Choosing a Cartesian coordinate $\{x, y, z\}$ system in the source, let's consider the propagation of a gravitational wave in the z direction. Then, the projector into the wave plane is simply $P_{ij} = diag(1, 1, 0)$. In this system the tensor $\ddot{M}_{ij}$ is a 3x3 matrix, and we can project it into the TT frame with the Lambda projector:

$$\begin{aligned}\Lambda_{ij,kl}\ddot{M}_{kl} &= \left(P_{ik}P_{jl} - \frac{1}{2}P_{ij}P_{kl}\right)\ddot{M}_{kl} \\ &= (P\ddot{M}P)_{ij} - \frac{1}{2}P_{ij}Tr(P\ddot{M}) \\ &= \begin{pmatrix} (\ddot{M}_{11} - \ddot{M}_{22})/2 & \ddot{M}_{12} & 0 \\ \ddot{M}_{21} & -(\ddot{M}_{11} - \ddot{M}_{22})/2 & 0 \\ 0 & 0 & 0 \end{pmatrix} .\end{aligned} \tag{168}$$

Recalling that in the TT frame the wave tensor can be written in terms of the two polarizations:

$$h_{ij}^{TT} = \begin{pmatrix} h_+ & h_\times & 0 \\ h_\times & -h_+ & 0 \\ 0 & 0 & 0 \end{pmatrix} , \tag{169}$$

we can obtain the amplitudes for the two polarizations in the quadrupole approximation, for a wave propagating in the z direction of the source frame:

$$h_+ = \frac{1}{r}\frac{G}{c^4}(\ddot{M}_{11} - \ddot{M}_{22}) , \tag{170}$$

$$h_\times = \frac{2}{r}\frac{G}{c^4}\ddot{M}_{12} \ . \tag{171}$$

To obtain the general expressions for a wave propagating in a direction $\mathbf{n}$ in the source frame, we introduce another Cartesian coordinate system $\{x', y', z'\}$ such that the propagation of the wave is in the z' direction. Now the amplitudes will be expressed in terms of $\ddot{M}'_{ij}$, the components of the second derivative of the quadrupole moment in the wave frame. We simply have to express these components in terms of the components in the source frame, $\{x, y, z\}$. The two frames are related by an Euler rotation of two angles:

$$R(\theta,\phi) = \begin{pmatrix} \cos\phi & \sin\phi & 0 \\ -\sin\phi & \cos\phi & 0 \\ 0 & 0 & 1 \end{pmatrix} \begin{pmatrix} 1 & 0 & 0 \\ 0 & \cos\theta & \sin\theta \\ 0 & -\sin\theta & \cos\theta \end{pmatrix} \ . \tag{172}$$

Since $\ddot{M}_{ij}$ is a 2-rank tensor, it transforms under the rotation as:

$$\ddot{M}_{ij} = R_{ik}R_{jl}\ddot{M}'_{kl} = (R\ddot{M}R^T)_{ij} \ , \tag{173}$$

or, inverting the relation:

$$\ddot{M}'_{ij} = (R^T\ddot{M}R)_{ij} \ . \tag{174}$$

Inserting the transformed components in the amplitudes (170) and (171), one finally obtains:

$$\begin{aligned} h_+ = \frac{1}{r}\frac{G}{c^4}[&\ddot{M}_{11}(\cos^2\phi - \sin^2\phi\cos^2\theta) + \ddot{M}_{22}(\sin^2\phi - \cos^2\phi\cos^2\theta) - \ddot{M}_{33}\sin^2\theta \\ &- \ddot{M}_{12}\sin 2\phi(1+\cos^2\theta) + \ddot{M}_{13}\sin\phi\sin 2\theta + \ddot{M}_{23}\cos\phi\sin 2\theta] \ , \end{aligned} \tag{175}$$

$$\begin{aligned} h_\times = \frac{1}{r}\frac{G}{c^4}[&(\ddot{M}_{11} - \ddot{M}_{22})\sin^2\phi\cos\theta + 2\ddot{M}_{12}\cos 2\phi\cos\theta \\ &- 2\ddot{M}_{13}\cos\phi\sin\theta + 2\ddot{M}_{23}\sin\phi\sin\theta] \ . \end{aligned} \tag{176}$$

5.2 Rotating neutron stars

The first astrophysical case of production of gravitational waves we are going to study is an isolated spinning neutron star. This is a potential target for detections in ground-based detectors. One of the principal characteristics of these system is that they produce continuous gravitational waves, so although the signal they produce is very weak, the statistical search of the signal into the noise of the detectors is enhanced by the long observational time they provide.

There are three main emission mechanisms for continuous gravitational waves in spinning neutron stars [Prix]:

- Non-axisymmetric distortions of the neutron star.
- Free precession.
- Unstable oscillation modes in the fluid part of the star (r-modes)

Here we are going to determine the form of a gravitational wave from the first mechanism (in the quadrupole approximation), non-axysimmetric distortions. We will follow the explanation given in [Maggiore, sec. 4.2.1]. Let us consider the star as a rigid body (this avoids the second mechanism commented before) which its rotation axis being one of the principal axes of the body (so no precession occurs).

For a non-relativistic source, the energy density quadrupole moment reduces to its moment of inertia: the second moment of the mass. This is because in the non-relativistic limit, $T^{00}/c \simeq \rho$, where ρ is the mass density. The inertia tensor of a rigid body can be computed as (see, for example, [Goldstein, sec. 5.3]:

$$I^{ij} = \int d^3x \rho(\mathbf{x})(r^2\delta^{ij} - x^i x^j) \ . \tag{177}$$

Because of our definition of the quadrupole moment in equation (162c), there is really an overall minus sign difference with the inertia tensor, $I^{ij} = -M^{ij}$, and when we project in (167) with the Lambda projector into the TT frame, we are losing the trace (it is a traceless gauge), so they differ in the trace of the inertia tensor too:

$$I^{ij} = -M^{TTij} + Tr(I) \ . \tag{178}$$

But the trace is constant, $Tr(I) = I_1 + I_2 + I_3$, where I_i are the eigenvalues of the inertia tensor (it is an hermitian tensor so by performing a rotation it is always possible to find a reference frame where the tensor is diagonal. In this frame, the axis are the principal axis of the body, and its eigenvalues are the principal inertia moments). As we are interested in the second time derivatives of the quadrupole moment, this constant difference is unimportant.

Let us consider we have a frame attached to the body, the body frame $\{x', y', z'\}$ with the axis along the principal axis of the star (so the frame rotates with the star) and the origin at the center of mass. In this frame, the inertia tensor is $I'^{ij} = diag(I_1, I_2, I_3)$ with the principal moments of inertia:

$$I_1 = \int d^3x' \rho(\mathbf{x'})(x_2'^2 + x_3'^2) \ , \tag{179a}$$

$$I_2 = \int d^3x' \rho(\mathbf{x'})(x_1'^2 + x_3'^2) \ , \tag{179b}$$

$$I_3 = \int d^3x' \rho(\mathbf{x'})(x_1'^2 + x_2'^2) \ . \tag{179c}$$

Now consider that the star rotates along its z' axis with angular frequency ω_{rot}. Then the angular momentum is directed in the z' axis too, $J = J_z = I_3\omega_{rot}$. Since this axis will not change in time, the angular momentum direction is constant and the star has no precession.

We define another Cartesian frame, $\{x, y, z\}$, such that its origin is at the center of mass too, and the z-axis coincides with the z'-axis of the star frame, but its orientation is constant in time. If at $t = 0$ the two frames coincide, after a time t the star frame will be rotated an angle $\omega_{rot}t$ respect the fixed frame. So the two frames are related by

a time-dependent rotation $R(t)$:

$$\begin{pmatrix} x_1' \\ x_2' \\ x_3' \end{pmatrix} = \begin{pmatrix} \cos\omega_{rot}t & \sin\omega_{rot}t & 0 \\ -\sin\omega_{rot}t & \cos\omega_{rot}t & 0 \\ 0 & 0 & 1 \end{pmatrix} \begin{pmatrix} x_1 \\ x_2 \\ x_3 \end{pmatrix} \ . \tag{180}$$

So $I' = (RIR^T)I$ and therefore $I = (R^TIR)I'$. After performing the rotation, and using the trigonometric formulas for the double angle, the inertia tensor components in the fixed frame read as:

$$I_{11} = 1 + \frac{I_1 - I_2}{2}\cos 2\omega_{rot}t \ , \tag{181a}$$

$$I_{12} = \frac{I_1 - I_2}{2}\sin 2\omega_{rot}t \ , \tag{181b}$$

$$I_{22} = 1 - \frac{I_1 - I_2}{2}\cos 2\omega_{rot}t \ , \tag{181c}$$

$$I_{33} = I_3 \ , \tag{181d}$$

$$I_{13} = I_{23} = 0 \ . \tag{181e}$$

So the only quadrupole components M_{ij} that are time dependent are:

$$M_{11} = -\frac{I_1 - I_2}{2}\cos 2\omega_{rot}t + constant \ , \tag{182a}$$

$$M_{12} = -\frac{I_1 - I_2}{2}\sin 2\omega_{rot}t + constant \ , \tag{182b}$$

$$M_{22} = +\frac{I_1 - I_2}{2}\cos 2\omega_{rot}t + constant \ . \tag{182c}$$

Now we can derivate twice this results respect to t and put them into the expressions for the amplitudes of the polarizations of the wave (175) and (176), for an observer whose line-of-sight (the direction in which the wave propagates) forms an angle ι with the z-axis of the rest frame (we choose, with no lose of generality, $\phi = 0$), at a distance r from the source:

$$h_+(t) = \frac{1}{r}\frac{4G\omega_{rot}^2}{c^4}(I_1 - I_2)\frac{1 + cos^2\iota}{2}\cos(2\omega_{rot}t) \ , \tag{183}$$

$$h_\times(t) = \frac{1}{r}\frac{4G\omega_{rot}^2}{c^4}(I_1 - I_2)\cos\iota\sin(2\omega_{rot}t) \ . \tag{184}$$

So we see that the spinning neutron star generates a continuous monochromatic gravitational wave with angular frequency $\omega_{gw} = 2\omega_{rot}$, twice the rotation angular frequency. Note that for producing a gravitational wave, I_1 and I_2 must be not equal. This is why this emission mechanism is called non-axisymmetric distortions. If we have an axisymmetric star, then $I_1 = I_2$ and the principal axis in the plane of rotation are degenerated: every pair of perpendicular directions in that plane are principal axes, so the rotation does not change the inertia tensor, and we have no emission. A rotating star is not a sphere, because the rotation form a centrifugal bulge, that is, the radius at the equator (the plane perpendicular to the rotation axis) is larger than the radius at the poles. But this centrifugal bulge is axisymmetric, so it does not produce gravitational waves. In order to have an emission, we need some distortions in the star surface, somehow like "montains".

The departure from the axial symmetry is quantified in the ellipticity, defined as:

$$\epsilon = \frac{I_1 - I_2}{I_3} \ . \tag{185}$$

In a first approximation, neutron stars are usually modeled as perfect fluid stable configurations, and a perfect fluid will not allow the appearance of these distortions needed for getting a non-zero ellipticity. However, in real neutron stars, exists a crust surface, which can have elastic strains allowing this distortions, and also exist strong magnetic fields, that can form these distortions in the surface. For a discussion of different types of ellipticy generations in neutron stars, see [Lasky, sec. 2]. In general, we will assume maximum ellipticities of the order $\epsilon \sim 10^{-6}$.

With this, and in terms of the frequency instead of the angular frequency $f_{gw} = \omega_{gw}/2\pi$, we can write the amplitudes as:

$$h_+(t) = h_0 \frac{1 + cos^2\iota}{2} \cos(2\pi f_{gw} t) \ , \tag{186}$$

$$h_\times(t) = h_0 \cos\iota \sin(2\pi f_{gw} t) \ , \tag{187}$$

with

$$h_0 = \frac{4\pi^2 G}{c^4} \frac{I_3 f_{gw}^2}{r} \epsilon \ . \tag{188}$$

5.3 Black Hole Binary Coalescence

The first detections of gravitational waves, the events GW150914, GW151226 and GW170104 detected by Advanced LIGO, corresponded to coalescence of a black hole binary system: two black holes orbiting around each other and finally coalescing to a final Black Hole. The process emits a great amount of energy in form of gravitational radiation: more than three solar masses emitted in gravitational waves for the first event. This is the main detection target for ground-based detectors due to the high Signal-to-Noise Ratio accumulated in the last orbits, merger and ringdown of the system, and due to extensive template of models available for match the signal.

In this section we will see the basic characteristics of the gravitational wave signal emitted by these systems. Unfortunately, the quadrupole formula is no longer a valid approximation for the emission of these systems, since the quadrupole formula was derived as the lowest order of a flat spacetime expansion, i.e, we were neglecting the self-gravitating nature of the source. It is necessary a most accurate approximation, the Post-Newtonian expansion, which is a non-linear expansion that takes into account the self-gravitation of the source. However, even this approximation finally breaks down in the last orbits of the inspiral stage, where the terms of the expansion diverge, and one needs to use the full set of Einstein equations to compute an accurate waveform. Thus, we will start sketching the basic features of the waveforms computed with the Post-Newtonian expansion, then we will introduce the necessity of the numerical relativity simulations in the final stages of the coalescence, and present one phenomenological model calibrated with these numerical simulations, PhenomD [Khan et al.], the model employed in this work.

The evolution of a coalescing binary system can be divided into three main stages:

- The inspiral: the two black holes orbit around each other losing energy by the emission of gravitational radiation. When the two black holes are far enough, the emitted power is low and the binaries slowly inspiral inwards. As the binaries get closer, the power of emission of gravitational waves increases, and they inspiral faster approaching each other. As long as the binaries do not reach high relativistic velocities, the Post-Newtonian expansion can be employed to obtain an approximate analytical form of the emitted gravitational wave signals. However, for the last orbits the binaries are so close and their velocity is so high that a numerical relativity treatment is needed.

- The merger: At some point, the two black holes get closer enough to collide and form a single black hole. In this process the emission of gravitational waves reach its intensity peak. It is a strong gravitational regime and even the Post-Newtonian expansion is no longer valid. One needs to use the complete highly nonlinear Einstein equations in a numerical simulation in order to get precise results.

- The ringdown: the final black hole is in an excited state, and it decays quickly to a stable configuration. During the decay, gravitational waves are emitted due to the damped oscillations of the event horizon. The frequency of the oscillations correspond to the quasinormal modes of the final black hole, and these depend on the intrinsic physical properties of it.

5.3.1 General aspects of Post-Newtonian expansion.

To a great accuracy, we can compute the inspiral part of the waveform using the Post-Newtonian expansion (PN). Now we are going to present the basic assumptions of this approximation scheme. Essentially, the PN expansion is an effective field theory of General Relativity, valid for self-gravitating systems such that the "gravitational force" between the objects forming the system (the two black holes in our case) is weak, but the objects can have a strong gravitational binding energy. In fact, far from the source, the Post-Newtonian expansion incorporates the multipole expansion treated in section 5.1, but additionally includes an expansion in the source, where the behavior of the source beyond the Newtonian level is taking into account. In the following explanation we are going to follow [Poisson].

Consider how we got the perturbed Minkowski metric in section 3.1: we use the energy-momentum tensor in the Newtonian limit, and compute a correction for the Minkowski metric, and then we analyzed the motion in this corrected metric to first order. The generalization of this beyond the Newtonian order is the basic idea of the Post-Newtonian expansion. Let us first introduce the Einstein equations (34) in the [Landau & Lifshitz] (LL) form:

$$\partial_\mu \partial_\nu H^{\alpha\mu\beta\nu} = -\frac{16\pi G}{c^4}(T^{\alpha\beta} + t^{\alpha\beta}_{LL}) \ , \tag{189}$$

where the tensor $H^{\alpha\mu\beta\nu} \equiv \mathfrak{g}^{\alpha\beta}\mathfrak{g}^{\mu\nu} - \mathfrak{g}^{\alpha\nu}\mathfrak{g}^{\beta\mu}$ is formed from the field variables $\mathfrak{g}^{\mu\nu} = \sqrt{-\det g}\, g^{\mu\nu}$, and $t^{\alpha\beta}_{LL} \sim \partial\mathfrak{g} \cdot \partial\mathfrak{g}$ is a field contribution to the energy-momentum tensor, which depends on derivatives of the field variables. Now we define new variables,

the potentials $h^{\mu\nu}$ (we use the same letter as for the gravitational waves, because gravitational waveforms are obtained from these potentials, as we will see), satisfying:

$$\mathfrak{g}^{\mu\nu} = \eta^{\mu\nu} + h^{\mu\nu} \ , \tag{190}$$

i.e, the potentials are the contributions to flat spacetime in order to obtain the complete field variables describing the physical spacetime. Choosing the harmonic gauge condition $\partial_\nu h^{\mu\nu} = 0$ (remember section 4.3) we can write the LL form of the Einstein field equations as a wave equation:

$$\Box h^{\mu\nu} = -\frac{16\pi G}{c^4}\tau^{\mu\nu} \ , \tag{191}$$

where $\Box$ is the flat d'Alembertian and

$$\tau^{\mu\nu} = -\det(g)(T^{\mu\nu} + t^{\mu\nu}_{LL} + t^{\mu\nu}_{H}) \ , \tag{192}$$

where $t^{\mu\nu}_{H} \sim \partial h \cdot \partial h + h\partial^2 h$ is a gauge contribution (from the harmonic gauge) added to the physical energy-momentum tensor $T^{\mu\nu}$ and the field energy-momentum $t^{\mu\nu}_{LL}$. The harmonic gauge condition imposes a conservation law for $\tau^{\mu\nu}$:

$$\partial_\nu \tau^{\mu\nu} = 0 \ . \tag{193}$$

The wave equation form of the Einstein field equations that we have just found looks similar to the wave equation (147) of the linearized theory, but in this case equation (191) with the above conservation law is an exact reformulation of the Einstein field equations, no information is lost. The conservation equation determines the behavior of the matter variables. Consider that for a particular problem there is a set of matter variables $\mathbf{m}$. Then, the energy-momentum tensor will be a functional of these variables, and then the potential is also a functional of these variables $h^{\mu\nu} = h^{\mu\nu}[\mathbf{m}]$. Then, if you solve the wave equation (191) you obtain the potential as a functional of the matter variables (*matter tells spacetime how to curve*), and then applying the conservation equation you determine how matter behavior in a spacetime constructed from $h^{\mu\nu}[\mathbf{m}]$ (*and spacetime tells matter how to move*), where in the parenthesis we reproduce the famous sentence from John Wheeler. So we need both equations (191) and (193) to obtain the true solutions to the Einstein equations.

Instead of searching for exact solutions, we can compute the potentials to a desired accuracy by an iterative procedure. Consider the formal expansion of the potentials in terms of Newton's constant G, called Post-Minkowskian expansion because we are looking for corrections to flat spacetime:

$$h^{\mu\nu} = k^{\mu\nu}_0 + Gk^{\mu\nu}_1 + G^2 k^{\mu\nu}_2 + \dots \ , \tag{194}$$

(rigorously, the expansion has to be in a dimensionless parameter constructed from G and other characteristic quantities of the specific problem, because G is a dimensionful parameter and then its value depend on the choice of units). Then we can search for approximate solutions truncating the above series at some order, for example the approximate potential to order 2 is $h^{\mu\nu}_2 = k^{\mu\nu}_0 + Gk^{\mu\nu}_1 + G^2 k^{\mu\nu}_2$. To zeroth order, we want the spacetime to be Minkowski, so $h^{\mu\nu}_0 = k^{\mu\nu}_0 = 0$. Then, if we relax the condition (193), we can use the wave equation (191) (called relaxed Einstein equations when they

are employed with that relaxation) to compute the next term in the potential from the zeroth term of $\tau^{\mu\nu}$:

$$\Box h_1^{\mu\nu} = -\frac{16\pi G}{c^4}\tau_0^{\mu\nu} \ . \tag{195}$$

Integrating the above equation we obtain $h_1^{\mu\nu}$ as a functional of the matter variables. From the potential we can construct the LL field to first order $\mathfrak{g}_1^{\mu\nu}$ and with that construct $\tau_1^{\mu\nu}$. Then, we can solved the relaxed Einstein equation for $h_2^{\mu\nu}$, and so on. It is an iterative procedure where one iterates n times to obtain the potentials to order n in G. When the desired order is obtained, one finally employs the conservation equation (193) to obtain the physical solutions.

The n-order potential will depend on the integration of all the $\tau_n^{\mu\nu}$, schematically:

$$h_n^{\mu\nu} \sim \sum_n \int \tau_n^{\mu\nu} \ . \tag{196}$$

In order to simplify the notation, let us forget about the tensorial indices, and rename the potential as ψ and the effective energy-momentum tensor as μ. As discussed in section 5.1, we need the retarded solutions to the wave equation, so formally the solution to the relaxed Einstein equations 191 for ψ is:

$$\psi(t, \mathbf{x}) = \int \frac{\mu(t - |\mathbf{x} - \mathbf{x}'|/c, \mathbf{x}')}{|\mathbf{x} - \mathbf{x}'|} d^3x' \ . \tag{197}$$

The integration domain is the region bounded by the past light cone of the point $\mathbf{x}$ (all the points that can have influenced the present of $\mathbf{x}$), and we can divide it into a near zone $\mathcal{N}$ and a wave zone $\mathcal{W}$ by considering a separation scale $R \sim \lambda$ of order of the wavelength of the emitted gravitational radiation:

$$\psi = \psi_{\mathcal{N}} + \psi_{\mathcal{W}} \ . \tag{198}$$

Since here, we developed a Post-Minkowskian expansion of the Einstein equations, regardless of the intrinsic velocities of the source. But now we apply the slow-motion condition which states as in section 5.1 that the intrinsic velocities are much slower than the speed of light, $v \ll c$. This implies that the source is deep inside the near zone. To see this, consider that we have following scales: r_s is the characteristic length scale of the source and t_s is the characteristic time scale of the source. Then, the characteristic velocity within the source is $v_s = r_s/t_s$, and the characteristic wavelength of the radiation is $\lambda_s = ct_s$. Thus, the slow-moving condition states that:

$$v_s \ll c \quad \Rightarrow \quad (r_s/t_s) \ll c \quad \Rightarrow \quad r_s \ll \lambda_s \ . \tag{199}$$

When $x = (t, \mathbf{x})$ (the point at which we want to know the value of ψ) is inside the near zone, the quantity $|\mathbf{x} - \mathbf{x}'|/c$ is small and we can expand the source term:

$$\mu(t - |\mathbf{x} - \mathbf{x}'|/c, \mathbf{x}') \simeq \mu(t, \mathbf{x}') - \frac{1}{c}\frac{\partial \mu}{\partial t}|\mathbf{x} - \mathbf{x}'| + \dots \ , \tag{200}$$

we have and expansion in terms of $(1/c)$, for instantaneous source potentials, i.e, evaluated at time t, not the retarded time. Thus the general expression of the near zone potential evaluated in points of the near zone (remember that we split the potential

into an integration in the near zone and an integration in the wave zone, but one can evaluate the resulting expression in any point of the total domain) is:

$$\psi_{\mathcal{N}}(x) = \sum_l \frac{(-1)^l}{l!c^l} \left(\frac{\partial}{\partial t}\right)^l \int \mu(t, \mathbf{x}')|\mathbf{x} - \mathbf{x}'|^{l-1} d^3x' \ . \tag{201}$$

For evaluating $\psi_{\mathcal{N}}$ in a point of the wave zone, one can realize that since $\mathbf{x} \gg \mathbf{x}'$ in this case, one can expand the source term μ as:

$$\frac{\mu(t - |\mathbf{x} - \mathbf{x}'|/c, \mathbf{x}')}{|\mathbf{x} - \mathbf{x}'|} \simeq \frac{\mu(t - r/c, \mathbf{x}')}{r} - x'^j \partial_j \frac{\mu(t - r/c, \mathbf{x}')}{r} + \dots \ . \tag{202}$$

When one integrates over $\mathbf{x}$', it is easy to see that the resulting terms are moments of μ, so one gets a multipolar expansion as in section 5.1, which each multipole evaluated at the retarded time $(t - r/c)$. For the integration in the wave zone we are not going to enter into the details, but essentially one integrates μ terms that are themselves solutions to the wave equation, and they generate back-scattering of gravitational waves in the near zone (known as gravitational wave tails) and also contribute to the propagating gravitational waves in the wave zone.

Finally, the idea is to obtain Ψ evaluated at the detector (in the wave zone). In this zone one has the multipole expansion obtained integrating in the near zone and the contribution of the integration in the wave zone. The multipole terms are however undetermined, and for fixing them one has to match with the Post-Newtonian expansion of the source (201) (including the tail effects of the wave zone integration). After that, one applies the TT gauge to ψ to finally obtain the propagated waveform at the detector.

Summarizing, we have an expansion of spacetime in terms of G (remember, rigorously a dimensionless parameter constructed from it and other characteristic quantities of the specific scenario) or equivalently an expansion of the source in terms of v/c. We say that we have a n PN order when we iterate until $(v/c)^{2n}$, or equivalently until $(\sim G)^n$. For example, for inspiralling binaries, the Post-Newtonian parameter that takes into account the order of the terms is $\gamma = GM/Rc^2$, where M is the total mass of the system and R is the separation between the binaries. But $(GM/R) \sim v^2$ (by the Virial theorem), so in terms of γ we see the equivalence of the order of the two expansions. For a system with relativistic intrinsic velocities such as black hole binary systems, one needs to compute to a high order in the Post-Newtonian expansion. The state-of-art of this field are the expressions for the 4PN order (so an expansion until $(v/c)^8$). The calculations involved in obtaining the expression for a gravitational wave produced in the inspiral stage of a binary system are long and difficult, a review of the procedure can be seen in [Blanchet]. Here we are going to show lower order expressions, only to comment on the general behavior of gravitational wave signals.

5.3.2 Inspiral emission according to Post-Newtonian expansion

First of all, note that for computing lensing effects, we need the frequency domain scalar wave description of gravitational waves. We can go to the frequency domain by

performing a Fourier transform of the time domain gravitational wave:

$$\tilde{h}_{\mu\nu}(f) = \int dt\ h_{\mu\nu}(t) e^{-i2\pi ft}\ . \tag{203}$$

We can construct a complex scalar waveform in the frequency domain for binary system sources encoding all the information of the gravitational wave as:

$$\tilde{h}(f) = \tilde{h}_{+}(f) - i\tilde{h}_{\times}(f)\ . \tag{204}$$

Let us comment that since the emission mechanism for gravitational waves is at least quadrupolar radiation, the emission of gravitational waves is direction-dependent. We can parametrize the waveform into a set of intrinsic (and some extrinsic) physical parameters of the source (λ), and into a set of angles defining the direction of emission respect to the source reference system (θ, ϕ):

$$\tilde{h}(f) = \tilde{h}(f; \lambda; \theta, \phi)\ . \tag{205}$$

As any function with angular dependence, we can decompose it into a basis of spherical harmonics (actually in the case of gravitational waves is a spin-weighted spherical harmonics basis, since gravitational waves are a spin-2 field) which carry the angular information:

$$\tilde{h}(f; \lambda; \theta, \phi) = \sum_{l=0}^{\infty} \sum_{m=-l}^{l} \tilde{h}_{lm}(f; \lambda)\ {}^{2}Y_{lm}(\theta, \phi)\ , \tag{206}$$

where $\tilde{h}_{lm}(f; \lambda)$ are the coefficients or modes of the waveform. For coalescing black hole binary systems, the dominant modes of emission are $l = 2$, $|m| = 2$, and they are related by $\tilde{h}_{2,-2}(f) = \tilde{h}^{*}_{2,2}(-f)$ (in the absence of precession, but in this work we do not consider precession).

Now we are going to follow the expressions of [Sintes & Luna], but the results are known since [Blanchet et al.]. Up to 2 PN order, the dominant (2,2) mode of the inspiral waveform for a non-precessing non-spinning binary system in the frequency domain can be written as :

$$\tilde{h}(f) = \mathcal{A}_{INS} f^{-7/6} e^{i\Psi(f)} \tag{207}$$

As a common guide, one can consider that this expression is valid until the innermost stable circular orbit frecuency, $f_{ISCO} = 1/(6^{3/2}\pi M)$, is reached, which corresponds to a separation of $6M$ between the binaries, where $M = m_1 + m_2$ is the total mass of the binary system. However, this result from Schwarzschild geometry does not make sense when the binary masses are comparable. In general one cannot predict at which concrete frequency the Post-Newtonian expansion will fail, because there is a gradual transition between inspiral and merger. The inspiral amplitude $\mathcal{A}_{INS}$ is given by:

$$\mathcal{A}_{INS} = -\frac{\mathcal{M}^{5/6}}{r}\sqrt{\frac{5\pi}{96}}\pi^{-7/6}\sqrt{F_{+}^{2}(1+\cos^{2}\iota)^{2} + F_{\times}^{2} 4\cos^{2}\iota}\ , \tag{208}$$

where $\mathcal{M} = (m_1 m_2)^{3/5}/(m_1 + m_2)^{1/5}$ is the chirp mass of the binary system, ι is the angle between the direction of the total angular momentum of the binary system and

the line-of-sight from the source to us, and F_+ and $F_\times$ are the antenna patterns of the detector (we will comment about them in section 6). The phase is given by:

$$\Psi(f) = 2\pi f t_c - \phi_c - \frac{\pi}{4} + \frac{3}{128}\sum_{k=0}^{4} A_k u^{k-5} \ , \tag{209}$$

where t_c is the coalescence time, ϕ_c is the phase at the coalescence instant, $u = (\pi \mathcal{M} f)^{1/3}$ and the coefficients A_k are:

$$A_0 = 1 \ , \tag{210a}$$
$$A_1 = 0 \ , \tag{210b}$$
$$A_2 = \frac{20}{9}\left(\frac{743}{336} + \frac{11}{4}\eta\right)\eta^{-2/5} \ , \tag{210c}$$
$$A_3 = -16\pi\eta^{-3/5} \ , \tag{210d}$$
$$A_4 = 10\left(\frac{3058673}{1016064} + \frac{5429}{1008}\eta + \frac{617}{144}\eta^2\right)\eta^{-4/5} \ , \tag{210e}$$

where $\eta = q/(1+q)^2$ is the symmetric mass ratio ($q = m_1/m_2$ with $m_1 \geq m_2$ is the mass ratio of the system), which maximum value is $1/4$ when $q = 1$. The corresponding time domain waveform is:

$$h_{+,\times}(t) = \frac{2M\eta}{r}(M\omega)^{2/3}\sum_{i=0,1/2,1,\ldots} v^i H^i_{+,\times}(t) \ , \tag{211}$$

where $v \equiv (M\omega)^{2/3}$, ω is the orbital frequency that increases with $1/R$ where R is the separation between the binaries, and the functions $H^i_{+,\times}(t)$ carry the time and angular dependence. For example, to lowest order $H^0_+(t) = -(1+\cos\iota)\cos\Phi(t)$ and $H^0_\times(t) = -2\cos\iota\sin\Phi(t)$.

As we see, in time domain the amplitude increases as the frequency increases in time, due to the binaries getting close towards the merger. However the amplitude in the frequency domain decreases with the frequency. This is due to the fact that at lower frequencies the binaries orbit more cycles, so the corresponding amplitudes of the Fourier modes are higher, but as they get close the frequency increases more quickly, so in each frequency they spent less cycles, corresponding to smaller amplitudes in the frequency domain at higher frequencies.

The amplitude decreases with the inverse law $1/r$, where r is the distance traveled to the observer, as in the neutron star case. This is a common feature for all gravitational waves. We see that the phase of the wave (which determines its shape in the time domain) depends besides of the frequency in the symmetric mass ratio and in the chirp mass (depends also on the time and phase of coalescence, but these are extrinsic parameters that depends on the conventions of the observer, not in intrinsic characteristics of the system). Furthermore, using the definition of symmetric mass ratio, we can write the chirp mass as $\mathcal{M} = M\eta^{3/5}$. If we define a dimensionless "mass frequency" as $Mf = f$ (in Hertz)$\times M$ (in seconds), then the shape of $\tilde{h}(Mf)$ only depends on the symmetric mass ratio. The total mass M, and the distance to the source r, only scale the amplitude of the waveform. If we have considered spins, then the waveform would also depend on the spin values of each binary.

5.3.3 Merger: necessity of numerical relativity simulations

The Post-Newtonian expansion is an accurate approximation to obtain the waveform in the inspiral stage, where the binaries are still far enough and spacetime between them is not so much curved, and their linear velocities are still not so much relativistic. However, when the separation between the binaries is small enough, the Post-Newtonian expansion does not converge. We can see this in terms of the factor in which we expand. As we said before, the expansion in powers of G is really an expansion in a dimensionless parameter constructed with G and specific quantities of the problem. For the case of a binary system, at nPN order we have the factor:

$$\left(\frac{Gm}{rc^2}\right)^n \sim \left(\frac{R_S}{r}\right)^n \ , \tag{212}$$

so when the separation is similar to the Schwarzschild radius of the system, then the expansion parameter is of order 1 and the series do not converge. If we regard the expansion parameter in the source, for nPN order we have:

$$\left(\frac{v}{c}\right)^{2n} \ , \tag{213}$$

so when the binaries reach relativistic velocities, again the expansion factor is of order 1 and the expansion does not converge. Besides, the Post-Newtonian method remains in the point particle approximation to the binaries, and despite one can add corrections to take into account the internal structure of the binaries, for BH binaries in the merger one needs to deal with apparent horizons and it is needed a full general relativity approach.

Thus, it is necessary to compute numerically the Einstein equations at this stage. The basic idea is to treat General Relativity as an initial value problem, an evolution problem. For this, one needs to slice spacetime in a family of spacelike 3-dimensional slices, and to evolve the initial data specified in some $t = 0$ slice through the slices. This decomposition of General Relavity relies on the work of [Arnowitt, Deser & Misner] in the 60s. Of course, despite the reformulation, the theory still has the "gauge" transformation group of all coordinate transformations, so the time evolution is not unique. But after fixing the gauge (choosing some coordinate system and some gauge conditions) one can evolve the metric components in a similar fashion as any other evolution problem in Physics.

Explaining even the basic ideas behind numerical relativity schemes is beyond the scope of this work, so here we will only comment that until the seminal work of [Pretorius] in 2005, the field was not developed enough to carry satisfactory binary systems simulations (the framework for dealing with numerical simulations of binary black holes was pioneered by [Smarr et al.] in 1976, almost thirty years before the work of Pretorius), but since then, the field has growth considerably in the last decade, due to the entering in the gravitational detectors era, for which numerical relativity improvements have been crucial. For a recent review of the procedures to extract gravitational wave information from numerical relativity simulations, one can read [Bishop & Rezzolla].

5.3.4 Ringdown emission: damped resonance

Although the ringdown emission is nowadays computed with numerical simulations for both merger-ringdown stages (we are going to talk soon about the phenomenological model employed in this work, PhenomD, which for the merger-ringdown has a phenomenological ansatz calibrated with numerical relativity simulations), it is instructive to mention the approximate analytic approximation for computing the waveform in this stage. Essentially is based on perturbations of the Kerr spacetime (the solution to Einstein equations that describe spinning black holes).

Following again [Sintes & Luna], we can write the dominant (2,2) mode ringdown frequency domain waveform approximately as:

$$\tilde{h}_{RD}(f) = \frac{\mathcal{A}_{RD}}{2\pi} e^{i2\pi f t_0} \left(\frac{e^{i\varphi_0}}{\frac{f_{QNR}}{Q} - 2i(f - f_{QNR})} + \frac{e^{-i\varphi_0}}{\frac{f_{QNR}}{Q} - 2i(f + f_{QNR})} \right) , \quad (214)$$

where t_0 is the start time of the ringdown (once the two black holes have merged into a final black hole), ϕ_0 is the phase at that time, f_{QNR} is the quasinormal mode frequency, i.e, the central frequency of the *ringing* of the final black hole's horizon, and Q is the quality factor. The amplitude is given by:

$$\mathcal{A}_{RD} = \frac{1}{r} \sqrt{\frac{128\eta^2 \epsilon M}{f_{QNR} Q}} . \quad (215)$$

We see that the waveform has the form of a Lorentzian distribution, which is the typical solution for resonance phenomena. The horizon of the final black hole resonates at $f = f_{QNR}$, the quasinormal ringdown frequency, which by the no-hair theorem only depends on the mass and the spin of the final black hole (if the black hole is charged then it will depend also on its total charge). A good fit for the quasinormal frequency and the quality factor of the (2,2) mode is:

$$f_{QNR} \approx [1 - 0.63(1 - a)^{3/10}] \frac{1}{2\pi M} , \quad (216)$$

$$Q \approx 2(1 - a)^{-9/10} , \quad (217)$$

where a is the Kerr parameter, essentially the dimensionless final spin of the black hole, $s_f = aM^2$, which varies between 0 (if the final black hole is a Schwarzschild, i.e, static non-spinning black hole) and ~ 0.98.

If we transform to the time domain, we can see that the waveform is in fact damped in time:

$$h_{RD}(t) = \mathcal{A}_{RD} \exp\left[-\frac{(t - t_0)\pi f_{QNR}}{Q} \right] \cos(-2\pi f_{QNR}(t - t_0) + \varphi_0) . \quad (218)$$

We have a sinusoidal wave damped by a negative exponential, which exponent increases (in absolute value) as time pass away from t_0. Physically, one can understand this as the final black hole produced in an excited state and radiating away gravitational waves (energy) until it reaches the equilibrium state, in which there are no more emission of waves.

5.3.5 PhenomD: a phenomenological model for spinning black hole binaries

One can observe that with numerical relativity simulations we could obtain the complete waveform without approximation schemes, losing accuracy only because using a discrete grid and the precision lost due to the numerical methods for solving the equations. However, a full numerical relativity simulation needs a lot of computational resources, and having analytic (despite approximate) expressions is always useful for qualitative analysis. So one intelligent way of generating a template bank of waveforms is to have a model based on the Post-Newtonian method adding higher order terms for the inspiral stage, and a phenomenological ansatz for the merger and ringdown stages , and calibrate this model with an ensemble of numerical relativity simulations. This is the idea behind the PhenomD model [Khan et al.], the model employed in this work to simulate gravitational waves.

The model deals with spin-aligned (and anti-aligned) binaries, so there is no precession motion of the orbital plane. As we said before, the waveform can be described in a basis of spherical harmonics (to be precise, spin-weighted spherical harmonics), and for aligned spins the dominant modes are still the $l = 2$, $|m| = 2$. Initially the model was designed to model only these modes (and in this work we will only use the dominant modes), but recently the model is being updated to consider higher modes [García et al.].

In terms of the dominant modes, we can write the frequency domain waveform as:

$$\begin{aligned}\tilde{h}(f;\lambda,\theta,\phi) &= \tilde{h}_+(f;\lambda,\theta,\phi) - i\tilde{h}_\times(f;\lambda,\theta,\phi) \\ &= \sum_{m=-2,2} \tilde{h}_{2m}(f;\lambda)\ {}^2Y_{2m}(\theta,\phi)\ ,\end{aligned} \tag{219}$$

where λ is the set of intrinsic parameters on which depends the waveform, and the angular dependence is encoded in the spin-weighted spherical harmonics ${}^2Y_{2m}(\theta,\phi)$. The components of the waveform in this basis satisfy $\tilde{h}_{2,-2}(f) = \tilde{h}^*_{2,2}(-f)$ (in no-precessing systems), so we only need to know the (2,2) component, that can be expressed in terms of amplitude and phase:

$$\tilde{h}_{2,2}(f;\lambda) = A(f;\lambda)e^{-i\Psi(f;\lambda)}\ . \tag{220}$$

The intrinsic parameters needed to describe the waveform are $\lambda = \{\eta, \chi_1, \chi_2\}$, where η is the symmetric mass ratio defined before (remember, $\eta = q/(1+q)^2$ where $q = m_1/m_2$ is the mass ratio, for $m_1 \geq m_2$) and χ_i are the individual dimensionless spin parameters of each BH, defined as:

$$\chi_i = \frac{\mathbf{s}_i \cdot \hat{\mathbf{L}}}{m_i^2}\ , \tag{221}$$

where $\mathbf{s}_i$ are the individual spin angular momenta of each BH and $\hat{\mathbf{L}}$ the direction of the total angular momenta of the system. The total mass of the system $M = m_1 + m_2$ and the distance to the source r only provide an overall scale for the waveforms, so we can use the dimensionless frequency Mf to evaluate the waveforms.

PhenomD provides the (2,2) mode (220) in the parameter space $\{\eta, \chi_1, \chi_2\}$ evaluated in the dimensionless frequency Mf. As showed in [Khan et al.], the waveforms

are very accurate in the calibration region, i.e, the parameter space covered by the numerical relativity simulations (really, hybrid simulations, since the early inspiral stage is calculated with Post-Newtonian method and the last inspiral, merger and ringdown with numerical relativity) employed in the calibration. In Figure 5 is showed the calibration points of PhenomD. As we can see the model is calibrated with a spin parameter

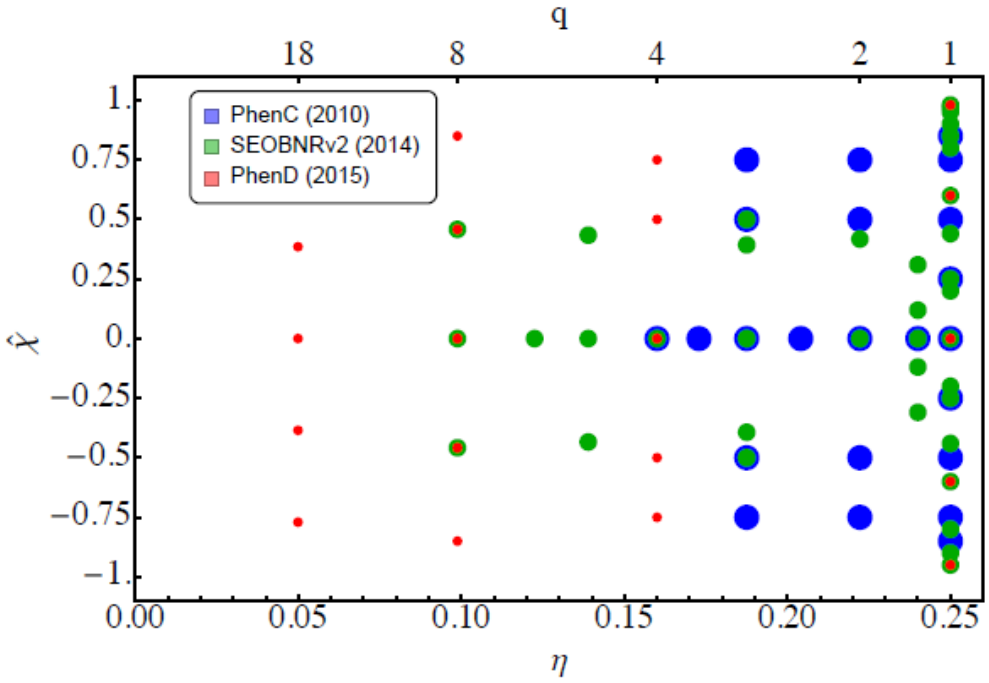

Figure 5: Calibration points for the PhenomD model. Reprinted from [Khan et al.]

$\hat{\chi}$ which is a combination of χ_1 and χ_2. Most of the hybrid waveforms used in the calibration have $\hat{\chi} = \chi_1 = \chi_2$, however in the paper is discussed that the calibration is accurate enough over a great region of the spins parameter space. Anyway, it turns out that the waveforms do not depend so much on the individual spin values, but on the combination $\hat{\chi}$, so in section 7 where we will use waveforms with spin we will only use equal values for both spins, reducing the dimension of the parameter space and saving computational time.

For obtaining the physical waveform (in the frequency domain), one has to multiply the dominant mode obtained with PhenomD with a factor M/r (in the same units) to physically scale the waveform, transform from the dimensionless frequency to the frequency in Hertz (dividing Mf by M in seconds), multiply by a factor M in seconds (since the time domain strain is a dimensionless quantity, its Fourier domain transform has to have dimensions of time due to the measure dt in the integral), and finally multiply the value of the spin-weighted spherical harmonics for some given angles. In this work we will use the average values of the spin-weighted spherical harmonics, since the angular dependence will be not much relevant for us. For obtaining the time domain waveform, one simply does the inverse Fourier transform. And, as we will comment in the next section, for getting the strain at the detector, one also needs to multiply by the antenna functions of the detector, which are functions of the relative angles between the detector and the source.

For getting an idea of the behavior of the PhenomD waveforms, we plot in Figure 6 three PhenomD waveforms for spin values $\chi_1 = \chi_2 = 0$ and three different values of the symmetric mass ratio $\eta = \{0.25, 0.15, 0.05\}$. As one can see, the amplitude decreases as the symmetric mass ratio decreases, which correspond to an increasing mass ratio q (remember that the maximum value of η is 0.25 and it corresponds to the minimum value of the mass ratio $q = 1$). In Figure 7, we plot the amplitude corresponding to $\eta = 0.25$ for three different spin values $\chi = \{0, 0.3, 0.7\}$ (we choose the same value for the two components χ_1 and χ_2). The amplitude is not modified so much for different spin values. The main difference is that for larger spins, the ringdown frequency is bigger (the frequency for which the amplitude curve begins to decrease more quickly). In Figure 8, we plot the phase of the three waveforms of Figure 7. In this case we see that the phase is much more dependent on the spin values than the amplitude. Finally, in Figure 9, we plot a time domain PhenomD waveform, corresponding to $\eta = 0.25$ and $\chi = 0$. The frequency and the amplitude are increasing with time until the merger. During the ringdown, the amplitude decreases exponentially.

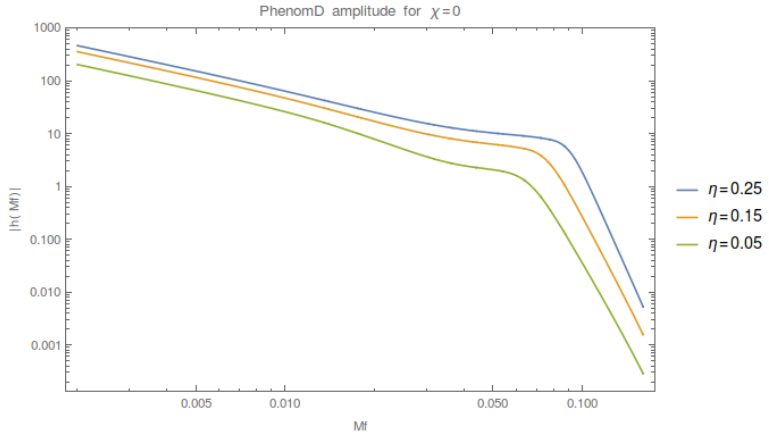

Figure 6: Double-logarithmic plot of the amplitude of PhenomD waveforms as a function of the symmetric mass ratio η.

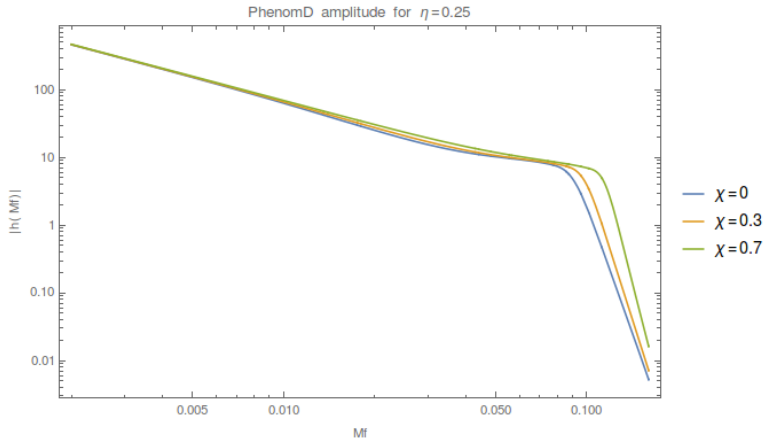

Figure 7: Double-logarithmic plot of the amplitude of PhenomD waveforms as a function of the dimensionless spins (with equal value).

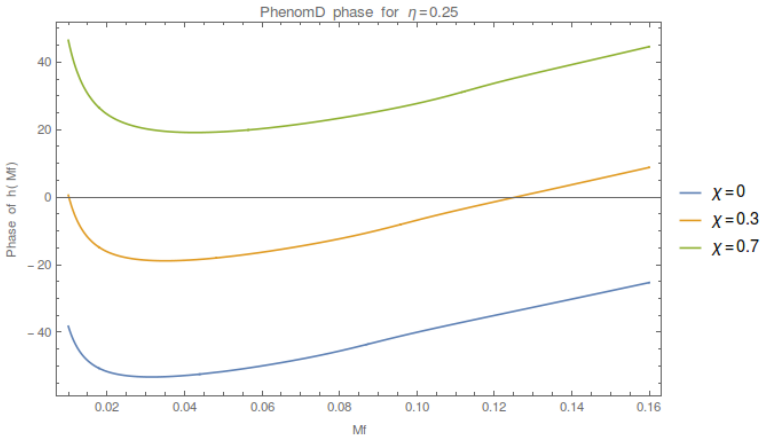

Figure 8: Phase of PhenomD waveforms as a function of the dimensionless spins (with equal value). Linear plot.

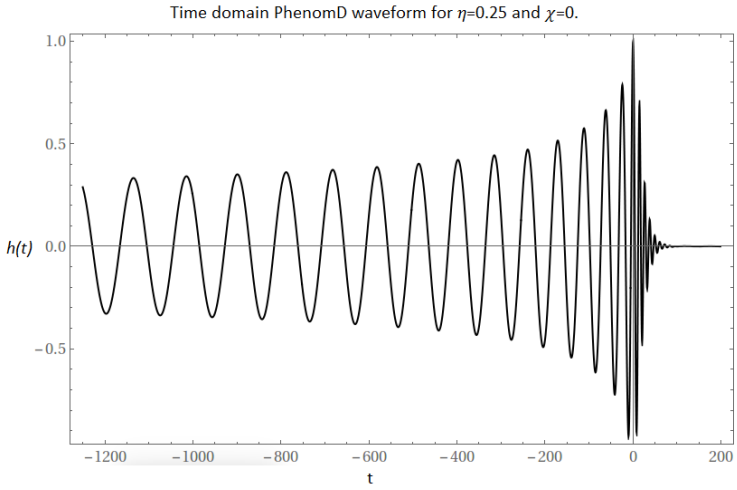

Figure 9: Phase of PhenomD waveforms as a function of the dimensionless spins (with equal value). Linear plot.

6 Detection and data analysis of gravitational waves

In this section we will treat briefly some of the statistical tools for the detection of gravitational waves, in particular the concept of Signal-to-Noise Ratio (SNR) and fitting factor (FF), which will be employed in the results of this work.

6.1 Strain at the detector: Antenna functions

The current most sensitive ground-based detectors, both detectors of advanced LIGO and the advanced VIRGO detector, are interferometric detectors. They detect the relative difference in the optical path length of a laser beam in a Michelson-like interferometer produced by the pass of a gravitational wave. This relative difference is the strain $h(t) = \Delta L/L$.

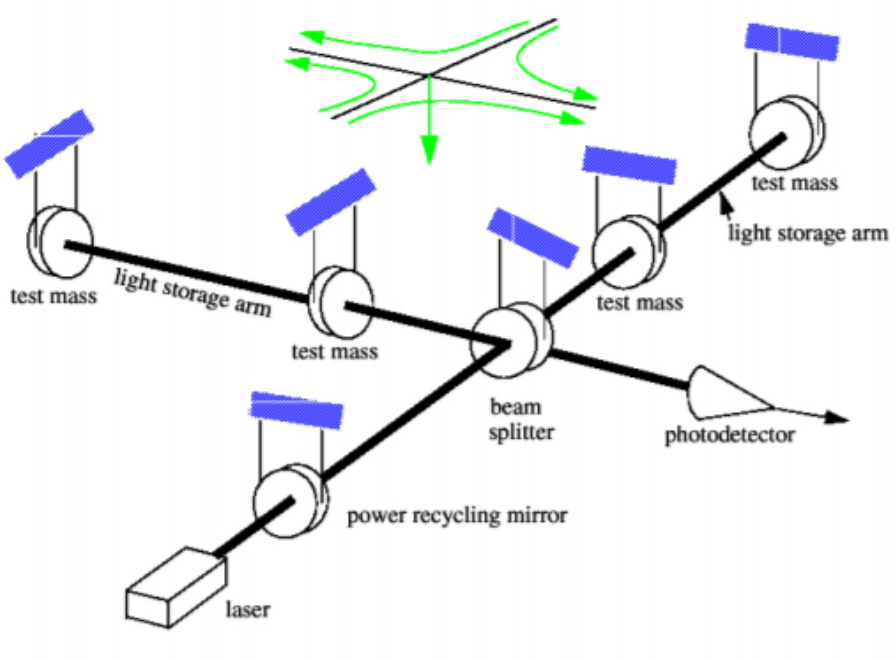

Figure 10: Scheme of a ground-based interferometric detector. Reprinted from [Whelan].

As we can see from Figure 10, ground-based detectors consist of two equal length L arms forming a $\pi/2$ angle, with two mirrors at the end of the arms. Although the mirrors are suspended against Earth's gravitational potential (so they are not in an inertial frame), one can consider that the orthogonal directions to the tension force are freely moving, so one can consider that they follow geodesics on this orthogonal plane. Then, let us consider the effect of a gravitational wave passing through the mirrors.

In the TT gauge, coordinates remain unchanged by the passing of a gravitational wave (see, for example, [Maggiore, sec. 1.3]). However, if we consider the travel of a photon from the beam splitter to one of the mirrors, the effect of a gravitational

wave on the arm will change the proper length of the geodesic followed by the photon, i.e, will change the optical path length of the photon, and this will induce a phase difference measurable in the photodetector. Let us establish a Cartesian coordinate system on the detector, with the x-axis aligned with one of the arms, and the y-axis aligned with the other, in such a way that the z-axis points towards Earth's surface, and the origin is at the beam splitter. The basis is a Cartesian basis:

$$\hat{\mathbf{x}} = (1,0,0),\ \hat{\mathbf{y}} = (0,1,0),\ \hat{\mathbf{z}} = (0,0,1)\ . \tag{222}$$

The position of the mirrors is mirror1$= (L,0,0)$ and mirror2$= (0,L,0)$. Consider the path of a photon from the beam splitter to mirror1, so the propagation is in the x-axis. We can obtain this path integrating the line element, which we can consider that is the Minkowski line element plus a perturbation due to the gravitational wave $h_{\mu\nu}$:

$$ds^2 \simeq -dt^2 + (1+h_{xx})dx^2 = 0\ . \tag{223}$$

Here, h_{xx} is not necessarily h_+ since it is the xx component of the wave tensor in the detector's frame, not in the wave's frame, and the line element is zero because photons follow null geodesics. So, to first order in $h_{\mu\nu}$, we can integrate the time interval spent by the photon in travelling from the beam splitter to mirror1 as:

$$\int_0^{T_1} dt = \sqrt{1+h_{xx}} \int_0^L dx \ \Rightarrow\ T_1 = \sqrt{1+h_{xx}}L \simeq (1+\frac{1}{2}h_{xx})L. \tag{224}$$

where in the last approximation we expand the squared root since $h_{xx} \ll 1$. In fact, we made another approximation to integrate the last equation. The component h_{xx} has a phase $\varphi = \omega t - \mathbf{k}\cdot\mathbf{r}$ as we have seen in section 4, so in principle we should integrate this phase, but if we consider that the wavelength $\lambda = 2\pi/\omega$ is much bigger than the size of the detector (or equivalently that the photon's travel time is much shorter than the time in which the phase changes significantly), then we can regard h_{xx} as constant. This is the long-wavelength limit, and for ground-based detectors the requirement is fulfilled (however, for the space-based detector eLISA one needs to consider correction terms to this approximation).

Thus, the total time from the beam splitter to mirror1 and to come back is $T_x = 2L(1+h_{xx}/2)$. With the same argument, the total time from the beam splitter to mirror2 is $T_y = 2L(1+h_{yy}/2)$. Thus, the relative time difference between the two beams due to a gravitational wave is:

$$s = \frac{\Delta T}{T} = \frac{T_x - T_y}{T_0} = \frac{(1+h_{xx}/2)L - (1+h_{yy}/2)L}{L} = \frac{1}{2}(h_{xx} - h_{yy})\ , \tag{225}$$

where $T_0 = L$ (remember, in units $c = 1$) is the travel time for a photon without the pass of a gravitational wave. This relative time difference is also the strain because $\Delta T/T = \Delta L/L$ since the speed of light is a fundamental constant.

We know the form of the gravitational wave in its associated reference frame, so we need to express h_{xx} and h_{yy} in terms of the components h_+ and $h_\times$ of that frame. Then, we have the coordinate basis of the detector $\{\hat{\mathbf{x}},\hat{\mathbf{y}},\hat{\mathbf{z}}\}$ and the TT coordinate basis attached to the wave $\{\hat{\mathbf{e}}_x,\hat{\mathbf{e}}_y,\hat{\mathbf{e}}_z\}$. In Figure 11 we see both reference frames (however with distinct names for the basis vectors) and the three angles relating them.

The components xx and yy in the detector frame are of course the following projections of the wave tensor $\mathbf{h}$ with the basis vectors:

$$h_{xx} = \hat{\mathbf{x}}^{\mathrm{T}} \cdot \mathbf{h} \cdot \hat{\mathbf{x}} \ , \quad h_{yy} = \hat{\mathbf{y}}^{\mathrm{T}} \cdot \mathbf{h} \cdot \hat{\mathbf{y}} \ . \tag{226}$$

Since both are Cartesian basis, we can go from one basis to another performing a general Euler rotation: $\hat{\mathbf{e}}_x = \mathbf{R} \cdot \hat{\mathbf{x}}$ (the same for the other basis vectors), so we have:

$$h_{xx} = \hat{\mathbf{x}}^{\mathrm{T}} \cdot \mathbf{h} \cdot \hat{\mathbf{x}} = \hat{\mathbf{e}}_x^{\mathrm{T}} \cdot \mathbf{R} \cdot \mathbf{h} \cdot \mathbf{R}^{\mathrm{T}} \cdot \hat{\mathbf{e}}_x = (\mathbf{R} \cdot \mathbf{h} \cdot \mathbf{R}^{\mathrm{T}})_{11} \equiv F_+(\theta, \phi, \psi) h_+ \ , \tag{227a}$$

$$h_{yy} = \hat{\mathbf{y}}^{\mathrm{T}} \cdot \mathbf{h} \cdot \hat{\mathbf{y}} = \hat{\mathbf{e}}_y^{\mathrm{T}} \cdot \mathbf{R} \cdot \mathbf{h} \cdot \mathbf{R}^{\mathrm{T}} \cdot \hat{\mathbf{e}}_y = (\mathbf{R} \cdot \mathbf{h} \cdot \mathbf{R}^{\mathrm{T}})_{22} \equiv F_\times(\theta, \phi, \psi) h_\times \ , \tag{227b}$$

where $(\mathbf{R} \cdot \mathbf{h} \cdot \mathbf{R}^{\mathrm{T}})_{11}$ is the component 11 of the tensor $\mathbf{R} \cdot \mathbf{h} \cdot \mathbf{R}^{\mathrm{T}}$ in the wave coordinate frame (the same for the 22 component), and we define the antenna functions $F_{+,\times}$ of the detector factorizing out the polarizations $h_{+,\times}$ from those components.

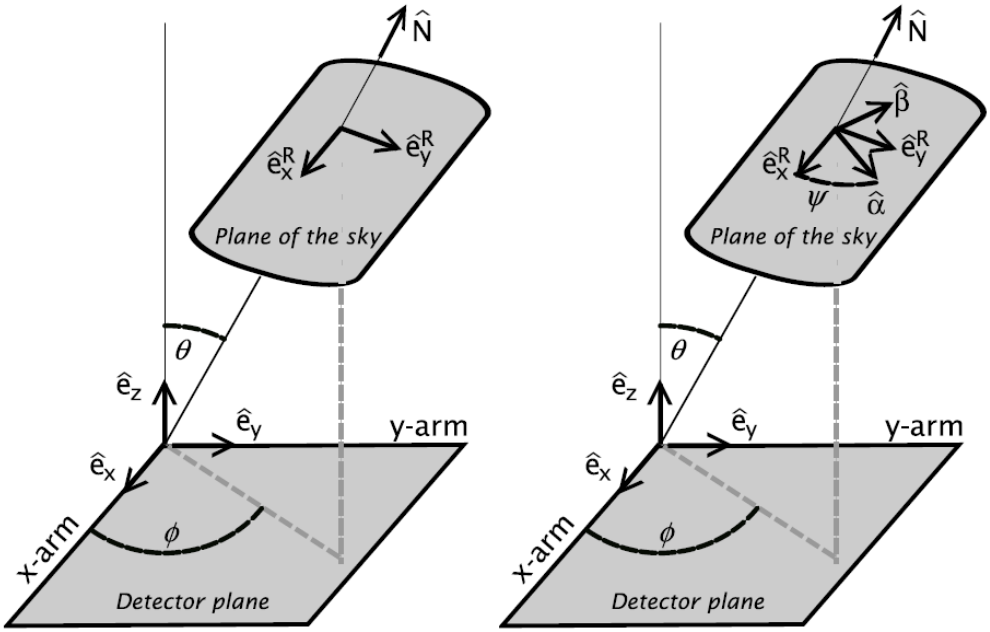

Figure 11: Relative orientation of wave and detector frames. Reprinted from [Schutz & Sathyaprakash].

From Figure 11 it is straightforward (if long) to get the trigonometric relations to express the Euler rotation matrix in the wave frame (for the derivation one can see [Trias], with another nomenclature), obtaining the following expressions for the antenna functions:

$$F_+(\theta, \phi, \psi) = \frac{1}{2}(1 + \cos^2\theta)\cos 2\phi \cos 2\psi - \cos\theta \sin 2\phi \sin 2\psi \ , \tag{228a}$$

$$F_\times(\theta, \phi, \psi) = \frac{1}{2}(1 + \cos^2\theta)\cos 2\phi \sin 2\psi + \cos\theta \sin 2\phi \cos 2\psi \ . \tag{228b}$$

The angles θ and ϕ only depend on the direction of propagation of the gravitational wave with respect to detector's frame, but for knowing ψ one needs to know the orientation of the source reference frame with respect to the detector frame, because this angle measures the polarization axes of the gravitational wave with respect to the rotated axes of the detector, and in order to know the polarization directions one needs to know the orientation of the emission.

6.2 Detector's noise

Besides the astrophysical signals, the detector contains also noise. Noise comes from several factors that cannot be completely suppressed. These include [Schutz & Sathyaprakash]:

- Ground vibration: external mechanical vibrations coming from seismic movements, mechanical machines operating near the detector, even road traffic or pressure sound waves from airplanes. One effective way to screen these effects is to suspend the mirror on pendulums, which are good filters for frequencies above their natural frequencies.

- Thermal noise: the pendulums and the mirrors and other subsystem of the detector have thermal vibrations due to their non-zero temperature. In the case of pendulums, these vibrations limit the minimum sensitive frequency of the detector, being about $f_{min} = 20$ Hertz for the advanced detectors. Mirrors have internal vibrations with natural frequencies of several kHz, limiting from above the range of frequencies with enough sensitivity to detect gravitational waves. Other unwanted effects are associated with thermal noise, as variable refractive index of the beam splitter due to laser heating, and so on.

- Shot noise: laser beams are coherent light states, so the photon number is not a defined quantity, and due to quantum fluctuations this number fluctuates. This provokes intensity fluctuations in the interferometer that can look like a gravitational wave signal. The variance of the intensity decays with $1/\sqrt{N}$, being N the number of photons, so using high intensity laser beams one can reduce this problem. To achieve great intensities, there are systems of light recycling in the detector. However, as one improves position sensing accuracy with these method, the uncertainty principle causes fluctuations in the momentum transferred to the detector. To fix this, the employ of squeezed light states is being developed.

- Gravity gradient noise: local changes in the gravitational potential will affect the mirrors as well as gravitational waves. The tidal forces due to these changes cannot be screened, and this imply that the frequency range below 1 Hz must be observed with space-based detectors.

Suppose that $x(t)$ is the data output of the detector. Then we can write it as:

$$x(t) = n(t) + h(t) \ , \tag{229}$$

where $n(t)$ is the noise contribution and $h(t)$ is an astrophysical signal (of course most of the time $h(t) = 0$). Thus, in order to correct identify a possible astrophysical signal from the output (i.e, detect a gravitational wave), one needs to know the contribution of the noise. However, noise usually is a random process, so in order to characterize it and extract the signal one needs to use statistical tools (if noise was a deterministic quantity, in the sense that we know its exact form at every instant, then subtracting the noise from the output we would get the possible astrophysical signal, but this is not the case).

Let us characterize the typical noise of a ground-based detector. We can assume the following properties:

- Gaussian noise: noise follows a Gaussian distribution function. This assumption is justified in several ways: By the Central Limit Theorem, any random process composed by a large number random subprocesses is approximately Gaussian, regardless of the probability distribution of the individual processes. Besides, if we only know the mean and the variance of the noise, then the least informative probability distribution is the Gaussian, so in a Gaussian distribution we encode all the information we have, minimizing the biases in the information that we do not know.

- Stationary noise: a random process is stationary if all its statistical properties are independent of time. In a real situation, noise is always time-dependent. However, for time periods smaller than the typical periods in which noise change, we can treat the noise as stationary.

- Noise with zero mean value. This in fact is not an assumption, we always can shift the origin of values to make the mean equal to zero, at least in a region where we can assume the mean to be constant (the stationary assumption).

One important characterization of noise is to know how its power is distributed in the frequency domain, i.e, what is the contribution to the power of each frequency. This is important because the amplitude of the gravitational waves signals is frequency dependent. If there is a lot of noise contribution to some frequency range, then it is difficult that we can extract the signal if it lies in that range. This power distribution is characterized by the Power Spectral Density (PSD):

$$S_n(f) = \lim_{T\to\infty} \frac{2}{T} \left| \int_{-T/2}^{T/2} dt\ n(t) e^{-i2\pi f t} \right| = \lim_{T\to\infty} \frac{2}{T} |\tilde{n}_T(f)|^2 \ , \tag{230}$$

so essentially the PSD is the square of the noise amplitude at each frequency. The factor 2 comes from the fact that we only consider positive frequencies, and since noise is real, $n(f) = n*(-f)$, so we count twice each mode. We can relate the PSD to the autocorrelation of noise in time, i.e, how well noise matches itself when it is shifted (respect to itself) by a time t. The autocorrelation function is:

$$C_n(t) = \lim_{T\to\infty} \frac{1}{T} \int_{-T/2}^{T/2} dt'\ n(t') n(t+t') \ , \tag{231}$$

but for stationary noise (and assuming that the process is ergodic) we can relate the time average with an ensamble average of different noise realizations:

$$C_n(t) = \langle n(t')(t+t') \rangle \ . \tag{232}$$

Using the Wiener–Khinchin theorem, we can relate the autocorrelation function with the Power Spectral density:

$$P_n(f) = \int_{-\infty}^{\infty} dt\ C_n(t) e^{-i2\pi f t} \ , \tag{233}$$

and using the ensemble average description of the autocorrelation and the Fourier transform of the noise, one can show:

$$\langle \tilde{n}(f) \tilde{n}^*(f') \rangle = \delta(f - f') P_n(f) \ , \tag{234}$$

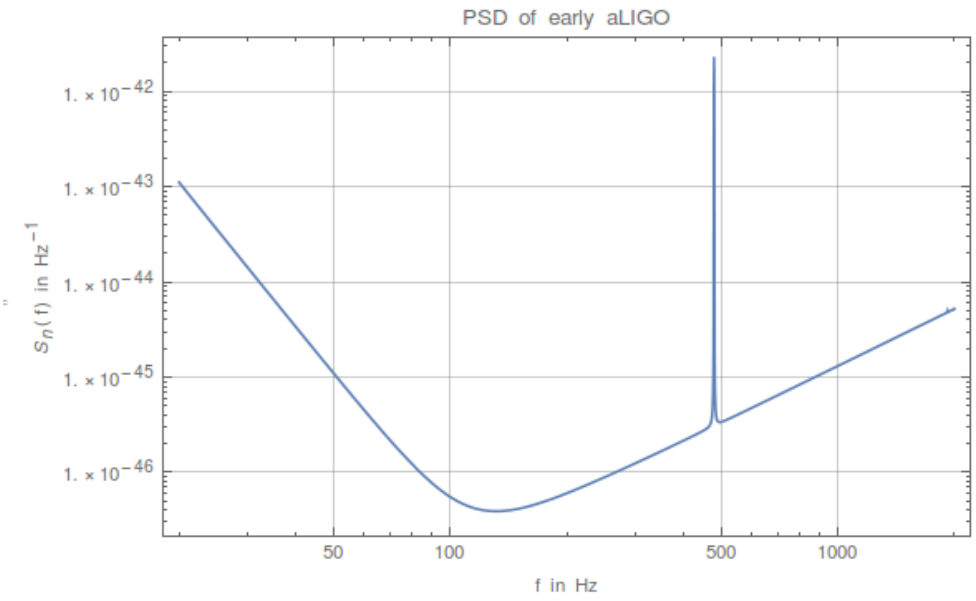

Figure 12: Power Spectral Density of early advance LIGO. This is the PSD employed in this work.

so different noise modes are uncorrelated in the frequency domain, as is indicated by the Dirac delta.

Generally, the Power Spectral density is estimated from noise samples. In the case of advance LIGO, we consider in this work the PSD estimated of the first observation run O1, which we plot in Figure 12.

6.3 Matched filtering and Signal-to-Noise Ratio

Once noise is characterized, the question is how to extract an astrophysical signal $h(t)$ from the detector's output $x(t)$. When one has a model for the signal, as in the case of compact binary coalescence signals, this can be done by a process called matched filtering. The idea is to filter the output of the detector to extract the signal:

$$y = \int_{\infty}^{\infty} dt\ x(t)K(t) = \int_{\infty}^{\infty} df\ \tilde{x}(f)\tilde{K}^{*}(f)\ , \tag{235}$$

where y is the filtered output, $\tilde{K}(f)$ is the filter function, and the last equality is due to Parseval's theorem. The idea is to recover the astrophysical signal the best we can, so we need to find the optimal filter to do that. As we can set the mean value of noise equal to zero, if we take the mean value of the filtered output, we get the mean value of the filtered signal:

$$S \equiv \langle y \rangle = \int_{\infty}^{\infty} dt\ \langle x(t) \rangle K(t) = \int_{\infty}^{\infty} dt\ h(t)K(t) = \int_{\infty}^{\infty} df\ \tilde{h}(f)\tilde{K}^{*}(f)\ , \tag{236}$$

because $\langle n(t) \rangle = 0$ and since $h(t)$ is a deterministic (in the sense of opposed to random) signal, its mean value is itself, because it has zero variance. We also need to know the contribution of the noise to the filtered output. We can compute this as the rms

(root-mean-square) value of the ouput without signal:

$$N \equiv \sqrt{\langle (y - \langle y \rangle)^2 \rangle_{h=0}} \ , \tag{237}$$

so:

$$\begin{aligned} N^2 &= \langle (y - \langle y \rangle)^2 \rangle_{h=0} = [\langle y^2 \rangle - \langle y \rangle^2]_{h=0} = \langle y^2 \rangle_{h=0} \\ &= \int_{-\infty}^{\infty} \int_{-\infty}^{\infty} dt dt' \ K(t) K(t') \langle n(t) n(t') \rangle \\ &= \int_{-\infty}^{\infty} \int_{-\infty}^{\infty} dt dt' \ K(t) K(t') \int_{-\infty}^{\infty} \int_{-\infty}^{\infty} df df' \ e^{i2\pi(ft - f't')} \langle \tilde{n}(f) \tilde{n}^*(f') \rangle \\ &= \int_{-\infty}^{\infty} \int_{-\infty}^{\infty} dt dt' \ K(t) K(t') \int_{-\infty}^{\infty} \int_{-\infty}^{\infty} df df' \ e^{i2\pi(ft - f't')} \delta(f - f') \frac{1}{2} S_n(f) \\ &= \int_{-\infty}^{\infty} \int_{-\infty}^{\infty} dt dt' \ K(t) K(t') \int_{-\infty}^{\infty} df \ e^{i2\pi f(t - t')} \frac{1}{2} S_n(f) \\ &= \frac{1}{2} \int_{-\infty}^{\infty} df \ |\tilde{K}(f)|^2 S_n(f) \ . \end{aligned} \tag{238}$$

We want a filter that maximizes the signal over the noise, so we want to maximize the Signal-to-Noise ratio (SNR):

$$SNR \equiv \rho = \frac{S}{N} = \frac{\int_{\infty}^{\infty} df \ \tilde{h}(f) \tilde{K}^*(f)}{\sqrt{\frac{1}{2} \int_{-\infty}^{\infty} df \ |\tilde{K}(f)|^2 S_n(f)}} \ . \tag{239}$$

To find the optimal filter for maximizing the SNR, let us introduce the following inner product in the space of real functions $f(t)$:

$$(A|B) \equiv \mathfrak{Re} \int_{-\infty}^{\infty} df \frac{\tilde{A}(f) \tilde{B}^*(f)}{(1/2) S_n(f)} = 4 \ \mathfrak{Re} \int_0^{\infty} df \frac{\tilde{A}(f) \tilde{B}^*(f)}{S_n(f)} \ . \tag{240}$$

Then, we can write the SNR as:

$$\rho = \frac{(u|h)}{\sqrt{(u|u)}} \ , \tag{241}$$

where $u(t)$ is a function such that its Fourier transform is:

$$\tilde{u}(f) = \frac{1}{2} S_n(f) \tilde{K}(f) \ . \tag{242}$$

It is easy to see that the SNR is maximized when the normalized function $u/\sqrt{(u|u)}$ is parallel (in the sense of a vector in the function space) with respect to $h(t)$. So the filter has to be:

$$\tilde{K}(f) \propto \frac{\tilde{h}(f)}{S_n(f)} \ , \tag{243}$$

where the proportionality constant is irrelevant since it cancels in the quotient. This is called the matched filter (also called Wiener filter) and it is the optimal filter when noise is gaussian and stationary and we can model the signal we want to find. With the matched filter, the SNR reads as:

$$\rho^2 = 4 \ \mathfrak{Re} \int_0^{\infty} df \frac{\tilde{h}(f) \tilde{h}^*(f)}{S_n(f)} = 4 \ \mathfrak{Re} \int_0^{\infty} df \frac{|\tilde{h}(f)|^2}{S_n(f)} \ . \tag{244}$$

As we can see, the matched filter is a noise-weighted filter, that assigns a lower weight to the frequency regions where the noise is higher. Regarding the SNR, we see that depends on the squared amplitude of the waveform, i.e, the phase cancels. If we regard the PhenomD waveform (220), we commented that the factor M^2/r (in geometrized units) scales the amplitude. So the SNR for this waveform will scale with the same factor. So there is an inverse proportionality between the distance to the source and the SNR: $\rho \propto 1/r$. We can use this to compute the distance at which some signal reaches a threshold SNR, i.e, the distance at which certain signal could be detected. Usually, this threshold is settled to $\rho_{th} = 8$. Thus, for a PhenomD waveform we can compute the detector's horizon distance as:

$$d_{DH}(M, \eta, \chi_1, \chi_2) = \frac{M^2}{8}\sqrt{4\,\mathfrak{Re}\int_0^\infty df \frac{|\tilde{h}_{PD}(f; \eta, \chi_1, \chi_2)|^2}{S_n(f)}}\ . \tag{245}$$

As we discussed, the frequency domain PhenomD waveforms are dimensionless (while frequency domain waveforms have to have dimensions of time due to the measure dt in the Fourier transform). So the integral has dimensions of frequency squared, due to the measure df and the PSD that has dimensions of time (but it is dividing). Then, with M in dimensions of time (recall that we are using geometrized units), d_{HD} is expressed in dimensions of time, seconds for example. To compute the distance in SI units one has to multiply by c. The distance obtained is a luminosity distance (remember 63).

6.4 Overlap, fitting factor and parameter detection bias

As we said, matched filtering is the optimal filtering when we know the form of the signal, i.e, when we can model accurately (ideally perfectly) the possible signal. However, in general a theoretical model always includes approximations, and it only reflects what we know. But it is possible that the true signal contains effects that we are not aware of. This is relevant in the case of lensing of gravitational waves. Consider that the detector receives a lensed signal, but we are searching only with unlensed models. Then, what is the chance to detect the signal with the incomplete unlensed model? And if detected, will the estimated parameters be biased due to the incorrect model?

We can analyze these questions using the inner product (240) as a measure of how well a model resembles the signal. Instead of using the optimal filter (243), i.e, the signal weighted by noise, we can employ a suboptimal filter: the template weighted by noise. Consider the inner product between the normalized signal $\hat{h}$ and the normalized template $\hat{u}$:

$$(\hat{h}|\hat{u}) = \frac{(h|u)}{\sqrt{(h|h)(u|u)}}\ . \tag{246}$$

If u is parallel (in the sense of functions as vectors in the function space) to h, then this product reaches its maximum value 1, but this is precisely the situation of matched filtering, because if u and h are parallel, then we are using the optimal filter. If they are not parallel, then the inner product reaches a smaller value. This product is called overlap, because it measures the overlapping of the two functions. Higher overlaps mean more similar functions.

The true signal depends on some parameter set λ. As we said in section 5, for coalescing BH binaries systems this set consists of the symmetric mass ratio η, the dimensionless spins ξ_i, which in the general case of not aligned spins sum 7 parameters, the total mass and the distance which scale the amplitude, the angular dependence of the emission codified by the spin-weighted spherical harmonics basis, the angular dependence of the detection codified in the antenna patterns of the detector, and coalescing parameters as the coalescing time t_c and the phase at that time ϕ_c. The modeled templates will depend on another set of parameters ξ which in general does not have neither the same dimension of the true parameter set. For example, in the PhenomD model, we consider aligned (or anti-aligned) spins so we reduce the spin parameters from seven to two. Or if the true signal is a lensed gravitational wave, then in λ we include the lens parameters M_L and y, while in an unlensed model this parameters are absent.

At some point of the model parameter space ξ, the overlap will reach a maximum value, which will be less than one if the model does not contain the true signal. We call the maximum overlap over the model parameter space the Fitting Factor of the model:

$$FF \equiv \max_{\xi} \frac{(h(\lambda)|u(\xi))}{\sqrt{(h(\lambda)|h(\lambda))(u(\xi)|u(\xi))}} \ . \tag{247}$$

We can understand the fitting factor as the ratio between the SNR with optimal filtering and the SNR reached with a suboptimal filter based on the model: $FF = \rho_{opt}/\rho_{subopt}$. From the fitting factor we can compute how much detection volume of space we are losing due to using an inexact model. To see this, consider that for the optimal filter we have the detection range given by r_{DH} (245). If we employ a suboptimal filter, then the SNR is the optimal SNR multiplied by the fitting factor, so the detection range will is also multiplied by the fitting factor. Now, the space volume on which possible events could be detected is proportional to r_{DH}^3, so the percentage of detection volume lost with the inexact model is equal to:

$$\Delta V_{lost} = \frac{V_{opt} - V_{subopt}}{V_{opt}} = \frac{r_{opt}^3 - r_{subopt}^3}{r_{opt}^3} = \frac{(1-(FF)^3) r_{opt}^3}{r_{opt}^3} = 1 - (FF)^3 \ . \tag{248}$$

Suppose for example that for a given model the fitting factor is $FF = 0.97$. This seems close to one, but the detection volume lost is $1 - 0.97^3 \simeq 10\%$, so we would loose ten percent of possible detections.

To end this section, we will discuss the parameter detection bias. We have seen that the fitting factor is the overlap for the model parameters that maximize it. Usually the set of signal parameters λ and the model parameters have parameters in common (the usual situation is that the model has a subset of the signal parameters). Then we can compare the value of the model parameters that maximize the overlap with the value of the true signal parameters, for the parameters that they have in common. If λ_i is some value of some signal parameter, and λ_i^m is the value for the same parameter maximizing the overlap, then we can define the parameter detection bias of the parameter λ_i as:

$$E_{\lambda_i} = \frac{\lambda_i^m - \lambda_i}{\lambda_i} \ . \tag{249}$$

7 Lensing effects on gravitational waves from black hole binary systems

We have presented in section 5.3 the gravitational wave signals emitted by binary systems of two black holes. As we said in that section, these signals are the current target for ground-based detectors as advanced LIGO and advanced VIRGO. We have seen in section 4 that gravitational lensing introduces amplitude and phase modulations to the signals, regulated by the amplification factor, a complex function dependent of the relative position to us of the source and the lens, the lens mass, and the signal frequency, and that the combination of these variables gives rise to a complicated scheme of regions where signals can be magnified and where interference effects are important due to the coherent nature of the gravitational waves signals.

Here we will focus on how lensing affects the statistical treatment of the signals, crucial to their detection in our current detectors. First, we are going to see how gravitational waves are modified in the frequency domain due to lensing, and then transform them to the time domain to see the actual look of a lensed signal. Then we will compute the fitting factor and the parameter detection biases for several cases where we represent the actual signal as a lensed waveform, and compare it to the unlensed signals of the PhenomD model. This will give us a estimation of how lensing can produce a loss of signals if unlensed templates are used for the search. Finally, we will compute the Signal-to-Noise Ratio in the lens parameter space to try to find how lensing can increase the detection range of events, and try to estimate a lensed events rate for Advanced LIGO.

7.1 Lensed waveforms

We will now discuss the amplitude and phase modulations on BH-BH binary systems due to gravitational lensing. We employ the PhenomD waveforms as an accurate model for the signal, and apply to them the amplification factor of a point mass lens. As discussed in section 4, the modulus of the amplification factor will affect the amplitude of the signal:

$$|h(f)|_{lensed} = |F(f, M_L, y)| \cdot |h(f)| \ , \tag{250}$$

while the argument of the amplification factor will affect the phase of the signal:

$$\phi_{lensed} = \phi + Arg(F) \ . \tag{251}$$

For the comparison, we select a PhenomD waveform reproducing the signal of the first detection GW150914, i.e, we employ the estimated parameters for this detection: As mentioned in section 4, for recover the physical waveforms from the PhenomD scaled

m_1	m_2	χ_1	χ_2	distance
$36M_\odot$	$29M_\odot$	0.33	0.33	440 Mpc

Table 1: Data release of the detection GW150914. Source: [GW150914data]. (We are assuming aligned spins since the estimated parameter is the final spin $\chi_f = 0.67$).

waveforms, we average the value of the dominant mode's spin-weighted spherical harmonic. Furthermore, we are not taking into account the orientation of the detector with

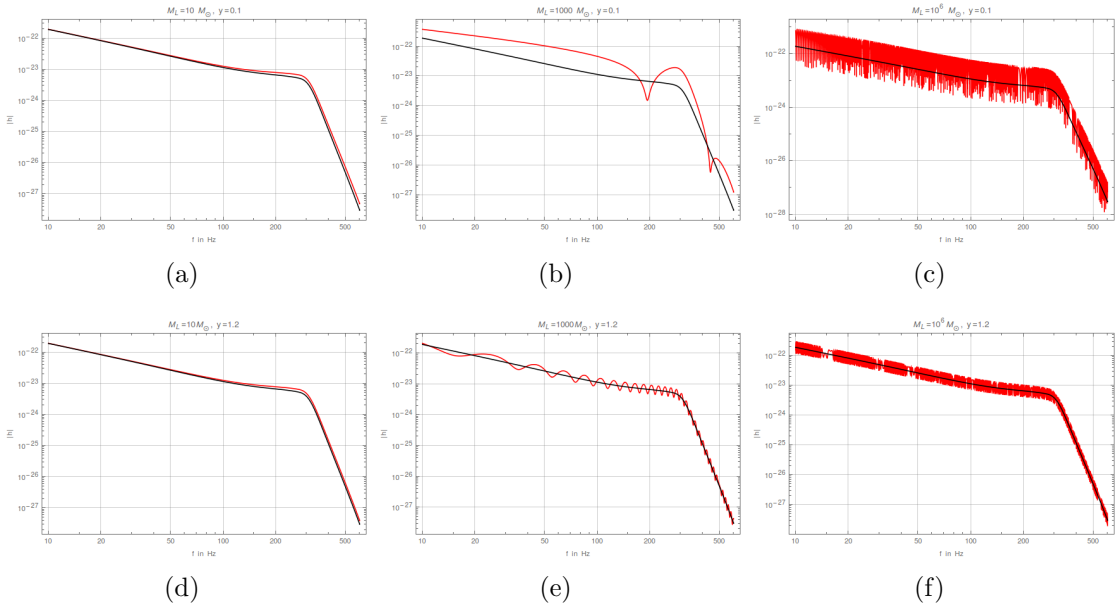

Figure 13: Amplitude comparison for unlensed and lensed event GW150914. The black line is the unlensed PhenomD waveform, and the red line is the lensed waveform. Double logarithmic plots.

respect to the wave, so this waveform is the optimally oriented version of GW150914.

In Figure 13, we see in the first row the lensing effect on the amplitude for a small impact parameter $y = 0.1$ and in the second row for a larger impact parameter $y = 1.2$. In each column the lens is a stellar black hole of mass $10M_{\odot}$, an intermediate mass black hole (IMBH) of mass $1000M_{\odot}$ and a supermassive black hole (SMBH) of mass $10^6 M_{\odot}$, respectively. We can see that for a stellar mass lens, the modification of the amplitude is small, and there is no a significant difference for the distinct impact parameters. For IMBH we see an important magnification of the signal but at some point it begins to oscillate. We see, as discussed in section 4, that as we increase the impact parameter, the frequency of the oscillations gets larger, but the amplitude of these oscillations is smaller (the total magnification is smaller in this regime). For a SMBH lens, the frequency of the oscillations is so large that we see a continuous band between the lowest and the highest magnification (the gaps in the figure are a plot artifact due to the number of points employed in the plot). We see that increasing the impact parameter has the effect of reducing the total magnification, i.e, the width of the band.

In Figure 14 we have the same scenario as in Figure 13, but now for the phase of the gravitational wave. We see again that for a stellar black hole lens there is no great phase modulation. For the IMBH lens we see an oscillation of the phase and a greater departure from the unlensed phase. As we increase the impact parameter y, the oscillations in the phase have a small period. For the SMBH lens, we see again a whole band of values for the lensed phase due to the rapid oscillatory behavior. As the impact parameter gets larger, the width of the band is reduced.

In Figure 15, we do the inverse Fourier Transform of the unlensed and lensed wave-

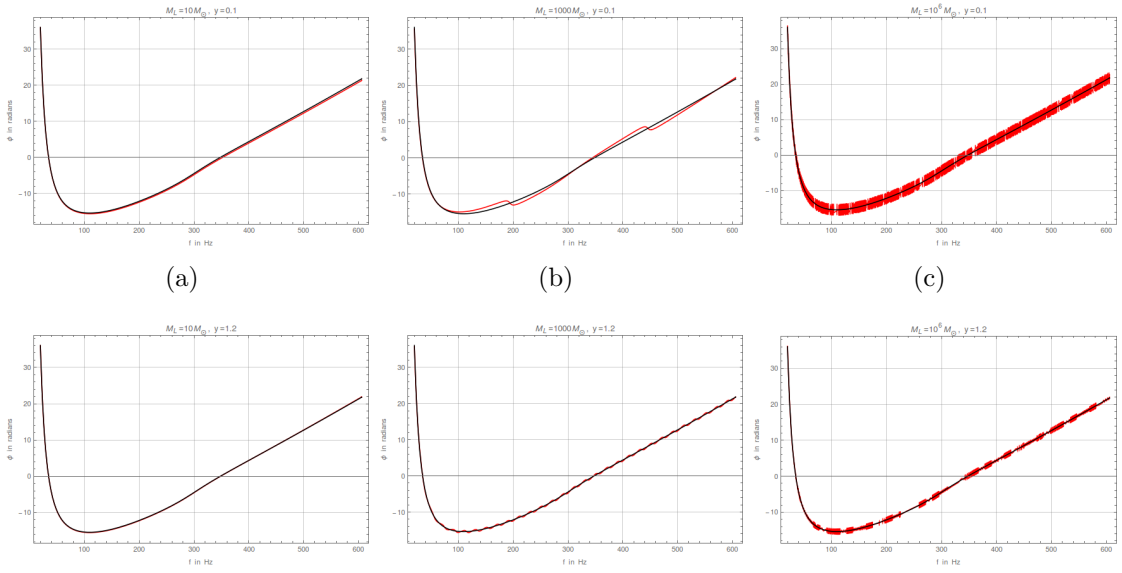

(a) (b) (c)

(d) (e) (f)

Figure 14: Phase comparison for unlensed and lensed event GW150914. The black line is the unlensed PhenomD waveform, and the red line is the lensed waveform.

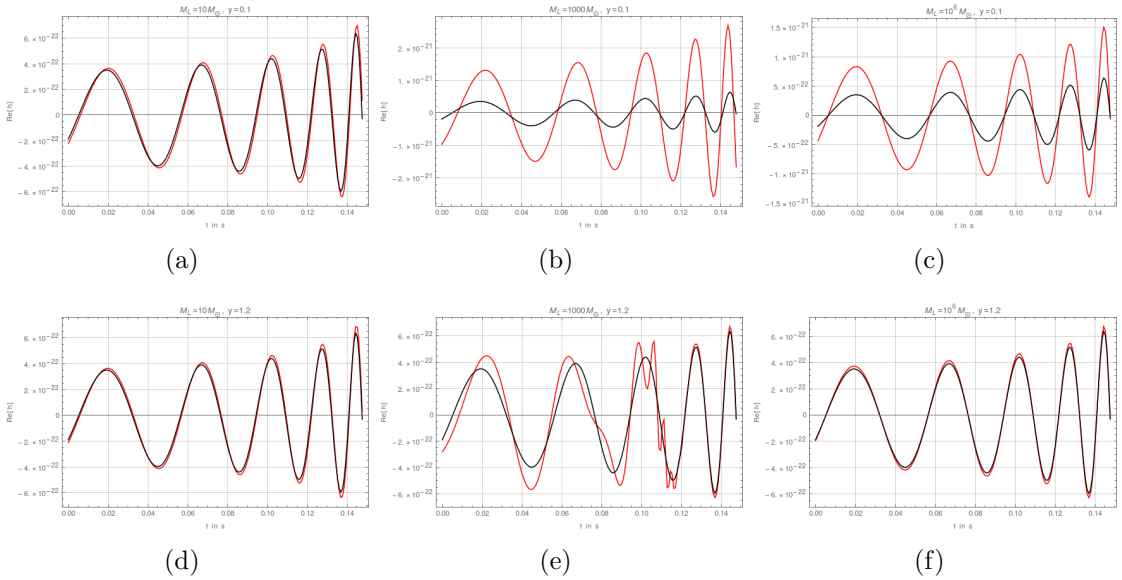

(a) (b) (c)

(d) (e) (f)

Figure 15: Comparison of time domain strains for the unlensed and lensed case. The black line is the unlensed PhenomD waveform, and the red line is the lensed waveform.

forms. We employ 4000 points to evaluate the waveforms, and show the last cycles before the merger. We can see again that for a stellar BH lens the waveform remains almost unchanged. One can appreciate some phase difference between the unlensed and lensed waveforms. For the case of IMBH in the strong magnification regime ($y = 0.1$), we see a bigger phase modulation, as we have seen in Figure 14(b), and a strong magnification. However, for the larger impact parameter case, we see a strange behavior of the lensed waveform. The magnification is small as expected (Figure 13(e)), but the shape is more distorted than in any other case. One possible explanation is that the oscillatory phase seen in Figure 14(e) provokes sums and cancelation of modes in the Fourier integral. For the SMBH lens, we see a much better behavior, that can look surprising due to the fast oscillations seen in the previous figures. However, one possible explanation is that for the frequency resolution we have employed, the Fourier transform acts as an average over a lot of oscillations for each mode, so we see a nice averaged waveform. This is encouraged by the fact that we do not observe any phase delay as in the other cases, because the phase difference in Figure 14(f) is averaged to zero. As we increase the impact parameter, the averaged magnification tends to one.

7.2 Fitting Factor and parameter detection bias between lensed signal and unlensed template

Remember from section 5 that how similar are two waveforms is computed with the overlap, a normalized inner product in the configuration space of waveforms. If we fix the parameters of the signal, we can vary the parameters of the model to search the maximum overlap. This is the fitting factor, and we remember that it computes the ratio between the SNR reached by a suboptimal filter (the unlensed model) and the SNR in optimal filtering (in our case the lensed waveform). We remember the expression:

$$FF = max_{\xi} \frac{(\tilde{h}_u(f,\xi)|\tilde{h}_l(f,\lambda))}{\sqrt{(\tilde{h}_u(f,\xi)|\tilde{h}_u(f,\xi))(\tilde{h}_l(f,\lambda)|\tilde{h}_l(f,\lambda))}} \ , \tag{252}$$

where $\tilde{h}_u(f,\xi)$ are the unlensed PhenomD waveforms in the Fourier Domain, that depend on some parameters ξ, and $\tilde{h}_u(f,\lambda)$ is the lensed signal in the Fourier Domain that depends on some parameters λ.

We are also going to compute the possible biases in the estimated parameters from the template with respect to the true parameters of the signal. We remember that this can be computed as:

$$E_{\lambda_i} = \frac{\lambda_i' - \lambda_i}{\lambda_i} \ , \tag{253}$$

where λ_i' is the parameter giving the fitting factor and λ_i is the true signal parameter.

7.2.1 Methodology

We choose the signal parameters to be:

$$\lambda = \{M, q, \chi; M_L, y\} \ , \tag{254}$$

i.e, the total mass of the system, the mass ratio, the mass-weighted spin (we only consider one spin parameter because as discussed in section 4, the PhenomD waveforms

are sensitive to a combination of the individual values of the spins, and reducing one dimension in the parameter space saves a lot of computational time), and the lens parameters: the lens mass and the impact parameter. We choose the binary parameters of the signal as the first detection GW150914 estimated parameters:

$$\{M = 65M_\odot, q = 39/26, \chi = 0.33\} \ , \tag{255}$$

(the sum of both equally valued spins gives the final spin 0.66). The lens parameters are varied in six different cases: we will study the Fitting Factor considering lensed signals from a stellar black hole of mass $M_L = 10M_\odot$, a IMBH of mass $M_L = 1000M_\odot$, and a SMBH of mass $M_L = 10^6 M_\odot$, each case in a strong lensing regime ($y = 0.1$) and a weak lensing regime ($y = 1.2$).

	case 1	case 2	case 3	case 4	case 5	case 6
M_L	$10M_\odot$	$10M_\odot$	$1000M_\odot$	$1000M_\odot$	$10^6 M_\odot$	$10^6 M_\odot$
y	0.1	1.2	0.1	1.2	0.1	1.2

Table 2: Different lensed cases analyzed in this section.

For the unlensed model, we will vary the following parameters:

$$\xi = \{M', q', \chi'\} \ , \tag{256}$$

thus we have a 3-dimensional parameter space on which to maximize the overlap. We have not found an analytical maximization, so we will compute the overlap for a sample of PhenomD waveforms in a region close to the signal parameters. We construct the following grid:

$$M' = \{62M_\odot, 68M_\odot; \Delta M' = 0.5M_\odot\} \ , \tag{257a}$$
$$q' = \{1.0, 1.1, 1.2, 36/29, 1.3, 1.4, 1.5, 1.6, 1.7, 1.8, 1.9, 2.0\} \ , \tag{257b}$$
$$\chi' = \{0.0, 0.5; \Delta\chi' = 0.01\} \ . \tag{257c}$$

Each waveform is evaluated at 1000 frequency points, between a minimum frequency $f_{min} = 20$ Hz and a maximum frequency of $f_{max} = 600$ Hz, twice the ringdown frequency of the signal. The integrals of the inner products are approximated as a sum of the integrands in each frequency point, multiplied by the frequency spacing $\Delta f = (f_{max} - f_{min})/1000$.

7.2.2 Results

In Table 3 we show the fitting factors of each case along with the model binary parameters for which the fitting factors are obtained. We also show the overlap between the signal and the unlensed waveform with the same binary parameters as the signal. In Figures (16−21) we show the contour plots of the overlap over the parameter space. In each subfigure we fix one of the three binary parameters to the value corresponding to the Fitting Factor, and we plot the overlap as a function of the other two parameters, showing with a red point where is allocated the fitting factor.

	Fitting Factor	M_F	q_F	χ_F	Overlap for signal parameters
case 1	0.997549	66 $M_\odot$	1.3	0.36	0.972394
case 2	0.997608	64 $M_\odot$	1.3	0.30	0.995568
case 3	0.867676	67.5 $M_\odot$	1.6	0.49	0.770319
case 4	0.952371	65 $M_\odot$	36/29	0.33	0.952371
case 5	0.741497	65 $M_\odot$	36/29	0.33	0.741497
case 6	0.952269	65 $M_\odot$	36/29	0.33	0.952269

Table 3: Fitting Factor of the different cases and overlap for equal binary parameters between the model and the signal.

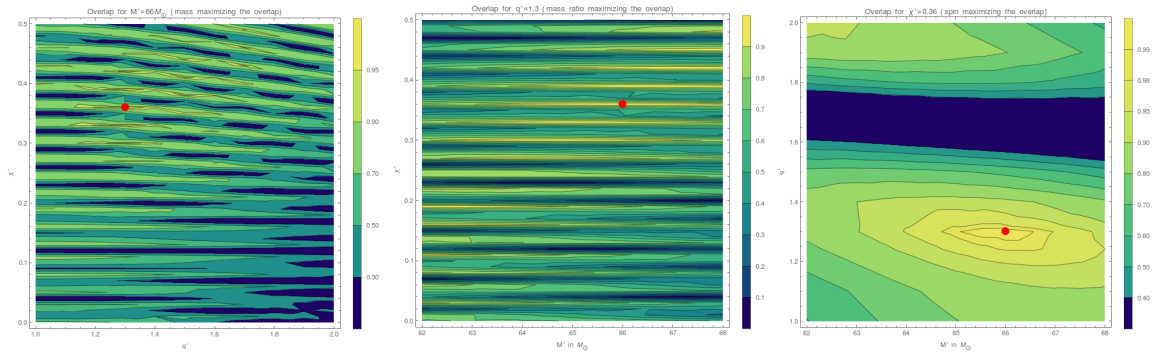

(a) (b) (c)

Figure 16: Contour plots of the overlap for case 1 ($M_L = 10M_\odot, y = 0.1$). Red point is the location of the Fitting Factor in the model parameter space.

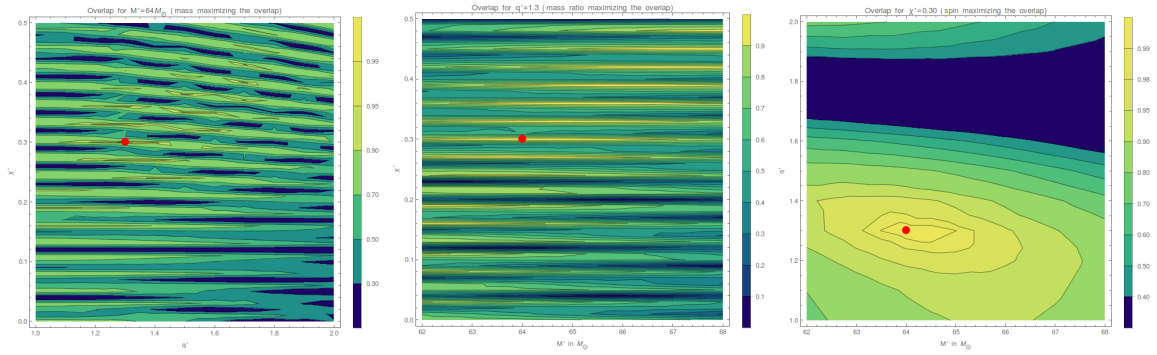

(a) (b) (c)

Figure 17: Contour plots of the overlap for case 2 ($M_L = 10M_\odot, y = 1.2$). Red point is the location of the Fitting Factor in the model parameter space.

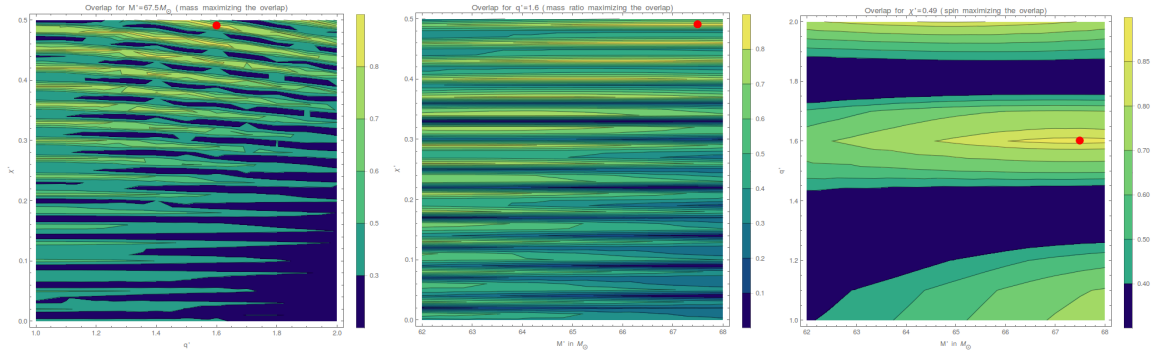

(a) (b) (c)

Figure 18: Contour plots of the overlap for case 3 ($M_L = 1000M_\odot, y = 0.1$). Red point is the location of the Fitting Factor in the model parameter space.

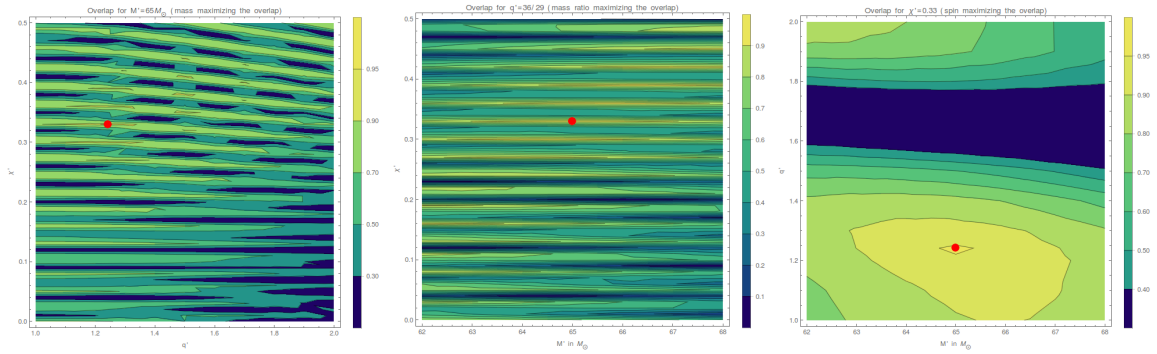

(a) (b) (c)

Figure 19: Contour plots of the overlap for case 4 ($M_L = 1000M_\odot, y = 1.2$). Red point is the location of the Fitting Factor in the model parameter space.

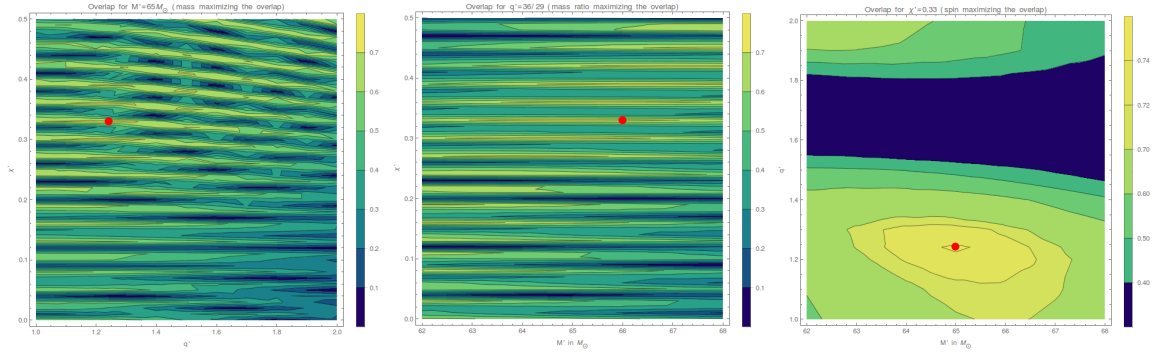

(a) (b) (c)

Figure 20: Contour plots of the overlap for case 5 ($M_L = 10^6M_\odot, y = 0.1$). Red point is the location of the Fitting Factor in the model parameter space.

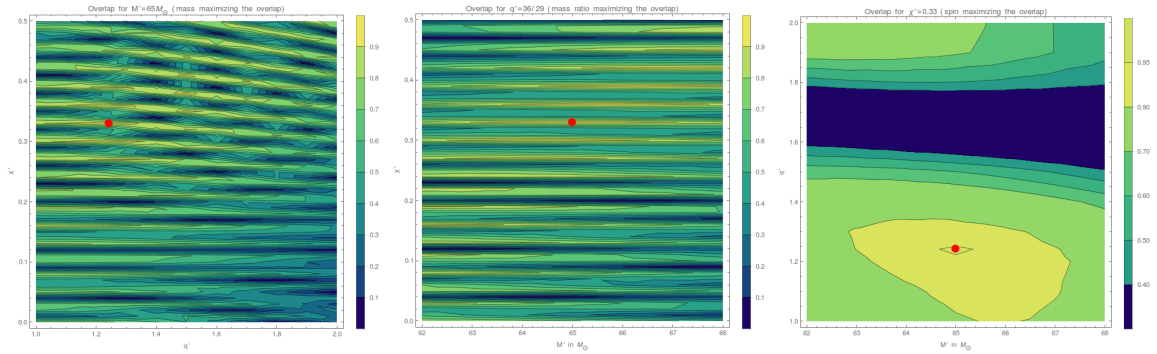

(a) (b) (c)

Figure 21: Contour plots of the overlap for case 6 ($M_L = 10^6 M_\odot, y = 1.2$). Red point is the location of the Fitting Factor in the model parameter space.

We can also study the parameter biases produced by lensing: the relative difference between the true signal parameters and the parameters inferred by the waveform giving the fitting factor. We show these parameter biases in table 4:

	E_M (%)	E_q (%)	E_χ (%)
case 1	1.538	4.722	9.091
case 2	-1.538	4.722	-9.091
case 3	3.846	28.89	48.48
case 4	0	0	0
case 5	0	0	0
case 6	0	0	0

Table 4: Parameter detection bias due to lensing in binary parameters.

7.2.3 Discussion

Looking at Table 3 and Table 4, we can comment the following aspects:

- We observe that the highest fitting factors are reached for a stellar mass lens: the situation of case 1, as we expected since in this case the wavelengths of the gravitational waves ($\sim km$) are larger than the Schwarzschild radius of the lens, and the signal does not feel the existence of a lens, so it is not greatly modified, as we can see in Figures 13(a, d), 14(a ,d) and 15 (a, d).

- As we increase the lens mass, then the fitting factor obtained is smaller. In the case of IMBH lens in the strong lensing regime (case 3), we have a mismatch of $\mathscr{M} = 1 - FF \simeq 0.14$, i.e, we lose 14% of SNR. If a lensed event of these characteristics can in principle be observed to a distance d corresponding to some threshold SNR, then the mismatch due to using unlensed templates reduces the observational volume of space by $1 - (0.868)^3 \simeq 45\%$. For the SMBH lens in the strong lensing regime (case 5) the situation is even worse.

- However, in the weak lensing regime ($y = 1.2$) all the fitting factors are higher than 0.95. Since in this regime the magnification is small, the overlaps between signal and model are large. For the stellar black hole lens, we obtain the best fitting factor, almost 1, in this situation. For the IMBH and SMBH lenses, we gain mismatch due to the oscillatory behavior of the signal (in the Fourier domain).

- In the first three cases (strong lensing for a IMBH lens and both regimes for a stellar BH lens) the value of the parameters maximizing the overlap are not the signal values, we have some parameter detection bias. For a stellar BH lens, we observe the same percentage of bias in both regimes, but the deviations are in opposite directions. In the strong lensing regime, the maximizing values are higher than the signal values. This can be understood considering that, even if weak, there is some magnification of the wave, so a more massive system can fit better the signal. However, in the weak lensing regime, we have a smaller magnification but possibly some weak interference, bigger than in the strong regime, and a waveform with smaller values than the signal seems to fit better. For strong lensing by a IMBH lens, we see much higher biases in the parameters. In particular, the mass of the model is almost at the limit of the sample region, and the effective spin too. We observe also a higher mass ratio than the signal, but it does not reach the highest values of the sample space.

- In the last three cases (weak lensing for IMBH lens and weak and strong lensing for SMBH lens) the value of the parameters maximizing the overlap are precisely the signal parameter values. This could mean that in the small region of the parameter space explored, in these cases there is no parameter combination that can mimic lensing effects.

- The last column of Table 3 shows the overlap for a model with signal values. We see that in the strong lensing regime it is significantly smaller than the fitting factor. This and the great biases of the strong IMBH lens case suggest that in a bigger region of the parameter space there can be some parameter values giving a best overlap for the last three cases. However, it can be possible that for a highly oscillatory behavior of the signal in the frequency domain, there is no waveform that can mimic this effect, so the unlensed signal waveform maybe the best fitting one since in average is the most similar to the lensed signal.

If we turn our attention to the contour plots of the overlap in the sample parameter space, we can make the following considerations:

- We see some periodic dependence on the effective spin value χ'. As we follow the spin values, we alternate high overlap fringes with low overlap fringes. The dependence of these fringes with M or q seems to be more slow varying. In the case of q (subfigure (a) of each case), for high spin values the fringes seem to follow descending path on the spin as the mass ratio q increases. This dependence is not seen in M (subfigure (b) of each case).

- For a fixed spin value, we see *island-like* regions where the overlap is increasing, and small overlap interzones between these regions (subfigure (c) of each case). We find the fitting factor in the only complete region that enters the domain of the sample space, but the appearance of other regions in the figures suggests that

maybe in a bigger sample space we could find larger overlaps in other regions. This is important for the last three cases, where there are not parameter bias, suggesting that maybe in regions outside the sample space we could find a better fitting factor.

- Concerning the resolution of the sample space, we conclude that ΔM and Δq are small enough to find the neighborhood where the fitting factor is allocated (this is suggested again by subfigures (c) of each case, and for the slow dependence of the high overlap fringes with q and M in subfigures (a) and (b)). Of course, increasing the resolution we could find a neighbor point where the overlap is still higher, but for localizing the approximate region the resolution seems enough. However, the oscillatory dependence on χ suggests that maybe is required more resolution in the spin parameter. The fringes seems to alternate between two consecutive points in the $\chi - q$ plot and between one consecutive point in the $\chi - M$ plot.

We can compare our results with the similar study realized in [Cao et al.], where the Fitting Factor for similar lens masses than in our case is computed using only the Post-Newtonian inspiral waveform without spins. In their results, they did not observe any significant parameter bias. However in our case, adding spins (and perhaps the employ of a more accurate model as PhenomD waveforms) reveals the appearance of biased parameters for the best fitting case (at least in the first three cases). Furthermore, we have observed that the overlap is highly dependent on the spin value, so we remark the necessity of including it in this kind of study. For unbiased parameters, our obtained overlaps are consistent with the overlaps obtained in that paper (Tables I to III of [Cao et al.]).

Our results however are preliminary and limited in scope. Further work should be done to get more general and accurate conclusions, in particular:

- One important scenario not treated in this study is the case of precessing binaries: those with the individual spins not aligned with the total angular momentum of the system. In that case, the orbiting plane is precessing, provoking some periodic modulation on the signal received at Earth. This effect in principle could mimic well the oscillatory behavior of a non-precessing lensed signal, so it is expected that we can find best fittings using precessing models.

- As we suggested, the resolution in the spin parameter χ should be improved, and the domain of the sample space should be bigger. For more accurate results we should also improve the resolution in the mass and the mass ratio. And more cases should be treated with intermediate values of the impact parameter y between the strong and weak lensing regime, and smaller values of y since in that region is where one expects to find large magnifications. As suggested in a recent paper by [Berry & Veitch], the first two detections of aLIGO could be produced by globular cluster lenses acting on further less massive binary systems than the estimates ones with magnifications of the order ~ 200, for which a small impact parameter would be required.

- However, in obtaining these results, tens of hours of computation in a six core computer were needed. Increasing the parameter space and the resolution, along

with including precessing effects (which would increase the dimension of the parameter space) can raise substantially the computation time needed for each case. One possible solution to this is to implement some stochastic algorithm (like Monte Carlo Markov Chains) to approach iteratively the best fitting values.

7.3 Increase in total number of detections due to lensing

In this section we are going to study how lensing can increase the number of detected events for ground-based detectors, in particular for advanced LIGO. Due to magnification, the SNR of lensed events is expected to be greater than the SNR for the same events without lensing, at least in some region of the lens parameter space. If the SNR increases due to lensing, then by the discussion of section 6.3 the horizon distance of the detector (the distance at which the SNR has a threshold value of 8) increases. We can compute how much potentially detectable volume we gain due to this. Knowing the merger rate density (the number of mergers per year per volume) we can compute the rate of potentially new events due to the increased volume. However, only those potentially detectable new events that are actually lensed will be detectable, so we need to multiply by the lensing probability of section 4.6, making some assumptions about the number density of compact lenses.

7.3.1 Methodology

We first sketch the procedure steps:

- We compute the SNR for lensed waveforms in a region of the parameter space.
- From the SNR we compute the corresponding detectable distance range, and then the observable volume. We also compute the unlensed observable volume for the binary parameters.
- We compute the detectable merger rate in lensed and unlensed cases multiplying the observable volume by the merger rate density.
- For the volume difference between lensed and unlensed cases, we compute the number of new potentially detectable events.
- From the new potentially detectable events, we compute the number of lensed events (and thus truly detectable events) multiplying by the lensing probability.

First we are going to compute the SNR in the reduced parameter space $\{q, M_L, y\}$ neglecting spin effects, to reduce the computation time. However, since the spin effects are more important for the phase than for the amplitude, and the SNR is computed with the amplitude, qualitatively it is an acceptable approximation:

$$\rho_L(q, M_L, y) = \sqrt{4\mathcal{R}e \int df \frac{|\tilde{h}_L(f; q, M_L, y)|^2}{S_n(f)}} \,, \tag{258}$$

where for the noise PSD $S_n(f)$ we use the data of the noise curve for early advanced LIGO (Figure 12). Since the total mass M and the distance d only scale the waveforms, the SNR is scaled too by these parameters, so we do not need to vary over them. In

particular, we compute SNR for $M = 10M_\odot$ and $d = 500$ Mpc.

Once we have the lensed SNR distribution in the parameter space, we can find the detector's horizon distance d_{HD} (i.e, the farthest distance the detector is sensitive to) defined as the distance at which we have a threshold SNR, enough to be able to make a detection, which is usually set as $\rho_{th} = 8$. For computing this distance we use the fact that SNR scales inversely with the distance to the source, so:

$$\frac{\rho(d)}{\rho(d_{HD})} = \frac{\rho(d)}{\rho_{th} = 8} = \frac{d_{HD}}{d} \ , \tag{259}$$

thus

$$d_{HD}(q, M_L, y) = \frac{\rho(d = 500Mpc; q, M_L, y)}{8}(500Mpc) \ . \tag{260}$$

But this is still for total binary mass $M = 10M_\odot$. However, using that the SNR scales with the total mass, then for any M:

$$d_{HD}(M, q, M_L, y) = \frac{M}{10M_\odot}\frac{\rho(M = 10M_\odot, d = 500Mpc; q, M_L, y)}{8}(500Mpc) \ . \tag{261}$$

We also compute the Horizon Distance for unlensed waveforms, as a function of q and M: $d_{unlensed}(q, M)$.

With the detector's horizon distance, we can compute the rate of detectable binary mergers (in mergers per year) if we know the merger rate density (mergers per year per observable volume). This last quantity has been estimated by the LIGO Scientific Collaboration with a Bayesian analysis based on the three detected events and some assumptions about the mass function of stellar black holes binaries. The actualized number after the third event is a merger rate density of 12 to 213 Gpc^{-3} yr^{-1} [Abbott et al.]. For this work we take the most probable value 103 Gpc^{-3} yr^{-1}. Once we know the merger rate density, we can compute the detectable merger rate without lensing multiplying by the observable volume $V = (4\pi/3)d^3_{unlensed}$.

The observable volume depends on the binary parameters M and q. However, the merger rate density is computed for total masses between $10M_\odot \leq M \leq 100M_\odot$ and mass ratios $1 \leq q \leq 19$. Thus, in order to take into account all the events at a given distance, we should choose the lower distance in that range of values, $d_{unlensed}(M = 10M_\odot, q = 19)$. In fact, we only computed distances until $q = 10$, so we take the lowest of our distances. For larger distances, we still can observe events, but the merger range density should decrease as we increase the minimum distance because some of the systems included in the merger rate density are now so far to cannot be detected, and we have no data of how this quantity decrease, so our conservative assumption is to take $d_{unlensed}(10M_\odot, q = 10)$. We will also examine the case with $10M_\odot$ and $q = 1$ as a more optimistic case, since systems with lower mass ratio are more expected (the three first detections have mass ratios close to one).

Now we go to the purpose of this section: compute the increase of the detectable merger rate due to lensing. For that, first we compute the merger rate corresponding to each horizon distance $d_{HD}(M, q, M_L, y)$. As before, we examine the cases with $M = 10M_\odot$ and $q = 1$, 10 for the reasons mentioned above, and we treat the horizon

distance as a function of the lens parameters. In the corresponding volume, only will be detectable the mergers whose signals are lensed by at least a lens with parameters M_L and y, so we need to compute the probability of being lensed by such a lens:

$$P(z_s) = \frac{3}{2}\Omega_{co} y^2 \int_0^{z_s} dz_L \frac{(1+z_L)^2}{H(z_L)/H_0} \frac{H_0 D_{LS}(z_L, z_s) H_0 D_L(z_L)}{H_0 D_S(z_s)} \ , \tag{262}$$

where z_s is the redshift of the source, z_L is the redshift of the lens, H_0 is the Hubble constant at the present time (zero redshift), $H(z_L)$ is the Hubble constant at the lens redshift, and Ω_{co} is the cosmological density of compact objects. Thus, we need to express the horizon distances, which are luminosity distances, in terms of the redshift. We have the equation for luminosity distance as a function of the redshift (63). To obtain the inverse function, we compute a list of luminosity distances for a redshift range $0 \leq z \leq 0.6$ and then interpolate a function $z(d_l um)$ (we can do this because the luminosity distance increases monotonically with the redshift). For that, we choose the ΛCMD cosmological model (the current standard model of cosmology), with the parameter values given by Wolfram Mathematica 11:

$$\Omega_m = 0.308 \ , \ \Omega_k = 0 \ , \ \Omega_\Lambda = 0.692 \ , \ H_0 = 67.8 \ . \tag{263}$$

Now we need to estimate the density of compact objects Ω_{co}. This is a highly undetermined parameter for the range of masses we are interested in. We choose the result of a Bayesian analysis by [Goobar et al.], which establishes as the most probable value (of their analysis) $\Omega_{co} = 0.11\Omega_m$. There are no precise estimations of the mass density of compact objects. For example, one of the most cited works from [Canizares] only establishes that $\Omega_{co} < \Omega_m$ for a mass range $1 - 10^5 \ M_\odot$. For more massive compact objects or subsolar mass compact objects there are more precise estimations, for example in that paper. As we need the number density as a function of mass, because our detectable volume depends on the lens mass, we multiply Ω_{co} by a mass probability distribution function. Several Bayesian analysis of X-Ray sources ([Farr et al.] and [Özel et al.]) suggest that the mass distribution function of stellar black holes follows a power law of the form:

$$\frac{dN}{dm} \propto m^{-\alpha} \ . \tag{264}$$

From [Abbott et al.] the exponent is estimated to be $\alpha \sim 2.3$ (but with a great variance) so we choose this value, and the minimum stellar black hole mass is about $5M_\odot$. So we normalize this distribution in the range $\{5M_\odot, \infty\}$ and we apply it to Ω_{co}. However, this distribution could be biased by the fact that in the analysis all black holes were stellar mass black holes and most of them with lower masses than the black holes detected by LIGO. We do not have any estimation of the distribution of intermediate mass black holes, which formation channels can be different than for stellar black holes, so in some sense this power law distribution could underestimate the number of higher mass black holes. So we perform additionally a calculation with a more optimistic mass distribution function:

$$\frac{dN}{dm} \propto m^{-1} \ , \tag{265}$$

and we normalize it in the range $\{5M_\odot, 1000M_\odot\}$ (because the logarithm diverges for $m \to \infty$).

7.3.2 Results

In the previous sections we saw that the higher magnifications are realized for small values of the impact parameter y, so first we plot the results for the detector's horizon distance for our smallest value of $y = 0.001$:

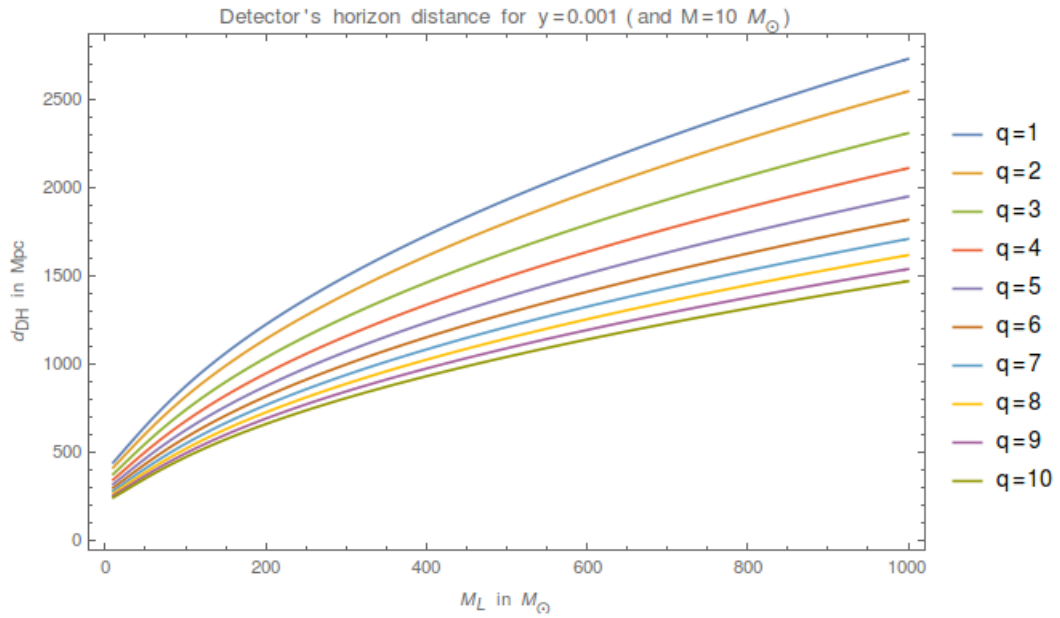

Figure 22: Detector's horizon distances for $y = 0.001$

As we see, for this value of the impact parameter the horizon distance is multiplied by a factor 5. As we discussed above, in order to use rigorously the estimated merger rate density of 103 Gpc^{-3} yr^{-1}, we should consider the distances for $q = 10$ in order to take into account all the systems considered for that rate, but we are also going to use the distances corresponding to a mass ratio $q = 1$, since it is expected that most of the detections will occur for low mass ratios. In Figure 23 we plot the behavior of the horizon distance as a function of the lens parameters for $q = 1$ and $q = 10$. We see a very similar behavior for the two mass ratios, changing only the value of the distances, that are greater for $q = 1$, but that is because in unlensed signals for lower q the SNR is higher. So we conclude that q is irrelevant for lensing effects at the level of the amplitude (remember that the SNR is computed only with the amplitude since the phase cancels in the inner product). Another comment about the figure is that for small values of y, the distance increases monotonically with the lens mass, but for greater values of the impact parameter we observe that the distance gets lower values as the lens mass increases, presumably due to the appearance of interference in the lensed waveform.

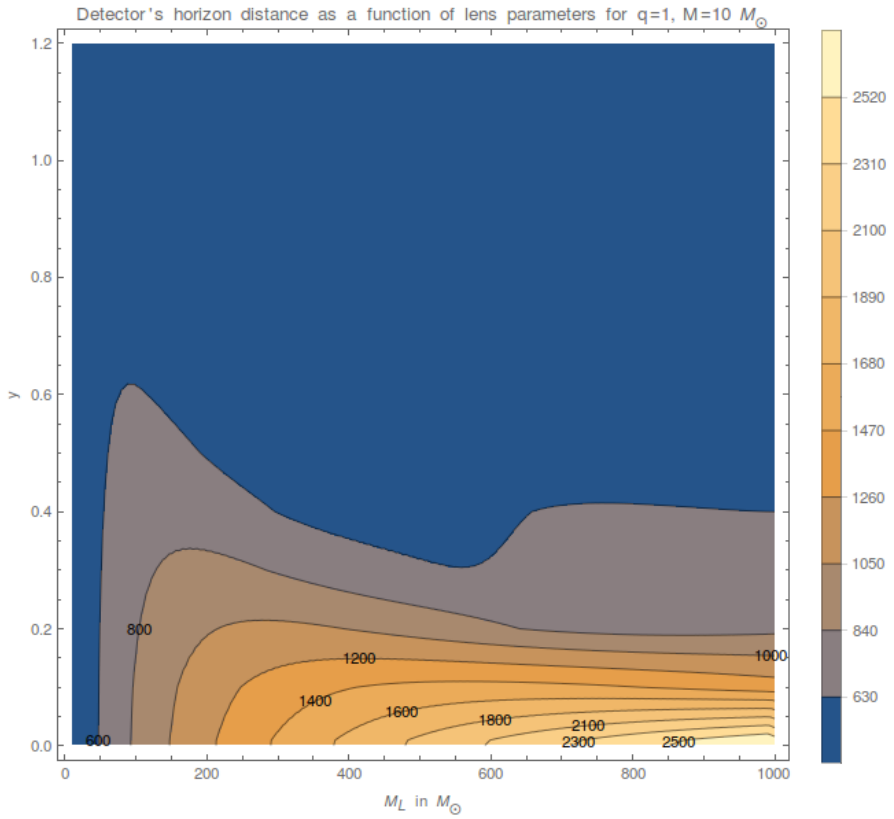

(a)

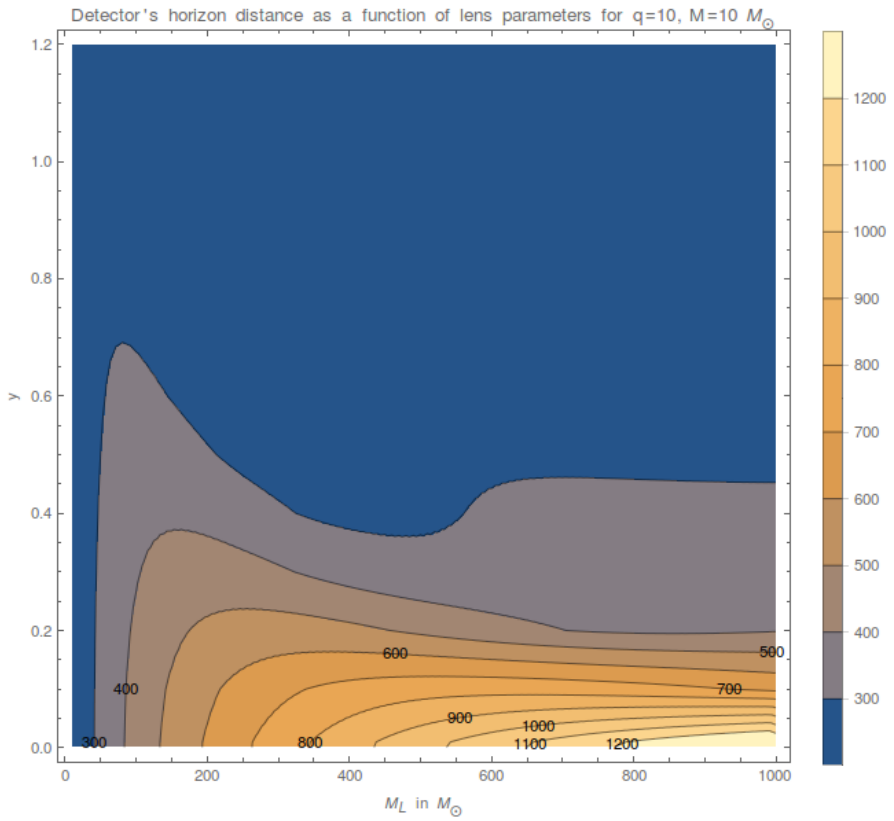

(b)

Figure 23: Detector's horizon distances (in Mpc) for $q = 1$ (up) and $q = 10$ (down).

In order to compute the increase in detectable volume between lensing situation and no lensing, we compute the detector's horizon distances for unlensed PhenomD waveforms for $q = 1$ and $q = 10$ (always for $M = 10M_\odot$):

$$d_{unlensed}(q = 1) = 388.837 \text{ Mpc} ,$$
$$d_{unlensed}(q = 10) = 213.436 \text{ Mpc} .$$

The volume increasing due to lensing for each par of values of the lens parameters is:

$$\Delta V(M_L, y) = \frac{4}{3}\pi[d^3_{HD}(M_L, y) - d^3_{unlensed}] . \tag{266}$$

Thus, the rate of new potentially detectable events is:

$$\frac{dN_L(M_L, y)}{dt} = \text{ERD} \cdot \Delta V(M_L, y) , \tag{267}$$

where ERD = 103 Gpc^{-3} yr^{-1} is the merger rate density. The actual detectable events are those who are actually lensed by a lens with parameters y' and M'_L such that $0 < y' \leq y$ and $M'_L \geq M_L$, so we need to multiply by the following lensing probability:

$$P(M_L, y) = \frac{3}{2}p(M_L)\Omega_{co}y^2 \int_0^{z_s} dz_L \frac{(1 + z_L)^2}{H(z_L)/H_0} \frac{H_0 D_{LS}(z_L, z_s) H_0 D_L(z_L)}{H_0 D_S(z_s)} , \tag{268}$$

where z_s is the redshift corresponding to the lensed horizon's distance, and $p(M_L) = \int_{M_L}^{\infty} dm\ f(m)$ is the probability that the mass lens is bigger than M_L according to the normalized mass distribution function $f(m) = k_1 m^{-2.3}$ for the conservative case or $f(m) = k_2 m^{-1}$ for the optimistic case (since the integral of the logarithm diverges at infinity, we integrate only to $M_L = 1000M_\odot$). Finally, as we want to count all possible new events, we sum for all y and all M_L (actually, we interpolate the data for all the points in the lens parameter space to get a function, and then integrate it). We show the results for $q = 1$, $q = 10$ and the two different mass distribution functions in Table 5, where N_L is the number of new events due to lensing per year, N_U is the number of unlensed events in the unlensed detectable volume, and $f(m)$ is the mass distribution function for compact lenses:

		N_L yr^{-1}	N_U yr^{-1}	$N_L/N_U(\%)$
q=1	$f(m) \sim m^{-2.3}$	0.0491191	6.05535	0.811
	$f(m) \sim m^{-1}$	1.74248	6.05535	28.8
q=10	$f(m) \sim m^{-2.3}$	0.00237353	1.00147	0.237
	$f(m) \sim m^{-1}$	0.0843154	1.00147	8.41

Table 5: Increase in the number of detectable events for aLIGO due to lensing.

7.3.3 Discussion

From Table 5 we see that for the more realistic mass distribution function estimated by the LIGO Scientific Collaboration, the increase in the number of events is small. For the detector's horizon distance corresponding to $M = 10M_\odot$ and $q = 10$ ($\sim 200Mpc$) we obtain a 0.2% of new detectable events, approximately two new lensed events per thousand years. When we increase the horizon distance to $\sim 400Mpc$ ($M = 10M_\odot$

and $q = 1$) then the percentage rises to 0.8%, approximately five new detectable events per century, because the lensing probability is bigger as we increase the detectable volume. This is a favorable perspective for future more sensitive detectors. When the detector is sensitive to higher distances, the probability that we could detect further lensed events rises.

For the more optimistic assumption about the mass distribution of lenses, we got much bigger percentage of new detectable events. The 28% of new events, roughly two new events per year, for the case with horizon distance $\sim 400Mpc$ is somehow too much optimistic. However, this reveals the highly dependent this analysis is in the mass distribution function. Possibly the uniform distribution in the logarithm of the masses overestimates considerably the number of more massive lenses, but if intermediate black holes (at the present time undetected) have a formation channel that allow a not so small population of these objects, then gravitational lensing of gravitational waves will be a non-negligible phenomena even for the current ground-based detectors.

The rates we have computed are a rough estimation. Despite we have not computed the associated errors, it is easy to see that the wide range for the merger rate ERD with the poor estimation for the number density of compact lenses produces a huge error in the rate estimation. Besides, we have to point out that a detectable event (an event with a higher SNR than the threshold) is not always detected. In order to make a detection, it is needed a process to accumulate statistical significance and the required confidence (a level of 5 sigmas) is not always reached. For example, the aLIGO candidate event LVT151012 reached a (network) SNR of 9.7, above the threshold, but its statistical significance was only 1.7σ. So our rate estimation is for *a priori* detectable events.

Another issue to comment is that we have only considered compact lenses, for which the point mass lens model is expected to be a good approximation. Furthermore, in this analysis we restrict to a maximum lens mass of $1000M_{\odot}$, but if a population of IMBH exists, there will be a range of masses above the thousand solar masses, and besides the population of SMBH (which existence is confirmed) with covers the range of millions of solar masses. So our analysis is quite restricted in this sense. One interesting type of lenses for cosmological horizon distances, as distances for which LISA will be sensitive enough, are galactic clusters and dark matter halos. This kind of lenses are better modeled with another well-known model, the singular isothermal sphere model.

In the paper of [Takahashi & Nakamura], they study the lensing probability for SMBH and dark matter halos (CDM halos) with these two models, the point mass lens and the singular isothermal sphere, for LISA, because the high redshift reached by LISA makes these lenses good candidates to produce lensed events. In their work they obtain in both cases a lensed event per year, approximately. Another lensing paper is [Broadhurst et al.], in which they study the lensed events rate for aLIGO in the geometrical approximation of section 3 considering as lenses elliptical galaxies. They obtain a lensed event rate between 0.2 and 14.2 lensed events per year, but with a great variance. So we think that our estimation covers a hole in the literature, the cases of compact lenses of stellar and intermediate masses for advanced LIGO. Our results (at least for the conservative mass distribution function) seem consistent with the rates for

other kind of lenses. However, we must point out that we did not compute the total rate of detectable lensed events, but the rate of new events not detectable without lensing, i.e, we do not consider lensed events in which the unlensed signal could be detectable due to have a higher SNR than the threshold.

Finally, we have to remark that we employ the sensitivity curve for the O1 run of aLIGO. In its design sensitivity, aLIGO will expect hundreds of detections per year, so maybe we are only a few years away from the first detection of lensed signals.

8 Conclusions

We review in this work the basic theory of gravitational lensing of gravitational waves, focusing on the point mass lens model. We have seen that for gravitational waves from astrophysical signals the wavelengths are long enough to have to take into account interference effects in lensing, and then one has to consider the wave optics formulation. We have seen that, opposite to the case for light, taking the geometrical limit of the wave optics does not eliminate the interference effects, due to the coherent emission of gravitational waves from astrophysical signals. Thus, one always needs to employ the wave optics formalism, incarnated in the amplification factor, to study lensing effects on the waveforms.

We studied two interesting situations. The first was the possible loss of SNR due to using unlensed templates in the search for a lensed signal for advanced LIGO detectors. This was previously analyzed in [Cao et al.], but ignoring spin effects in the waveforms, and considering only the inspiral part in the Post-Newtonian approximation. We upgrade the analysis employing more accurate phenomenological waveform models from the PhenomD model, which include the merger and ringdown signals and that is calibrated with fully numerical relativity simulations. Also the PhenomD model includes spin effects (although only for the aligned-antialigned cases). We have found that spins play an important role in determining the fitting factor, the highest normalized SNR reached with unlensed models, showed in the highly oscillatory behavior of the overlap in the spin range. However, we also conclude that a future analysis with a bigger parameter space needs to be done, specially for IMBH and SMBH lenses, including precession effects, that could mimic the oscillatory behavior of the lensed signals.

The second situation was the possible gain in detectable events rate due to lensing magnification. Magnification can make detectable a signal far enough to be undetectable due to have a SNR smaller than the threshold of the detector. We estimate the rate of new detectable events due to lensing by compact objects, based on an estimation of the merger rate density done in [Abbott et al.] and some assumptions on the number density of compact lenses. We found a small number of new detectable events (less than five in a century) for the conservative assumptions and a significant number (upon one a half event per year) with the optimistic assumptions. This study covers a hole in the literature about lensed events rate, complementing [Takahashi & Nakamura] which study SMBH and CDM halos lenses for LISA and [Broadhurst et al.] which study elliptical galaxy lenses for LIGO.

We conclude that lensing is an interesting phenomenon that has to be taken into account for the future sensitivity upgrades of LIGO and VIRGO, and for future planned detectors as LISA and Einstein Telescope. As the sensitivity of the detector grows and further distances can be observed, the lensing probability rises, and future detectors could loose a significant number of signals if lensed templates are not used for the search. Besides, the employ of lensed templates allows to detect more distant signals than those expected by the designed sensitivity of the detector. Possibly in a near future we could detect the first lensed gravitational wave signal.

Further studies need to be done, in particular a rigorous study of parameter es-

timation for lensed signals: how precisely can be estimated the lens and the binary parameters from a detection, the possible correlations between lens and binary parameters, etc. This is also analyzed in [Cao et al.], but with the restrictions mentioned above due to neglect spin effects and to employ only a inspiral waveform. Another interesting situation to study in the future is lensing of spinning neutron star signals. We introduce the basic theory of signals from these sources in section 5.2, however, a quantitative lensing study was beyond the scope of this work.

References

[Abbott et al.] LIGO Scientific and VIRGO Collaboration, GW170104: *Observation of a 50-Solar-Mass Binary Black Hole Coalescence at Redshift 0.2*, Phys. Rev. Lett. 118, 221101, 2017.

[Arnowitt, Deser & Misner] R. Arnowitt, S. Deser, C. W. Misner, *The Dynamics of General Relativity*, 7th chapter of L. Witten (editor), *Gravitation: an introduction to current research*, John Wiley & Sons, 1962.

[Baraldo, Hosoya & Nakamura] C. Baraldo, A. Hosoya, T. T. Nakamura, *Gravitational induced interference of gravitational waves by a rotating massive object*, Physical Review D, Volume 59, 083001.

[Berry & Veitch] C. Berry, J. Veitch, *What if the gravitational waves detected in 2015 were strongly lensed by massive galaxy clusters?*, https://dcc.ligo.org/P1700140/, 2017.

[Bishop & Rezzolla] Nigel T. Bishop, Luciano Rezzolla, *Extraction of gravitational waves in numerical relativity*, Living Reviews in Relativity, 19:2, 2016.

[Blanchet] Luc Blanchet, *Gravitational Radiation from Post-Newtonian Sources and Inspiralling Compact Binaries*, arXiv:1310.1528v4, 2016.

[Blanchet et al.] L. Blanchet, B.R. Iyer, C.M. Will, A.G. Wiseman, *Gravitational Radiation from inspiralling compact binaries to second-post-Newtonian order*, Class. Quantum Grav., 13, 1996.

[Born & Wolf] Max Born, Emil Wolf, *Principles of Optics*, 6th edition, Cambridge University Press, 1980.

[Broadhurst et al.] K.Y. Ng, W.K. Wong, G.F. Li, Tom Broadhurst, *Precise LIGO Lensing rate Predictions for Binary Black Holes*, 6th edition, Cambridge University Press, 1980.

[Canizares] C.R.Canizares, *Manifestations of a cosmological density of compact objects in quasar light*, Astrophysical Journal, 263, 1982.

[Cao et al.] Z. Cao, Li-Fang Li, Yan Wang, *Gravitational lensing effects on parameter estimation in gravitational wave detection with advanced detectors*, Phys. Rev. D, 90, 062003, 2014.

[Carot] Jaume Carot, *Aspectos geométricos de la Relatividad General*, notes for the subject Geometry & Relativity, MFMA, UIB, 2017 (unpublished).

[Carroll] Sean Carroll, *Spacetime and Geometry: An Introduction to General Relativity*, Addison Wesley, 2004.

[Etherington] I. M. H. Etherington, *On the definition of distance in general relativity*, Philosophical Magazine ser.7, vol.15, 761 (1933).

[Farr et al.] Will M. Farr, N. Sravan, A. Cantrell, L. Kreidberg, C. D. Bailyn, I. Mandel, V. Kalogera, *The mass distribution of stellar-mass black holes*, The Astrophysical Journal, 741, 2, 2011.

[García et al.] Cecilio García, Sascha Husa, Geraint Pratten, Marta Colleoni, Xisco Jiménez Forteza, *Toward calibrating phenomenological waveform models with subdominant harmonics to Numerical Relativity*, Talk at IGWM2017, Bilbao, 2017.

[Goobar et al.] A. Goobar, E. Mörtsell, L. Bergström, *Determining the fraction of compact objects in the Universe using supernova observations*, The Astrophysical Journal, 559:53-58, 2001.

[Goldstein] Herbert Goldstein, Charles Poole, John Safko, *Classical Mechanics*, 3rd edition, Addison Wesley, 2000.

[Khan et al.] Sebastian Khan, Sascha Husa, Mark Hannam, Frank Ohme, Michael Pürrer, Xisco Jiménez Forteza, Alejandro Bohé, *Frequency-domain gravitational waves from non-precessing black-hole binaries. II. A phenomenological model for the advanced detector era*, arXiv:1508.07253v2, 2015.

[Landau & Lifshitz] L.D. Landau, E.M. Lifshitz, *The Classical Theory of Fields*, 4th ed., Butterworth-Heinemann, 1975.

[Lasky] Paul D. Lasky, *Gravitational waves from neutron stars: a review*, Publications of the Astronomical Society of Australia, 2015.

[GW150914data] losc.ligo.org/events/GW150914/

[Maggiore] Michele Maggiore, *Gravitational Waves, Volume 1: Theory and Experiments*, Oxford University Press Inc., 2008.

[Nambu] Yasunada Nambu, *Wave Optics and Image Formation in Gravitational Lensing*, International Journal of Astronomy and Astrophysics, 2013, 3, 1-7.

[Özel et al.] F. Özel, D. Psaltis, R. Narayan, J. E. McClintock, *The black hole mass distribution in the Galaxy*, The Astrophysical Journal, 725, 2, 2010.

[Poisson] Eric Poisson, *Introduction to Post-Newtonian theory (slides)*, www.dpg-physik.de/dpg/pbh/aktuelles/pdf/Poisson.pdf, 2015.

[Pretorius] Frans Pretorius, *Evolution of Binary Black-Hole Spacetimes*, Phys. Rev. Lett. 95, 121101, 2005.

[Prix] Reinhard Prix, *Gravitational Waves from Spinning Neutron Star*, Chapter 24 of W. Becker(ed.) *Neutron Stars and Pulsars*, Astrophysics and Space Science Library 357, Springer-Verlag, 2009

[Schneider, Ehlers & Falco] P. Schneider, J. Ehlers, E. E. Falco, *Gravitational Lenses*, Springer, 1992.

[Schutz & Sathyaprakash] B.S. Sathyaprakash, Bernard F. Schutz, *Physics, Astrophysics and Cosmology with Gravitational Waves*,Living Rev. Relativity, 12, 2, 2009.

[Sintes & Luna] Alicia M. Sintes, Manuel Luna, *Parameter estimation of compact binaries using the inspiral and ringdown waveforms*, arXiv:gr-qc/0601072v2, 2006.

[Smarr et al.] Larry Smarr, Andrej Cadez, Bryce DeWitt, Kenneth Eppley, *Collision of two black holes: Theoretical framework*, Phys. Rev. D, Volume 14, n.10, 1976.

[Takahashi & Nakamura] Ryuichi Takahashi, Takashi Nakamura, *Wave effects in gravitational lensing of gravitational waves from chirping binaries*, arXiv:0305055v2, 2003.

[Trias] Miquel Trias, *Gravitational wave observation of compact binaries: detection, parameter estimation and template accuracy*, http://hdl.handle.net/10803/37402, 2011.

[Wald] Robert M. Wald, *General Relativity*, The University of Chicago Press, 1984.

[Wambsganss] Joachim Wambsganss, *Gravitational Lensing in Astronomy*, www.livingreviews.org/Articles/Volume1/1998-12wamb

[Whelan] John T. Whelan, *The Geometry of Gravitational Wave Detection* notes from School of Gravitational Waves, Warsaw, 2014.